Imaging of Early Distal Tarsal Osteoarthritis in Icelandic Horses

Charles J. Ley
Faculty of Veterinary Medicine and Animal Science
Department of Clinical Sciences
Uppsala

Doctoral Thesis
Swedish University of Agricultural Sciences
Uppsala 2014

Acta Universitatis Agriculturae Sueciae
2014:53

Cover: Radiograph (left) and anaglyph three-dimensional volumetric reconstruction computed tomography (right) of tarsal joints from two horses used in the study. Note that the anaglyph image appears as a three-dimensional image when viewed using red-cyan colour filter spectacles. Images assembled by Charles Ley.

ISSN 1652-6880
ISBN (print version) 978-91-576-8054-9
ISBN (electronic version) 978-91-576-8055-6

Print: SLU Service/Repro, Uppsala 2014

Imaging of Early Distal Tarsal Osteoarthritis in Icelandic Horses

Abstract

The early stages of osteoarthritis (OA) are characterised by focal morphological changes that may slowly progress if joint repair fails. Validated, non-invasive and affordable methods to diagnose the early stage of OA in horses are lacking. The objectives of this thesis were to investigate and validate OA detection methods, and describe the morphological OA changes in the distal tarsal region of a group of young Icelandic horses.

Radiography, computed tomography (CT) and magnetic resonance imaging (MRI), light microscopy histology, backscattered electron scanning electron microscopy, and confocal scanning light microscopy were used to investigate osteochondral changes in the joints of the distal tarsal region in 38 two-and-a-half year old Icelandic horses. Radiographs were taken of live horses standing, all other examinations were performed 2-3 months later on non-weight bearing cadaver specimens from the same horses.

The results showed that a novel CT and MRI guidance method for osteochondral tissue specimen collection improved detection of early OA changes in centrodistal (distal intertarsal) joints compared to standardised specimen collection from predetermined locations. Diagnostic imaging and microscopy showed that early OA morphological changes primarily occur in the articular hyaline and calcified cartilage rather than the subchondral bone. The lesions articular mineralisation front defect, central osteophytes and hyperdense mineralisation front protrusions were described in detail in the joints of the distal tarsal region using combined microscopic imaging of embedded block specimens. A comparison of clinical diagnostic imaging methods found that radiography was equal or better than low-field MRI for the detection of early OA in centrodistal joints. Articular mineralisation front defects were identified as a highly specific imaging feature in radiographs for early OA.

This thesis provides a detailed morphological description of the osteochondral changes occurring in the early stages of OA in the centrodistal joint of Icelandic horses and proposes a validated, non-invasive, cost-effective radiography method for proceeding with future longitudinal studies of early OA in Icelandic horses.

Keywords: Magnetic resonance imaging, computed tomography, radiology, radiography, equine, bone spavin, osteoarthrosis, degenerative joint disease, articular cartilage, microscopy.

Author's address: Charles J. Ley, SLU, Department of Clinical Sciences,
P.O. Box 7054, 750 07 Uppsala, Sweden
E-mail: charles.ley@slu.se

Dedication

To Cecilia, Timothy, Kristoffer and Edward.

Increasing magnification teaches more and more about less and less, and for this reason a sensible compromise must be reached.

Alan Boyde and Elwyn Firth 2008

Contents

List of Publications

This thesis is based on the work contained in the following papers, referred to by Roman numerals in the text:

I Ley, C.J., Ekman, S., Dahlberg, L.E., Björnsdóttir, S. & Hansson, K. (2013). Evaluation of osteochondral sample collection guided by computed tomography and magnetic resonance imaging for early detection of osteoarthritis in centrodistal joints of young Icelandic horses. *American Journal of Veterinary Research* 74(6), 874-887.

II Ley, C.J., Ekman, S., Hansson, K., Björnsdóttir, S. & Boyde, A. (2014). Osteochondral lesions in distal tarsal joints of Icelandic horses reveal strong associations between hyaline and calcified cartilage abnormalities. *European Cells and Materials* 27, 213-236.

III Ley, C.J., Björnsdóttir, S., Ekman, S., Boyde, A. & Hansson, K. Detection of early osteoarthritis in the centrodistal joints of Icelandic horses: Evaluation of radiography and low-field magnetic resonance imaging (submitted).

The contribution of Charles J. Ley to the papers included in this thesis was as follows:

I Conception and design of the study, acquisition, analysis and interpretation of data, drafting the article, statistical analysis, critical revision of the article.

II Conception and design of the study, acquisition, analysis and interpretation of data, drafting the article, statistical analysis, critical revision of the article.

III Conception and design of the study, acquisition, analysis and interpretation of data, drafting the article, statistical analysis, critical revision of the article.

Abbreviations

2D	two-dimensional
3D	three-dimensional
BSE SEM	backscattered electron scanning electron microscopy
CSLM	confocal scanning light microscopy
CT	computed tomography
DICOM	digital imaging and communications in medicine
FSE	fast spin echo
GRE	gradient echo
MRI	magnetic resonance imaging
OA	osteoarthritis
PMMA	polymethyl methacrylate
STIR	short tau inversion recovery
T1W	T1 weighted
WATSf	water selective fluid

1 Introduction

1.1 General background

Osteoarthritis (OA) is a disease of joints that results from the failure of the joint tissue repair mechanisms (Lane *et al.*, 2011). The disease has a high prevalence in horses (Innes & Clegg, 2010; Egenvall *et al.*, 2006), particularly in the joints of the distal tarsal region of Icelandic horses (Björnsdottir *et al.*, 2000b; Eksell *et al.*, 1998), and the joint pain and lameness that are caused by OA are a common reason for loss of use or euthanasia of horses (Egenvall *et al.*, 2006; Björnsdottir *et al.*, 2003; Bergsten, 1983). There is currently no cure for OA (Martel-Pelletier *et al.*, 2011; Bay-Jensen *et al.*, 2010; Wieland *et al.*, 2005).

The reason why Icelandic horses commonly develop distal tarsal OA is currently uncertain. Studies of adult Icelandic horses show a medium to high heritability for radiographic changes of distal tarsal OA, and the combination of hindlimb lameness after a flexion test and radiographic changes of distal tarsal OA (Arnason & Björnsdóttir, 2003; Björnsdottir *et al.*, 2000a). This means that identification of horses with distal tarsal OA before breeding age and removal of these horses from the breeding population has the potential to reduce the prevalence of the disease. This would be of major benefit to the horses, their owners and the Icelandic horse industry. Furthermore, if accurate early identification of distal tarsal OA was possible this information could provide a valuable model for the development of early intervention treatments to limit or slow the progression of OA. Non-invasive diagnostic imaging methods including radiography and standing magnetic resonance imaging (MRI) may be suitable imaging biomarkers for screening horses for early OA of the joint in the distal tarsal region, but the stage at which these methods can detect the disease and the morphological changes that indicate a high risk of developing clinical distal tarsal OA are currently uncertain.

When a diagnosis of OA is made clinically there will usually be a permanent alteration to the joint tissue structure and function. At this stage of the disease multiple tissues in the joint will be affected, changes in the tissues will be advanced, and the chance of identifying the initial lesions and triggering pathophysiological causes is low. For development of OA treatments and research aimed at investigating the causes of OA, studies of this clinical phase of the disease are frustrating and generally unrewarding (Bay-Jensen *et al.*, 2010; Burstein & Hunter, 2009). This has resulted in a focus on the development of non-invasive biomarker methods that can detect OA at an early preclinical stage of the disease when tissue changes might be reversible and initial lesions can still be identified (Baum *et al.*, 2012; Luyten *et al.*, 2012; Heinegard & Saxne, 2011; Quatman *et al.*, 2011; Ding *et al.*, 2010). Studies of early OA provide information about the pathogenesis of OA and this can be used to develop OA preventative strategies (Palmer *et al.*, 2013; Ding *et al.*, 2010; Squires *et al.*, 2003). Furthermore, availability of an accurate non-invasive biomarker for early OA would pave the way for studies of treatments aimed at slowing, stopping or even reversing joint changes before clinical signs occur (Palmer *et al.*, 2013).

Traditionally radiography has been used to assess joints for morphological evidence of OA, but radiography is considered to be poor at detecting the early stages of OA (Hunter *et al.*, 2011a; Quatman *et al.*, 2011; Jones *et al.*, 2004). Major technological advances during recent years have resulted in a rapid evolution of the multiplantar (cross-sectional) imaging techniques computed tomography (CT) and, in particular, MRI for the assessment of OA (Hayashi *et al.*, 2012b; Quatman *et al.*, 2011; Roemer *et al.*, 2011; Aula *et al.*, 2009; Vande Berg *et al.*, 2002). Both these techniques offer three-dimensional (3D) imaging at resolutions that allow detection of the small and often focal changes that occur in the early stages of human OA (Palmer *et al.*, 2013; Ding *et al.*, 2010).

Clinical diagnostic imaging is used as an imaging biomarker for human OA (Hunter & Eckstein, 2011). Clinical diagnostic imaging biomarkers for OA have several major advantages over other biomarker methods; they are non-invasive, provide spatial information about the tissue and are repeatable (ESR, 2013). Before an imaging biomarker can be considered accurate for detection of the intended disease or tissue change the method requires validation (ESR, 2013; Wang *et al.*, 2012; Murray *et al.*, 2007). Validation is done by comparing image changes with a 'gold' standard (also sometimes called reference or criterion standard). 'Gold' standards for abnormalities or features detected in clinical diagnostic images are based on microscopic methods where the tissue change can be evaluated at a cellular level (for example light microscopy histology) or methods where it is possible to see the tissue lesion

directly (for example arthroscopy). Once validated, diagnostic imaging methods can be used to follow patients and study groups over time without having to perform invasive 'gold' standard procedures such as osteochondral sampling. These types of longitudinal studies are essential for understanding the events that occur during OA development.

Animal models have a major role in human OA research particularly for the investigation of the early stages of the disease when access to human tissues is highly restricted (Heinegard & Saxne, 2011; Aigner *et al.*, 2010; Innes & Clegg, 2010; Ameye & Young, 2006; Squires *et al.*, 2003). The high incidence of naturally occurring OA in Icelandic horses and the similarities between equine and human articular cartilage and subchondral bone structure and thickness make Icelandic horses a suitable research model (McIlwraith *et al.*, 2011; Innes & Clegg, 2010).

1.2 The joints of the equine distal tarsal region

The equine tarsus is a complex joint region composed of eight or nine bones which articulate by four joint regions (Fig. 1) (Shively, 1982). The term "distal tarsal region" also called "distal portion of the tarsus" is considered to be the region of the tarsus that includes the talocalcaneal-centroquartal (previously called proximal intertarsal), centrodistal (previously called distal intertarsal) and tarsometatarsal joints (Fig. 1) (Tranquille *et al.*, 2011; Labens *et al.*, 2007a; Branch *et al.*, 2004; Axelsson *et al.*, 2001; Björnsdottir *et al.*, 2000b; Eksell *et al.*, 1999; Laverty *et al.*, 1991). These joints are low-motion and predominantly flat joints. They allow mild rotation and translation of the distal tarsal region (Sisson, 1975), have an important shock absorbing function (Lanovaz *et al.*, 2002; Pool, 1996) and are exposed primarily to compressive loading (Schamhardt *et al.*, 1989).

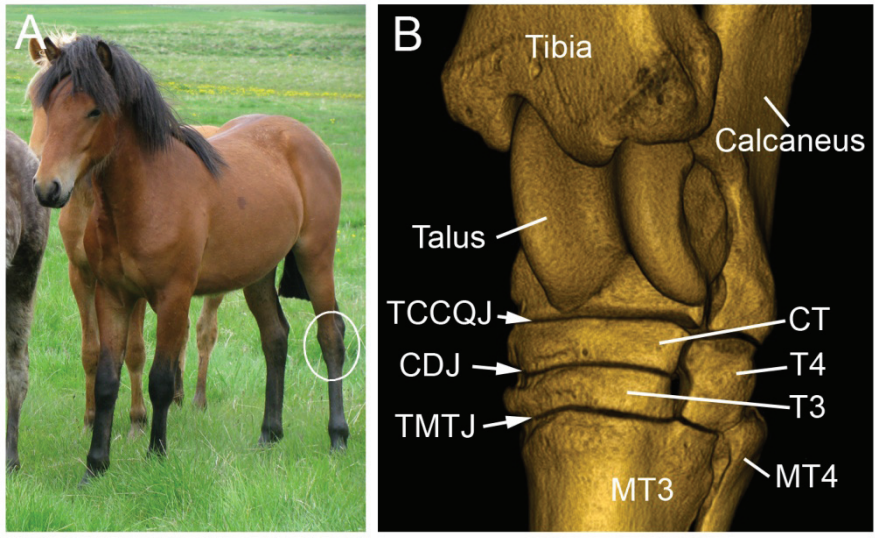

Figure 1. Equine tarsal region bones and joints. (A) An Icelandic horse from the study. The left tarsus region is within the white circle. (B) Three-dimensional volumetric reconstruction computed tomography image showing the dorsolateral aspects of bones and joints of the tarsal region. TCCQJ = talocalcaneal-centroquartal joint; CDJ = centrodistal joint; TMTJ = tarsometatarsal joint; CT = central tarsal bone; T3 = third tarsal bone; T4 = fourth tarsal bone; MT3 = third metatarsal bone; MT4 = fourth metatarsal bone.

The joint surfaces are covered by a thin layer of articular cartilage which is attached to the underlying subchondral bone by a wavy chondro-osseus junction called the 'cement line' (Fig. 2). Articular cartilage is a highly specialised tissue. It does not contain blood vessels, lymphatic vessels or nerves and it provides a durable, cushioning and almost frictionless surface for the joint (Buckwalter & Hunziker, 1999). The cartilage is divided into the hyaline articular cartilage that forms the articular surface and the deeper articular calcified cartilage. The gently undulating junction between the hyaline and calcified articular cartilage is called the 'mineralisation front' and this junction is represented by a basophilic line called the 'tidemark' in decalcified haematoxylin and eosin stained tissues viewed with light microscopy histology (Fig. 2) (Madry *et al.*, 2010; Oegema *et al.*, 1997). The hyaline articular cartilage is divided into three zones: superficial, middle and deep (Fig. 2) (Madry *et al.*, 2012; Pritzker & Aigner, 2010; Pritzker *et al.*, 2006). In the superficial zone chondrocytes have a flattened shape and are aligned approximately parallel to the articular surface, in the middle zone chondrocytes are spheroid shaped and in the deep zone chondrocytes are spheroid to ellipsoid in shape are often arranged in columns orientated perpendicular or mildly obliquely to the articular surface (Fig. 2). The articular calcified cartilage contains smaller chondrocytes surrounded by mineralised matrix (Fig. 2) (Madry *et al.*, 2012; Pritzker *et al.*, 2006; Buckwalter & Hunziker, 1999). The bulk of the articular cartilage volume is made up of extracellular matrix, which is predominantly interstitial water and the proteoglycans in the hyaline cartilage and hydroxyappatite and proteoglycans in the calcified cartilage. Proteoglycans are negatively charged and this has a key role in controlling the amount of interstitial water that is present within the hyaline articular cartilage (Heinegard, 2009; Mow *et al.*, 1992). The structural framework that provides the tensile strength of articular cartilage is formed by type II collagen (Cluzel *et al.*, 2013). This collagen is arranged in an arcade-like structure and is firmly attached to the underlying subchondral bone (Buckwalter & Hunziker, 1999; Jeffery *et al.*, 1991).

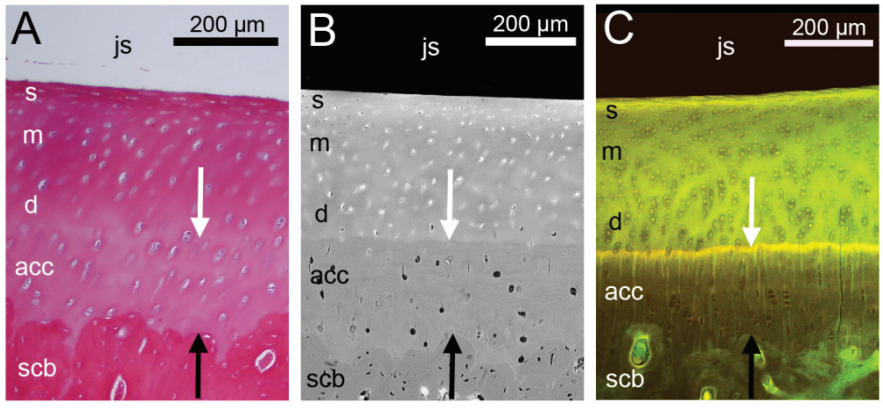

Figure 2. Microscopic morphology of the articular osteochondral tissues from a centrodistal joint from the study. (A) Light microscopy histology with hematoxylin and eosin stain. (B) Backscattered electron scanning electron microscopy (BSE SEM) with iodine staining. (C) Confocal scanning light microscopy (CSLM). The hyaline articular cartilage is divided into superficial (s), middle (m) and deep zones (d). Note the clear definition of the mineralisation front/tidemark (white arrow) in the BSE SEM and CSLM images compared to the light microscopy image. In contrast there is clearer definition of the chondro-osseus junction/cement line (black arrow) in the light microscopy image compared to BSE SEM and CSLM. s = superficial zone, m = middle zone, and d = deep zone of the hyaline articular cartilage; acc = articular calcified cartilage; scb = subchondral bone; js = joint space. Panel (B) and (C) images by A. Boyde.

The joint capsules and ligaments in the distal tarsal region are very important in maintaining alignment and stability of the tarsal joints. The joint capsules are thick and fibrous and have strong attachments to the external surfaces of the tarsal bones. Ligaments surrounding the distal tarsal region provide firm external support for the joints and include collateral ligaments, the talocentrodistalmetatarsal ligament and the plantar ligament (Sisson, 1975). Interosseus ligaments within non-articular depressions are present in the talocentroquartal, centrodistal and tarsometatarsal joints and these provide firm internal support for the joints (Raes *et al.*, 2011; Sisson, 1975). The tendons of the peroneus tertius and tibialis cranialis muscles attach on the dorsal bone surfaces of the distal tarsal and proximal metatarsal regions giving further external support to the joints in the area (Sisson, 1975).

There are variable communications between the joints in the distal tarsal region. The centrodistal and the tarsometatarsal joints are reported to communicate in 9-38% of horses (Bell *et al.*, 1993; Kraus-Hansen *et al.*, 1992; Sack & Orsini, 1981; Brown & Valko, 1980). There is communication between the centrodistal and talocalcaneal-centroquartal joints in approximately 4% of horses and in some cases all three joints communicate (Bell *et al.*, 1993).

1.3 Osteoarthritis (OA)

The definition of OA is evolving as more is understood about the disease. Concepts that classify OA as primary or secondary and emphasize OA as a degenerative disease have been challenged during the last decade (Heinegard & Saxne, 2011; McGonagle *et al.*, 2010; Brandt *et al.*, 2009). The use of these classifications is now rare. Inflammation has been recognised to be a key event in OA and thus the term 'osteoarthrosis', which was previously used to describe the disease, is no longer recommended (Heinegard & Saxne, 2011).

During 2009 a working group established by the Osteoarthritis Research Society International (OARSI) presented a general definition of the disease state of OA (Lane *et al.*, 2011). The working group consensus was that OA is "usually progressive and represents failed repair of joint damage initiated by an abnormality in any of the synovial joint tissues" and that this "ultimately

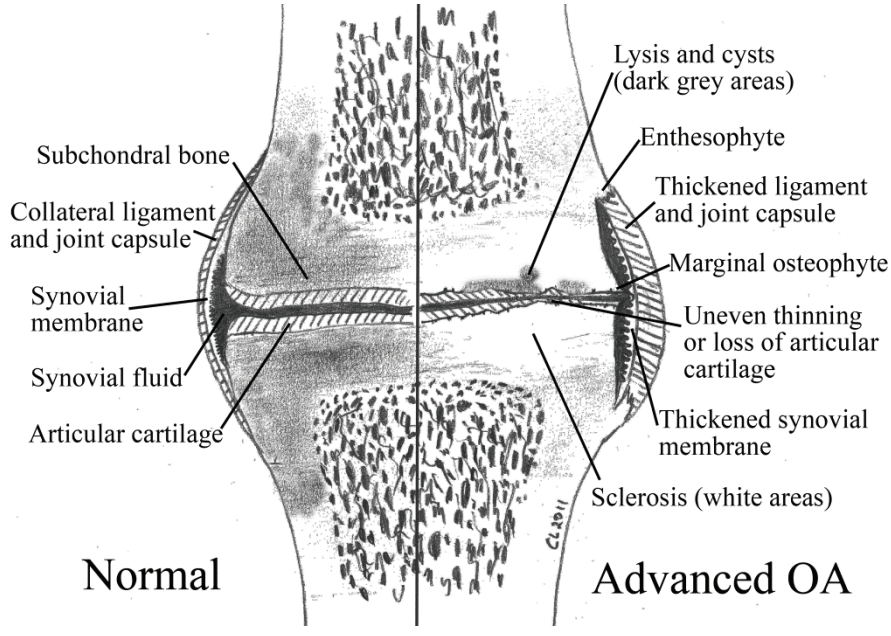

Figure 3. Schematic drawing showing the major tissues of the joint organ and common morphological changes of OA. The left side of the joint shows normal morphology. The right side of the joint shows abnormalities of these joint tissues that are typical of late or advanced OA. (Modified from Caron, J.P. (1996). Neurogenic factors in joint pain and disease pathogenesis. In: McIlwraith, C.W and Trotter, G.W. (Eds.) Joint disease in the horse. P73. Philadelphia: W.B. Saunders Company.)

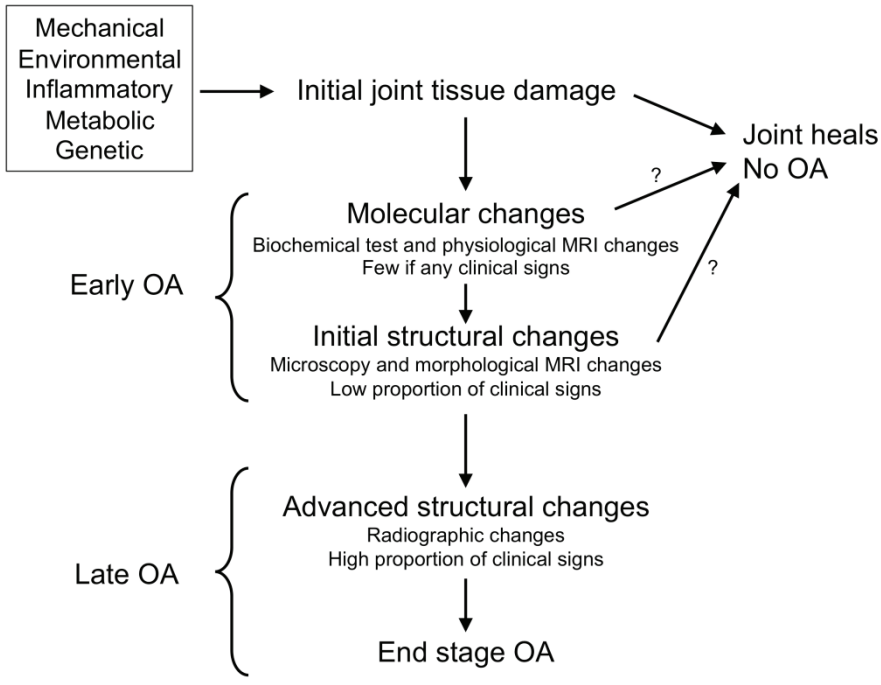

Figure 4. Flow chart showing the initiating factors, disease pathways and stages of OA. It is unknown whether or not it is possible for early OA changes to completely heal and revert to a normal joint. Once the late OA stage is reached it is no longer possible for the joint to heal and regain normal morphology.

results in the breakdown of cartilage and bone, leading to the symptoms of pain, stiffness and functional disability" (Lane *et al.*, 2011). Additionally the working group introduced the concept of the "disease OA" defined as the structural joint changes that can be detected with diagnostic imaging, microscopic imaging and arthroscopy and the "illness OA" defined as the patient-reported symptoms (Lane *et al.*, 2011). OA is considered to involve the entire joint organ (Fig. 3), which constitutes all of the synovial tissues (articular cartilage, subchondral bone, ligaments, joint capsule, synovium and if present menisci) and even the structures that surround the joint (peripheral nerves, periarticular muscles, bursa, local fat pads and tendons) (Loeser *et al.*, 2012; Brandt *et al.*, 2009; Peterfy *et al.*, 2004; Waldschmidt *et al.*, 1999). The disease pathway of OA can be considered as a continuum with an early and a late stage (Fig. 4). Initial joint tissue damage caused by mechanical, environmental, inflammatory, metabolic or genetic factors is followed either by healing, or, if healing fails, OA (Ding *et al.*, 2010). The development of OA is an interplay between the initiating causes and the likelihood of OA development increases as the number of causal factors present increases

(Felson, 2013). Strong arguments have been made for the mechanical factors joint overload and/or abnormal joint anatomy (congenital or acquired) as being the predominant initiators and the driving forces behind the progression of OA (Felson, 2013; Brandt *et al.*, 2009) and that in conjunction with inflammatory mediators this results in a cascade of destructive, degenerative and proliferative joint changes (Loeser *et al.*, 2012; Heinegard & Saxne, 2011).

1.3.1 Early OA

The term 'early' or 'pre-clinical OA' has been applied to the period of the first molecular and structural changes of OA during the time that clinical signs of OA are not present (Chundru *et al.*, 2013; Palmer *et al.*, 2013; Luyten *et al.*, 2012; Bay-Jensen *et al.*, 2010; Ding *et al.*, 2010; Burstein & Hunter, 2009). Molecular changes that can be detected with biochemical tests or physiological imaging techniques (Palmer *et al.*, 2013; Bansal *et al.*, 2011; Gold *et al.*, 2009; Goldring & Goldring, 2007) represent the earliest changes (Heinegard & Saxne, 2011). Simultaneously or following the molecular changes, morphological changes develop in the joint tissues, and these are characteristically focal or multifocal (Pritzker *et al.*, 2006; Squires *et al.*, 2003; Veje *et al.*, 2003; Dieppe & Kirwan, 1994). It is now generally accepted that conventional radiographs detect only late/advanced OA (Palmer *et al.*, 2013) and thus the term 'pre-radiographic OA' has become synonymous with 'early OA' (Bay-Jensen *et al.*, 2010; Cibere *et al.*, 2009).

The OA detection method selected determines at which stage of the OA disease pathway a diagnosis of OA can be made (Fig. 4). This is of particular importance in studies that attempt to classify patients into a group with early OA compared to a group without OA. Methods that measure a substance, structure or process that predicts the incidence or outcome of a disease are termed biomarkers (ESR, 2013; Strimbu & Tavel, 2010; WHO, 2001). Biomarkers for early OA include bio-signal imaging biomarkers (high-resolution morphological diagnostic imaging techniques such as MRI and CT, arthroscopy), bio-signal biochemical biomarkers (physiological MRI), and bio-specimen biomarkers (microscopy and biochemical tests of joint tissue specimens). Between and within these biomarker techniques there is variation for the stage of early OA that can be detected and the sensitivity of the test (Palmer *et al.*, 2013; Quatman *et al.*, 2011; Cibere *et al.*, 2009). This range of early OA biomarker sensitivity has resulted in variation and some controversy about the definition of OA and the point when OA should be classified as early (Schiphof *et al.*, 2014; Hayashi *et al.*, 2012a; Luyten *et al.*, 2012; Heinegard & Saxne, 2011; Hunter *et al.*, 2011a; Quatman *et al.*, 2011; Pritzker *et al.*, 2006).

In post mortem studies of equine OA it is common to use light microscopy histology of specimens harvested from standard sampling sites as the 'gold' standard to classify cadaver joints for OA (Lacourt *et al.*, 2012; Smith *et al.*, 2012; Olive *et al.*, 2010b; Olive *et al.*, 2009; Murray *et al.*, 2007; Björnsdottir *et al.*, 2004; Laverty *et al.*, 1991). The high magnification of tissues that makes microscopy suitable as a 'gold' standard for OA has a weakness when evaluating a joint for the presence of early OA. This is because microscopy evaluates small specimens taken from a much larger joint and the locations of focal regions of early OA change in joints and are likely to vary among individuals (Pritzker *et al.*, 2006; Veje *et al.*, 2003). Thus it is possible that OA will fail to be detected because the associated lesions were not included in the collection site (Smith *et al.*, 2012; Murray *et al.*, 2006). For this reason, a method that can evaluate the entire joint organ and guide osteochondral specimen collection from regions of suspected OA changes might be beneficial, particularly for detection of early OA (Veje *et al.*, 2003).

The precise point where the joint tissue damage becomes irreversible in OA is currently unknown (Bay-Jensen *et al.*, 2010). Studies using MRI that have followed human patients with mild osteochondral lesions for up to two years have found that although the majority of these lesions worsen some do improve (Buck *et al.*, 2010; Ding *et al.*, 2010; Ding *et al.*, 2006; Wang *et al.*, 2006; Biswal *et al.*, 2002). This variation in progression from the early stages of OA has led to the theories that the presence of early OA changes reduces the healing response of the joint to the initiating causes (Ding *et al.*, 2010) so that early structural OA should be considered as a "risk factor" rather than a certainty for the development of end stage OA (Hunter & Eckstein, 2011).

1.3.2 Structural joint changes in early OA

There is controversy regarding which structures of the joint that are first affected by OA (Brandt *et al.*, 2009; Burr, 2004a; Felson & Neogi, 2004). Some authors believe that the articular cartilage is the first part of the joint to be damaged (Madry *et al.*, 2012; Heinegard & Saxne, 2011) and that the loss of the cartilage cushioning effect results in damage to the bone under the cartilage. Others propose that the bone below the articular cartilage changes first to become stiffer and this increases the stresses on the cartilage resulting in injury to the cartilage (Brandt *et al.*, 2006; Burr, 2005; Burr, 2004b). However, there are studies that have found lesions of reduced subchondral bone density in early OA (Chiba *et al.*, 2012; Lacourt *et al.*, 2012). The junction region of the articular cartilage and the bone, particularly the articular calcified cartilage, has also been suggested as a location for the initial OA

lesions (Suri & Walsh, 2012). Regardless of which tissues are first affected and in what sequence, the interrelations and biochemical communications that exist between the joint tissues mean that changes in one tissue type will commonly result in simultaneous changes to other tissue types in the joint organ (Loeser *et al.*, 2012; Scanzello & Goldring, 2012; Brandt *et al.*, 2009; Sanchez *et al.*, 2005).

A range of structural changes are described in joint tissues considered to have early OA, and during this early stage of the disease these changes occur in small focal regions of the joint (Madry *et al.*, 2012; Pritzker *et al.*, 2006; Veje *et al.*, 2003; Dieppe & Kirwan, 1994). The type and degree of changes varies according to the type of joint involved (Lane *et al.*, 2011), animal species (Aigner *et al.*, 2010) and the definition for early OA that is used (Luyten *et al.*, 2012; Madry *et al.*, 2012; Pritzker *et al.*, 2006). Hyaline cartilage lesions are described in early OA of all studied species and joints with changes ranging from focal regions of chondrocyte loss and necrosis to regions of chondrocyte proliferation (cluster formation) and hypertrophy (van der Kraan & van den Berg, 2012; Pritzker *et al.*, 2006). The hyaline cartilage may initially have an increased thickness due to oedema (Calvo *et al.*, 2004) but may also have a reduced thickness due to surface fibrillation or defects (Luyten *et al.*, 2012; Pritzker *et al.*, 2006). Subchondral bone and articular calcified cartilage lesions may include mild advancement of the subchondral bone plate into the articular calcified cartilage, simple linear splits in the calcified cartilage and mild disruption of the subchondral bone plate structure (Chiba *et al.*, 2012; McIlwraith *et al.*, 2010; Sokoloff, 1993). Whether or not osteophytes, marginal or central, are a typical feature of early OA is unclear and the status of osteophytes in OA is somewhat controversial (van der Kraan & van den Berg, 2007). In a recent study that attempted to define MRI OA it was concluded that definite osteophyte formation was a cardinal feature of OA but it was not possible to give an exact definition of a definite osteophyte (Hunter *et al.*, 2011a). Synovial membrane hyperplasia and inflammation are often present in early OA (Scanzello & Goldring, 2012; Oehler *et al.*, 2002; Myers *et al.*, 1992) with the proportion of patients with synovitis increasing as OA progresses. Ligament abnormalities have been reported in early OA and the joint instability caused by these abnormalities have been reported as initiating causes of the development of OA (McGonagle *et al.*, 2010; Quasnichka *et al.*, 2005)

1.3.3 Early distal tarsal OA in Icelandic horses

A high detail radiograph and histology study of centrodistal joint specimens from 82 young (0 - 4 years old) unridden Icelandic horses found articular cartilage lesions indicative of early OA in 33% of the joints (Björnsdottir *et al.*,

2004). These lesions included chondrocyte necrosis, chondrocyte loss, chondrocyte clusters, decreased staining of the cartilage matrix for proteoglycans, occasional hyaline cartilage fibrillation and in several cases focal disruptions of the cartilage/bone interface (seen adjacent to regions of chondrocyte necrosis). Cartilage lesions detected with microscopy were strongly associated with subchondral bone plate defects seen in radiographs. Sclerosis of the subchondral bone was detected in radiographs and this was associated with adjacent cartilage lesions within the lateral regions of the joint but not within the medial regions of the joint. Osteophytes were occasionally detected on the joint margins and were only found in specimens with cartilage abnormalities. No abnormalities were detected in synovial membranes or periarticular ligaments. Similar lesions are reported in centrodistal joints from Dutch Warmblood foals (Barneveld & van Weeren, 1999) and in young horses and foals (≤ 2 years old) from several breeds (Laverty *et al.*, 1991). The high prevalence of histological lesions in young Icelandic horses, and of radiographic findings in older Icelandic horses (Björnsdottir *et al.*, 2000b; Eksell *et al.*, 1998), strongly suggests an early onset and slow progression of OA in Icelandic horses.

1.4 Imaging of early OA in horses

Imaging in medicine is the process of making a visual representation of tissues of the body by scanning with a detector. Imaging methods can be broadly divided into clinical diagnostic imaging methods that usually have macroscopic resolution (equivalent to the detail seen by the naked eye) and do not require a tissue sample or biopsy, and the higher resolution microscopic imaging methods that do require a tissue sample or biopsy to be taken from the patient.

Imaging methods result in either planar or multiplantar images. Planar imaging method produces two-dimensional (2D) images of the entire specimen volume or body part that is examined and these techniques suffer from superimposition and summation of anatomical structures in the image. This can both hide structures and create summation artefacts. Multiplantar methods allow examination of entire regions from multiple angles without the problems of summation of surrounding structures and when acquired at higher resolutions these images can produce 3D images of the tissue volume examined.

The ability to separate and accurately depict two objects or structures in an image is called the image spatial resolution. Spatial resolution is controlled by multiple equipment and patient/specimen factors and varies between imaging techniques. The majority of imaging techniques are now digital and in these

techniques the image pixel (2D imaging) or voxel (3D imaging) sizes are a limiting factor for the image spatial resolution. Additionally the amount of signal (information in the image that is due to actual differences in the imaged object) in an image compared to the noise (variation in the image information that is not due to the patient) has a major influence on the image spatial resolution. Typical minimal sizes of objects that can be defined with the clinical imaging techniques used in this thesis are; digital radiography 0.17 mm, MRI 1 mm and CT 0.3 mm (Bushberg *et al.*, 2012). Microscopy techniques usually allow sub-micron resolution.

1.4.1 Clinical diagnostic imaging

Radiography

Radiography (Fig. 5A) is a widely available and relatively cheap imaging method and it is currently the most commonly used diagnostic imaging method in equine practice for diagnosing and screening horses for joint disease (Gaschen & Burba, 2012; Hinz & Fischer, 2011) but the technique has limitations (O'Brien *et al.*, 2011). Radiographs of joints only show the morphology of the mineralised tissues in detail, since soft tissues appear as a homogeneous single opacity. Thus in a radiograph, non-mineralised tissue structures involved in OA such as the hyaline articular cartilage, the joint capsule and ligaments cannot be clearly defined from one another (Loeuille *et al.*, 1998). Furthermore, it is a planar imaging method and thus produces a 2D image of the complex 3D joint structure. For this reason radiographs are most sensitive for detecting abnormalities in peripheral joint regions when the change is located on or close to the edge of the joint image, in other words when the area of interest is tangential to the x-ray beam (O'Brien *et al.*, 2011). Thus multiple angles of projections are routinely taken of horse joints, and when the projections are taken at 45 degree intervals it is possible to more or less assess the margins around the entire joint. Small changes in the angle of the horses' leg and the x-ray beam can result in large changes in the appearance of the radiograph and so it is common that several attempts may be required to get the desired angle of projection.

A radiograph is made by passing x-rays through a selected region of the body in a collimated beam to form a grey scale image that is a type of relief map, where the relief values indicate the attenuation of the x-rays by the tissues in the region examined. Tissues with the highest density, atomic number and electrons per gram, such as bone, result in the highest attenuation of the x-rays and these tissues appear whitest in the radiograph. The radiographic image is

captured on a flat x-ray detector, either an electronic detector system (computed radiography or digital radiography) or silver emulsion film. X-rays for exposure of a radiograph are produced by heating a metal filament (usually tungsten) in a vacuum to produce free electrons which are then attracted to a metal anode (usually tungsten or copper) using a high voltage. When the beam of electrons hit the anode they interact with the metal atoms to produce x-rays by either Bremsstrahlung (bending and slowing of the trajectory of the incident electron by the metal atom) or characteristic interactions (the incident electron knocks an orbital electron out of a metal atom). The x-rays produced form the 'primary beam' that is directed by the angle of the metal anode surface and restricted by a lead collimator so that it passes to the body tissue intended for examination. The x-rays that pass through the body tissue are then detected and a radiographic image formed.

Radiography is still frequently used as the 'gold' standard technique to detect OA in human medicine and research (Kellgren & Lawrence, 1957) but the recognised limitations of radiography (Jones *et al.*, 2004) and the expanding availability and rapid technical improvements mean that increasingly the multiplanar imaging techniques of MRI and CT are replacing radiography in human OA research (Guermazi *et al.*, 2013a; Guermazi *et al.*, 2013b).

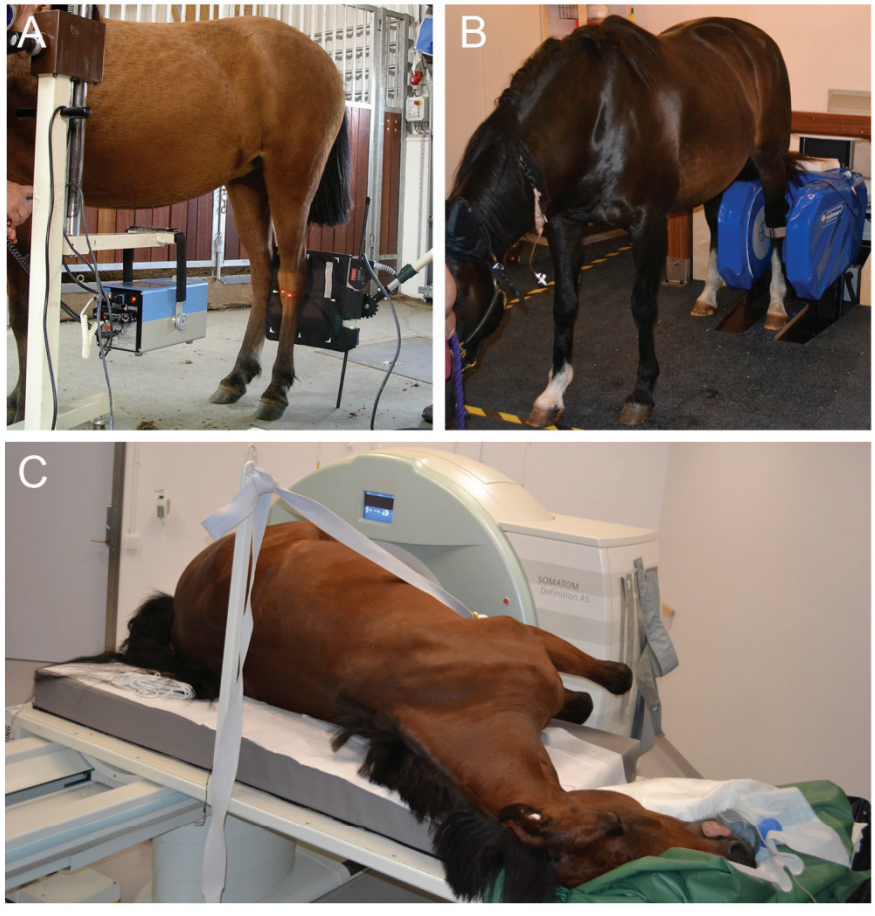

Figure 5. Examples of clinical diagnostic imaging methods for examination of the distal tarsal region. (A) Radiography of a sedated horse. (B) Low-field magnetic resonance imaging of a sedated horse. (C) Computed tomography of an anesthetised horse.

Magnetic resonance imaging (MRI)

During the last decade MRI has developed as the diagnostic imaging method that carries the greatest promise for the detection and monitoring of progression of early OA in research settings (Hunter & Guermazi, 2012; Roemer *et al.*, 2011), although recently the sensitivity of MRI for human OA detection in a clinical setting has been questioned (Menashe *et al.*, 2012). A major advantage of MRI compared to the imaging methods that use x-rays is that it produces high quality images of soft tissue structures such as ligaments, tendons, synovial tissues and hyaline articular cartilage and it is very sensitive to changes in water content of all tissues in the body (Loeuille & Chary-Valckenaere, 2012). Compared to radiography, MRI detects pathological

changes of human OA at a much earlier stage of the disease (Palmer *et al.*, 2013; Guermazi *et al.*, 2012; Jones *et al.*, 2004; Raynauld *et al.*, 2004; Wluka *et al.*, 2002). High-field MRI has been shown to be superior to radiography for detecting structural joint changes (Wirth *et al.*, 2013; D'Anjou *et al.*, 2008; Ding *et al.*, 2007; Amin *et al.*, 2005). It has recently been suggested that high-field MRI should replace radiography for OA assessment in research (Guermazi *et al.*, 2011) and several semi-quantative grading systems for MRI detected osteochondral changes associated with human OA have been developed (Guermazi *et al.*, 2013b). However, a universally accepted and validated MRI definition for OA still does not exist although several recent studies have investigated this issue and have provided a framework for a definition (Schiphof *et al.*, 2014; Hayashi *et al.*, 2012a; Hunter *et al.*, 2011a).

Magnetic resonance imaging forms multiplantar images from radiowaves that are produced by a body region as a result of placing the body region within a strong magnetic field and exposing it to pulses of radiowaves. Most of the MRI image information comes from protons and most of the protons are located within the water that is found within tissues and the fluid filled tissue spaces. A radiofrequency (RF) coil both produces the pulses of radiowaves that are sent into the body region and receives and records the radiowaves subsequently produced by the body region. The strong magnetic field aligns the magnetic moments of the protons in the body region. This is used to coordinate the position of the magnetic moments for the initial pulse of radiowaves (which 'flips' these magnetic moments) and causes the subsequent realignment (relaxation) of the magnetic moments of the protons. Different types of MRI images (called sequences) that show different amounts of signal (called intensity) from specific tissue and fluid types are possible. These sequences are weighted to show features of the protons in a variety of ways, including showing the density of protons in a tissue or the binding of the protons in the tissue structure or fluid. The intensities of the tissue or fluid depend on the timing and type of the pulses of radiowaves emitted by the RF coil and the timing of the receiving period of the RF coil. Clinical MRI machines have preinstalled sequences that result in predicable intensity of specific tissue types and some modification of the sequence settings is usually possible. Sequence types and names vary between manufacturers although commonly used sequences are found as standard in all modern clinical MRI machines. Sequences can be further divided according to whether scans are performed by sequentially acquiring information as narrow tissue slices (2D sequence) or if information is acquired from the entire tissue volume simultaneously (3D sequence). Sequences vary from those that produce images that show the morphology of a wide range of tissue types (e.g. proton density)

to those that show only intensity from a limited range of tissues and low or no signal from other selected tissues (e.g. Water Saturation fluid sequence (WATSf)).

Human OA research that utilises MRI is currently done almost exclusively with high-field (≥ 1 Tesla) MRI, but in equine OA research both high- and low-field (≤ 0.3 Tesla) MRI are utilised (Smith *et al.*, 2012; Werpy *et al.*, 2011; Olive, 2010; Olive *et al.*, 2010b; Murray *et al.*, 2009b). Magnetic fields result in predicable effects on the spin behaviour of the protons (called precession) in body tissue with the frequency of precession of tissue protons increasing as the magnetic field increases according to the Larmor equation. Additionally stronger magnetic fields result in higher amplitude of the radiowaves produced by a body tissue. Thus high-field MRI produces images with high signal per unit of acquisition time compared to low-field MRI and this allows imaging at higher resolution whist maintaining reasonable scan times.

A dedicated equine low-field MRI system (Fig. 5B) designed for the limbs of standing horses is available (Mair *et al.*, 2005). A standing low-field MRI system offers advantages for screening programmes particularly if frequent follow up examinations are planned, since the examinations can be performed with the horse sedated rather than under general anaesthesia, which is required for other MRI systems. However, lower signal and motion of the horses' leg during the scan have been shown to decrease the accuracy of low-field MRI compared to high-field MRI systems for the detection of mild osteochondral changes (Werpy *et al.*, 2011).

Computed tomography (CT)

Computed tomography is a multiplanar imaging technique and multidetector CT is able to produce volumetric image information. Thus, this technique does not suffer from the problems of summation, superimposition and angle of projection (Dalrymple *et al.*, 2005). The high sensitivity of CT to mineralisation changes in bone means it should be possible to detect early skeletal changes of OA (Bousson *et al.*, 2012; Chiba *et al.*, 2011). However, compared to MRI, CT has a lower sensitivity to non-mineralised tissue changes and since early OA lesions may occur in soft tissues there is doubt regarding how useful CT is for detecting early OA in humans (Palmer *et al.*, 2013). Compared to other clinical diagnostic imaging techniques there are relatively few publications that investigate the use of CT for OA in horses and humans (Turmezei *et al.*, 2014; Bousson *et al.*, 2012; Chiba *et al.*, 2011; Olive *et al.*, 2010a). Currently almost all CT examinations of the equine limbs are performed with the horse under general anaesthesia lying on a specially

designed table (Fig. 5C), although standing CT of the hoof has been described (Desbrosse *et al.*, 2008).

The basic component of a CT gantry is a large ring which has an x-ray tube (with the same components as an x-ray tube used for radiography) on one side of the ring and an electronic detector (single slice) or rows of electronic detectors (multislice) on the opposite side. A fan shaped x-ray beam is turned on while the gantry is rotated about the body part at the same time as the body part is moving at a constant speed on the CT table through the centre of the ring. The detectors determine the attenuation (a measure of x-ray absorption) of the x-ray beam by the body part, measuring this information multiple times during each gantry rotation and the computer records the radial position of each beam that contributes to each measurement. Using a mathematical technique called backprojection, the recorded geometry and attenuation values are converted into multiple radial lines of shades of grey corresponding to attenuation values within a slice and these are added to form a cross-sectional image.

1.4.2 Microscopic imaging

Light microscopy histology

Light microscopy is the traditional method for examining microscopic changes in biological tissues. The technique involves transilluminating a thin slice of paraffin embedded material on a glass slide with a focused beam of visible light and viewing the magnified light transmitted through the glass slide. Osteochondral joint specimens for light microscopy are prepared by sectioning joints with a bandsaw or diamond saw to give slabs or blocks of joint tissues. The small joint specimens are first preserved in formalin and then decalcified in chemicals such as sodium formiate and formic acid after which specimens can be further sectioned. Following decalcification the specimens are dehydrated and then embedded in paraffin to form paraffin blocks that are typically sectioned into 3-6 μm thick slices with a microtome. Slices are placed on glass slides, stained, coverslipped, and the prepared sections are viewed using light microscopy at magnifications that are usually between 40x and 1000x. There are many stains used for the examination of osteochondral tissues (Schmitz *et al.*, 2010). The two component stain hematoxylin and eosin is most commonly used for examining cell and tissue morphology (Fig. 2A). Hematoxylin is an alkaline dye that stains acidic structures (such as nucleic acid) a purplish-blue colour, and eosin is an acidic dye that stains alkaline structures (such as the cytoplasm) a red-pink colour. Stains that can be used to evaluate proteoglycan content include Toluidine blue and Safranin-O (Schmitz

et al., 2010). These stains are alkaline (cationic) dyes that stain acidic (anionic) structures such as proteoglycans. Stains for collagen fibres include picrosirus red and the Goldner's trichrome staining method (Schmitz *et al.*, 2010).

Several studies have investigated the microscopic appearance of the joints in the distal tarsal region of horses using conventional light microscopy. These studies include descriptions of lesion free tarsometatarsal joints (Murray *et al.*, 2009a), descriptions of osteochondral lesions in the joints of the distal tarsal region of young horses and foals (Björnsdottir *et al.*, 2004; Barneveld & van Weeren, 1999; Laverty *et al.*, 1991; Watrous *et al.*, 1991) and descriptions of osteochondral lesions in the centrodistal and tarsometatarsal joints of adult horses (Tranquille *et al.*, 2011).

Backscattered electron scanning electron microscopy (BSE SEM)

This technique uses a beam of electrons in a vacuum environment to examine the surface regions of block embedded specimens and study the 3D features of the surfaces of mineralised tissues. The electrons required for BSE SEM are produced by a thin V-shaped tungsten wire cathode filament that is operating within a vacuum, in the same way electrons are produced in an x-ray tube. The electrons are formed into a beam by a negatively charged caplike structure that covers the filament and repels the electrons so they are forced to exit through a narrow aperture forming a beam of electrons. The electron beam is further accelerated by a hollow cylinder shaped anode. The high velocity of the electrons, when they reach the anode, means that many electrons pass through the hollow anode and form a divergent beam. This beam is focused on the surface of the specimen by a second aperture and a series of electromagnetic lenses in a column. The specimen is scanned by incrementally moving the beam. When the electrons enter the specimen they can either pass through the specimen, or interact with the electrons in the specimen and cause secondary electrons or they can collide with the atom nucleus and bounce back out of the specimen to become backscattered electrons. Higher atomic number materials cause more backscatter of the electron beam. The backscattered electrons are detected by a positively charged circular detector plate located in the sample chamber between the last focussing lens and the specimen, which has a central hole for passage of the scan electron beam. The amount of backscatter detected is combined with the location of the electron beam in the specimen to form an image of the of the mean atomic number of the components of the specimen (Stokes, 2009). The surface topography of a specimen results in variations of the backscattered electron signal and this allows images that show this surface topography in great detail (Vajda *et al.*, 1999; Howell & Boyde, 1994). Rather than the diameter of the scan electron beam it is the volume from which

backscattered electrons are able to escape from the surface of the specimen that determines the resolution limit of BSE SEM (Howell & Boyde, 2003). This volume depends on the composition of the specimen itself. In practice, with a 20 kV accelerating voltage, structures down to 0.2 μm can be resolved.

Block embedded specimens are produced by setting the specimen in plastic such as polymethyl methacrylate (PMMA), then grinding and polishing the block surface back to the level of the specimen using silicon carbide papers and diamond abrasives to produce a smooth and flat specimen surface for examination (Boyde, 2012a). Using this method there is no decalcification of the specimen and block surfaces of several centimetres in area can be examined.

Recently it has been shown that the BSE coefficient of soft tissues can be enhanced in already embedded tissues by 'staining' with elemental iodine using triiodide solutions (iodine dissolved in potassium or ammonium iodide) or by sublimation of pure elemental iodine (Boyde, 2012b). This raises the BSE signal level from soft tissues to values that can easily be seen alongside the naturally high scattering from mineralised tissues, thus allowing evaluation of both mineralised and non-mineralised tissues (Fig. 2B).

For examination of the 3D features of the surfaces of mineralised tissues a maceration method using an alkaline pronase enzyme detergent or hydrogen peroxide solution can be used to remove the soft tissues from specimens leaving all mineralised tissue intact (Boyde, 2012a).

Studies of equine joints with BSE SEM have focused on the high-motion metacarpo/metatarsophalangeal joints in Thoroughbred racehorses and the effects of exercise on the osteochondral tissues (Boyde *et al.*, 2011; Boyde & Firth, 2008; Doube *et al.*, 2007; Boyde & Firth, 2005; Boyde & Firth, 2004).

Confocal scanning light microscopy (CSLM)

A major advantage of CSLM over other forms of epi-illumination microscopy techniques is its ability to examine regions on and immediately below the surface of thick specimens such as PMMA embedded specimens. The combination of CSLM (Fig. 2C) with BSE SEM imaging of the same unstained bone block surfaces has been used produce high detail images which contain both mineralised tissue and soft tissue information (Boyde *et al.*, 2005). This method has been used to evaluate lesions in the equine fetlock (Boyde *et al.*, 2011) and to study articular calcified cartilage canals in the third metacarpal bone (Boyde & Firth, 2004).

The aim of confocal techniques is to illuminate a very small volume of the specimen at any one instant, and image only the reflected or fluorescent light emanating from that same volume. Light of specific wavelength in the form of

a laser causes autofluorescence of specific biological tissues (Monici, 2005; Aubin, 1979). A laser with wavelength 488 nm results in autofluorescence of collagen and chondrocytes that is strong in the green (498-578 nm) and red (>600 nm) spectral regions. A key feature of CSLM is the pinhole aperture in the microscope which removes light arising from regions that are deeper and shallower than the selected focus plane and this allows high resolution 2D image acquisition at a specific depth from the specimen surface (Inoué, 1995). By changing the mechanical focus images can be made at a series of equally spaced depths, typically at 2-10 μm below the specimen surface, creating a series of extremely thin high-resolution image slices. Stacks of image slices from up to 50-100 μm below the specimen surface can be combined to give 3D images of the surface region of a thick specimen.

Micro-CT

Micro-CT is a specialised CT technique that results in very high resolution images. The micro-CT equipment can only accommodate small objects such as osteochondral biopsies and in some cases small laboratory animals. The technique for producing and acquiring the images is the same as clinical CT, the difference being the much smaller size of the CT equipment (which allows the higher resolution) and longer scan times. Micro-CT produces 3D images with voxels sizes generally around 10 μm (De Clerck & Postnov, 2007).

1.5 Validation of clinical diagnostic imaging methods for OA detection

Validation is the process of proving the accuracy of a biomarker or test by comparing it to a 'gold' standard (ESR, 2013). 'Gold' standards are often invasive microscopic methods that require tissue specimens since they usually require a detailed analysis of the tissues in question. Thus validation studies for early OA often require cadaver material (ESR, 2013). Validation of the lesions detected or tissue measurements made in diagnostic images require techniques that provide spatial alignment of the clinical diagnostic image and the 'gold' standard image, so that the lesion detected or the tissue type measured in the clinical diagnostic image can be compared to the true tissue morphology. Several animal cadaver and human arthrectomy OA studies have compared MRI and CT images of normal and abnormal joints with light microscopy histology using spatial alignment techniques. In most cases these techniques align the images of the joint to the location of a standard predetermined joint tissue specimens using varying degrees of anatomical localisation (Olive *et al.*, 2010b; Olive *et al.*, 2009; Murray *et al.*, 2005; Calvo *et al.*, 2004; Dawson *et*

al., 1999; McGibbon *et al.*, 1998; Gahunia *et al.*, 1995; Modl *et al.*, 1991). In one study lesions were identified in the image and the site of the sampling was determined by visual inspection of the joint surface and anatomical localisation (Trattnig *et al.*, 1998), and there are more complex methods that involve Ethi®-pin markers (Bittersohl *et al.*, 2009) or use of custom made containers (McGibbon *et al.*, 2003; McGibbon & Trahan, 2003).

Joint tissue sampling followed by light microscopy histology is the most widely used 'gold' standard for validating diagnostic imaging studies in equine OA research (Smith *et al.*, 2012; Olive *et al.*, 2010b; Olive *et al.*, 2009; Murray *et al.*, 2007; Murray *et al.*, 2006; Björnsdottir *et al.*, 2004; Laverty *et al.*, 1991). Light microscopy histology is a widely available, relatively cheap, well proven method and general OA grading methods (Pritzker *et al.*, 2006; Mankin *et al.*, 1971) and methods for specific equine joints (McIlwraith *et al.*, 2010) are well described. Despite this, there is still variation in how light microscopy grading criteria are applied in studies (Aigner, 2012; Kerkhof *et al.*, 2011; Quatman *et al.*, 2011). Furthermore, the paraffin embedding method used for light microscopy is not optimal for the evaluation of mineralised tissues due to the decalcification required for microtome cutting of the specimens. Microscopic methods which do not require specimen decalcification such as BSE SEM and CSLM have been used to evaluate OA changes in equine joints (Boyde *et al.*, 2011; Boyde & Firth, 2008) but these microscopic methods have not been used to validate clinical diagnostic imaging methods.

Arthroscopic evaluation of joint surfaces is also considered suitable as a 'gold' standard for validation of OA detection with clinical diagnostic imaging and although it requires an invasive procedure no tissue samples are required (Kijowski *et al.*, 2009; Wong *et al.*, 2009; Yoshioka *et al.*, 2004). In studies of cadaver material visual inspection of the joint surfaces including staining of the articular surface with Indian ink may be used as a 'gold' standard (Schmitz *et al.*, 2010). A weakness of arthroscopy and visual inspection of the joint surfaces is that they are only able to assess the articular surface of the joint cartilage and not the tissues deep to the articular surface, since OA changes may occur within the osteochondral tissues without resulting in changes to the articular surface (Lacourt *et al.*, 2012). Furthermore, the short, strong extra- and intra-articular ligaments, the low volume joint spaces, and the surrounding firm, fibrous joint capsule of the joints in the distal tarsal region mean that arthrotomy of this joint is only possible after extensive dissection of the peri-articular soft tissues. This dissection results in loss of the positional relationship of apposing articular surfaces and peri-articular tissues, and damage to tissues that may be important in the assessment for OA lesions.

1.6 Radiographic and clinical distal tarsal OA in horses

1.6.1 The general horse population

Distal tarsal OA is a common chronic hindlimb joint disorder of horses (Moyer, 1978). Joint problems are reported to be the most common cause of death or euthanasia in the general Swedish horse population (Egenvall *et al.*, 2006). Furthermore a study of Swedish insurance data found distal tarsal OA accounts for approximately 9% of all cases of equine lameness that result in loss of use (Bergsten, 1983). There is an extremely large variation in reported prevalence of equine distal tarsal OA as diagnosed by radiography. A study based on prepurchase radiographs found distal tarsal OA changes in 39% of the 160 horses of various breed (van Hoogmoed *et al.*, 2003). Another study, also based on prepurchase radiographs, found distal tarsal OA in 92% of 3566 sport horses (Winter *et al.*, 1996). A radiographic study of 590 randomly chosen 3- and 4- year-old Dutch Warmblood mares found a 3.1% incidence of distal tarsal OA (van der Veen *et al.*, 1994). These large variations in prevalence are likely a result of varying interpretation of the criteria for radiographic distal tarsal OA and a quantitative rating scale for distal tarsal OA has been developed in response to this (Labens *et al.*, 2007a).

Radiographic changes that are commonly described in joints in the distal tarsal regions with OA are periarticular osteophytes, enthesophytes, areas of articular cartilage loss causing apparent narrowing of the joint space, irregular widening of the joint space, increased (sclerosis) and decreased (lysis) subchondral bone mineral density, cyst-like changes in the subchondral bone and in advanced cases partial or complete ankylosis of the joint (Pool, 1996; Shelley & Dyson, 1984). For many years it was considered that the radiographic changes of distal tarsal OA most commonly occurred on the dorsomedial margin (Verschooten & Schramme, 1994) of the distal tarsal joints. However, subsequent studies have shown that distal tarsal OA lesions occur on multiple aspects of the joint and that taking less than the 4 standard angles of projection reduces the sensitivity of radiography for detecting distal tarsal OA (Labens *et al.*, 2007b; Eksell *et al.*, 1999).

1.6.2 Icelandic horses

Distal tarsal OA has a high prevalence in Icelandic horses (Björnsdottir *et al.*, 2000b; Axelsson *et al.*, 1998). Studies in Sweden of Icelandic horses 0-19 years of age show a prevalence of 23% for radiographic changes of distal tarsal OA and radiographic changes were only detected in horses older than 4 years of age (Axelsson *et al.*, 1998; Eksell *et al.*, 1998). A study in Iceland of Icelandic horses 6-12 years of age shows a prevalence of 30.3% for

radiographic signs of distal tarsal OA (Björnsdottir *et al.*, 2000b). A survey follow up of the Icelandic prevalence study group (Björnsdottir *et al.*, 2000b) obtained five years later found that distal tarsal OA was the most common cause for loss of use (culling) due to disease in 7 to 17 year old Icelandic horses used for riding in Iceland (Björnsdottir *et al.*, 2003). It is more common for radiographic changes of distal tarsal OA to be detected in both hind legs rather than unilaterally (Björnsdottir *et al.*, 2000b).

Risk factors known to be associated to the detection of distal tarsal OA in adult Icelandic horses include: sire (Arnason & Björnsdóttir, 2003; Björnsdottir *et al.*, 2000a), increasing age (Björnsdottir *et al.*, 2000b; Eksell *et al.*, 1998), and 'sickle hock' conformation of the tarsal joint (Eksell *et al.*, 1998). In contrast, the use of the horses for riding and workload is not a risk factor (Björnsdottir *et al.*, 2000b). As a result of these studies a screening program for distal tarsal OA using tarsal radiography of stallions 5 years of age or older has been established for Icelandic horses and the results of these radiographs are made public (Finn, 2006). The International Federation of Icelandic Horse Associations strongly encourages Icelandic horse breeders not to use stallions with radiographic changes of distal tarsal OA.

2 Aims of thesis

The general aims of this thesis were to investigate the early stage of distal tarsal OA in young Icelandic horses using complementary imaging techniques, both to guide sampling for microscopic studies of the joints, to describe osteochondral lesions and to evaluate the potential of clinical diagnostic imaging methods to detect early changes of distal tarsal OA. Microscopy was used to verify and validate diagnostic imaging abnormalities. The combined microscopy and diagnostic imaging information was used to propose pathogenesis theories for equine distal tarsal OA.

The specific aims were:

- Investigate whether a diagnostic imaging guided method for sampling cadaver equine centrodistal joints results in improved accuracy for early OA detection (paper I).
- Correlate osteochondral abnormalities detected with CT and high-field MRI with OA detected by microscopy in young Icelandic horses (paper I)
- Describe in detail the osteochondral lesion morphology in the early stages of distal tarsal OA in young Icelandic horses (paper II).
- Evaluate radiography and low-field MRI, for detecting early OA lesions in the centrodistal joints of young Icelandic horses (paper III).

3 Hypotheses

The following hypotheses were raised for the distal tarsal joints:

- Compared to predetermined site sampling a diagnostic imaging guided sampling method would result in a higher rate of detection of histological OA changes (paper I).
- Specific osteochondral lesions detected with CT and high-field MRI would be associated with the presence of histological OA (paper I).
- Morphological changes of early OA would occur primarily in the tissue surrounding the mineralisation front and involve both the hyaline articular cartilage and articular calcified cartilage (paper II).
- Low-field MRI of cadaver specimens using clinical sequences would be superior for detecting early OA lesions (defined by microscopy) compared to radiography of standing horses (paper III).

4 Materials and methods

This section summarises the material and methods used in the studies performed for this thesis. Detailed descriptions of the procedures are presented in each of the papers.

4.1 Horses (papers I-III)

The Icelandic horses that were used for the studies were bred from parent horses selected according the presence or lack of radiographic changes of distal tarsal OA. Calculations based on Björnsdottir *et al.* (2004) suggested that a random sample of 40 horses were likely to provide 28 centrodistal joints with early OA changes. The goal of parent selection was to breed a study group that provided joints showing the full spectrum of morphologies from normal to early OA. An effort was made to breed study horses from parents that had either radiographic OA in the distal tarsal region in both hindlegs or had no evidence of radiographic OA in the distal tarsal region. The parent horses consisted of 28 mares and nine stallions. A summary of the OA status and ages of the parent horses is given in table 1. Stallions sired between one and seven study horses (median = 5). A summary of the radiographic changes detected in the joints of the distal tarsal region of the parent horses is given in table 2. Two of the study horses were lost, one was aborted and another died as a result of an accident when it was 1 year old. Thus the study group consisted of 38 Icelandic horses (23 males and 15 females) and centrodistal joints of both hind legs were examined (n = 76). Ethical approval from the Iceland National Animal Research Committee was obtained before the studies commenced.

Horses were bred in two groups. Group-07 horses (n = 24) were born in spring 2007 and group-09 horses (n = 14) were born in spring 2009. Both groups lived on the same farm in the north of Iceland. Horses within each group lived together from birth and were exposed to the same environmental

and husbandry conditions. Horses were fed together ad libitum with hay and mineral supplement, and dewormed regularly. The horses were not trained or exercised. No musculoskeletal abnormalities in the tarsal regions or obvious lameness's were detected in the horses prior to the imaging examinations although complete lameness and orthopaedic examinations were not possible in these young untrained horses.

Table 1. *Summary of the number and ages of the parent horses used to breed the horses used in the studies in this thesis according to osteoarthritis status and gender,*

	Number of parent horses	Age range (yrs)	Age median (yrs)
OA negative mares	14	5-18	12
OA positive mares	24	4-18	11.5
OA negative stallions	3	5-17	15
OA positive stallions	6	4-8	6

OA = osteoarthritis; yrs = years old.

Table 2. *Summary of the joints in the distal tarsal region of parent horses that had radiographic osteoarthritis. Values shown indicate the number of legs,*

	Mares OA positive in both hindlegs	Mares OA positive in only one hindleg	Stallions OA positive in both hindlegs	Stallions OA positive in only one hindleg
Both hindlegs TCCQJ only	0	-	0	-
Both hindlegs, CDJ only	8	-	2	-
Both hindlegs, TMTJ only	0	-	0	-
Both hindlegs, CDJ and TMTJ	14	-	4	-
One hindleg, TCCQJ only	0	0	0	0
One hindleg, CDJ only	10	0	2	1
One hindleg, TMTJ only	0	0	0	0
One hindleg, CDJ and TMTJ	9	3	2	0
One hindleg, TCCQJ, CDJ and TMTJ	1	0	0	0

OA = osteoarthritis; TCCQJ = talocalcaneal-centroquartal joint; CDJ = centrodistal joint; TMTJ = tarsometatarsal joint; - = not applicable

Radiographic evidence of distal tarsal OA was present in both hindlegs of both parents in 19 of the horses, in neither parent in nine horses, in both hindlegs of one parent and one hindleg of one parent in two horses, in both hindlegs of one parent in two horses, and in one hindleg of one parent in six horses. The radiographic classification of the parent horses was made by three experienced equine radiologists (CJL, KH, SB) using consensus with the presence of either subchondral bone sclerosis/lysis, narrow or uneven joint space, marginal osteophyte, periarticular bone bridge or ankylosis considered to indicate OA.

Study I used the right tarsal joints from group-07 horses, study II used the left tarsal joints from group-07 horses and study III used both left and right tarsal joints from group-07 and group-09 horses.

4.2 Clinical diagnostic imaging methods (papers I-III)

Radiographs were taken when the horses were 28 ± 1 months old. A portable x-ray unit (Ajex 9020H, Ajex Meditech, Seoul, Republic of Korea) and a digital radiography system (DR3 Mark IIIG RapidStudy, Sound-Eklin, Carlsbad, CA, USA) with exposure settings 80 kVp and 5 mAs, and pixel pitch 0.16 mm were used. Horses were sedated with 0.3–0.4 ml intravenous detomidine hydrochloride (Domosedan®, Orion Pharma Animal Health, Sollentuna, Sweden) and made to stand square with the metatarsal portion of the limb in a vertical position. Four standard angles of projection were acquired for each tarsal joint (lateromedial [LM], dorsoplantar [DPl], dorso-35º-lateral-plantaromedial oblique [D35L-PlMO] and plantaro-10º-distal-45º-lateral-dorsoproximomedial oblique [Pl10Di45L-DPrMO]).

The horses were slaughtered at 30 ± 1 months old at an abattoir in Iceland 35 km from the paddock where they were kept. This age for the slaughter was selected to provide materials from horses that were at the point of skeletal maturity (Strand *et al.*, 2007) and in the age range were early distal tarsal OA changes are reported (Björnsdottir *et al.*, 2004). Horses were slaughtered two at a time, once a week. Carcasses were processed at the abattoir and the meat was used for human consumption. The tarsal joints were removed during the processing of the carcasses by sawing through the leg at the level of the distal third of the tibia and disarticulating the metatarsophalangeal joint. The tarsal joints were labelled, sealed in plastic bags and transported in foam refrigeration boxes in refrigerated conditions by truck, car and plane to Uppsala in Sweden. Time from slaughter to when the joints arrived in Uppsala was 24-50 hours.

In Uppsala the tarsal joints were examined with 1.5 Tesla MRI (Intera, Philips Medical Systems, Best, The Netherlands), 0.27 Tesla MRI (Hallmarq

EQ2 Scanner, Hallmarq Veterinary Imaging Ltd, Guildford, Surrey, UK) and 64-slice CT (Definition, Siemens Medical Systems, Erlangen, Germany). Images were acquired using sequences and exposure values to maximise the resolution of the mineralised and soft tissues of the distal tarsal joints including; articular cartilage, subchondral bone, articular margins and intra-articular ligaments, and when possible images were acquired to allow 3D post-acquisition (Tables 3 and 4). The temperatures of soft tissues caudal to the distal tibia were monitored immediately before low-field MRI examinations with a digital meat thermometer (Meat thermometer, ART 65 RF, Coop Norden AB, Stockholm, Sweden) and found to range between 6.7 ºC and 20.7 ºC.

For 1.5 Tesla MRI and CT examinations each disarticulated tarsal joint was held in position by foam pads in a lying position so the dorsal surface was facing the table top. For 0.27 Tesla MRI the tarsal joints were held in place using foam pads in an upright position with the long axis of the leg perpendicular to the static magnetic field. The joints were not loaded during the examinations. The isocentre of the magnetic field and the mid level of the radiofrequency coil were centred at the level of the centrodistal joint. The short tau inversion recovery (STIR) sequences used had a relatively short inversion time following recommendations for tissue scanning at temperatures between refrigeration and room temperature (Adrian *et al.*, 2012). Images were transferred to a diagnostic imaging work station with DICOM viewing software (OsiriX v 4.1.2, Pixmeo, Geneva, Switzerland) for evaluation.

Within 16 hours after completion of the MRI and CT studies the unopened distal tarsal joints were manually sectioned with a bandsaw (KT-400, Klaukkala, Finland) using parallel saw cuts to make five to ten millimetre thick frontal plane slabs. The positioning and angulation of the saw cut was done according to a described method (Björnsdottir *et al.*, 2004). All tarsal slabs except the second from dorsal slab in group-07 tarsal joints were immersed and fixed in 10% neutral buffered formalin. The second from dorsal slabs in group-07 tarsal joints were or placed in plastic bags and frozen (-20 ºC). The time between slaughter and tarsal slab fixation/freezing ranged from 45 to 69 hours. After fixation in formalin specimens for embedding in PMMA (Paper II) were transferred into 70% ethanol five to seven days before subsampling.

Table 3. *Settings used during magnetic resonance imaging sequences of cadaver distal tarsal joints (papers I and III),*

	1.5 Tesla sequences			0.27 Tesla sequences			
	WATSf	STIR	T1W 3D FFE	T2*W-GRE	T2W-FSE	STIR-FSE	T1W-GRE
Scan plane	Sagittal	Sagittal	Sagittal	Sagittal	Sagittal	Sagittal	Sagittal and dorsal
Echo time (ms)	10.1	60	5.3	13	87	27	8
Inversion time (ms)	—	140	—	—	—	60	—
Repetition time (ms)	21.7	3422	25	140	1969	2700	100
Flip angle (^{o})	50	90	35	32	90	90	75
No. of signal acquisitions	4	3	2	6	4	2	6
Bandwidth (Hz)	145	212	145	33	49	98	65
Slice thickness and gap (mm)	0.7 and -0.35*	3 and 3.3	1 and -0.5*	3.5 and 4.2	3.5 and 4.2	5 and 6	3.5 and 4.2
Field of view (mm)	80	100	100	170	170	170	170
Phase encoding steps	272	125	147	192	195	165	192
Frequency encoding steps	272	160	192	384	384	336	384
In-plane pixel resolution (mm)	0.3 x 0.3	0.8 x 0.6	0.7 x 0.5	0.9 x 0.4	0.9 x 0.4	1 x 0.5	0.9 x 0.4
Reconstruction matrix (pixels)	512 x 512	288 x 288	384 x 384	512 x 512	512 x 512	256 x 256	512 x 512
Approximate scan time (min)	54	4	11	8.1	5.2	3.1	5.8

— = Not applicable; WATSf = water saturated fluid; STIR = short tau inversion recovery; W = weighted; 3D = three dimensional; FFE = fast field echo; GRE = gradient echo; FSE = fast spin echo. *Slice gaps -0.35 and -0.5 refer to contiguous slices with a 0.35 mm and 0.5 mm overlap respectively.

Table 4. *Settings used during computed tomography examinations of cadaver distal tarsal joints (paper I),*

Parameter	Whole tarsus	Bone slab
Position in gantry	Head-foot-prone	Head-foot-prone
Tube voltage (kVp)	120	120
Tube current (mA)	400	100
Exposure time (s)	0.5	1
Focal spot (mm)	1.2	0.7
Spiral pitch factor	0.8	0.5
Convolution kernel	B70f	U70u
Slice thickness (mm)	0.6	0.4
Slice increment (mm)	0.4	0.2
Single collimation width (mm)	0.6	0.3
Acquisition plane reconstruction diameter (mm)	124	50-80
Acquisition plane reconstruction matrix (pixels)	512 x 512	512 x 512

4.3 Osteochondral sampling methods (papers I-III)

4.3.1 Predetermined sampling (paper I)

One slab, containing the full joint width, was removed from each joint at the location described by Björnsdóttir *et al.* (2004). The pathologist (SE) who removed the specimens had no knowledge of the originating horse's parentage, and no attempt was made to identify gross lesions. The centrodistal joint of the selected bone slab was removed by transversely dividing the central, third, and fourth tarsal bones. The joint was then divided into lateral and medial halves by sawing sagittally through the centrodistal fossa. This resulted in two 8 mm to 30 mm blocks representing lateral and medial aspects of the centrodistal joint.

4.3.2 Image-guided sampling of centrodistal joints (papers I-III)

The MRI and CT images from the tarsal joints were analysed using a semi-quantitative grading system (Table 5) modified from similar grading systems used in human and veterinary OA research (Olive *et al.*, 2010a; Hunter *et al.*, 2008; Kornaat *et al.*, 2005; Peterfy *et al.*, 2004). Lesions were graded on three

point scales as follows: grade-0, unremarkable appearance; grade-1, abnormal with a small or mild change; and grade-2, moderate to severe or large change. Anatomic sites for osteochondral specimen collection were selected from the anatomic region of the centrodistal joint with the highest grade total. When grades were equal, selection priority was given to the region with the highest-grade lesions on the articular aspect of the joint, over lesions on the articular margin. The image-guided specimen collection sites were selected semiquantitatively by taking into account the lesion grades, groupings, and type. The aim was to identify specimen collection sites that were < 5 mm in diameter and contained the highest degree of pathologic change according to the MRI and CT images.

Table 5. *Grading system used to characterize the type and severity of suspected osteoarthritis lesions in centrodistal joints from equine cadavers as identified with computed tomography and 1.5 Tesla magnetic resonance imaging,*

Lesion	Modality	Grade-1	Grade-2
Articular cartilage hypointensity	MRI	—	Focal hypointense signal within the articular cartilage
Articular cartilage thickness and joint space (Figs. 7 - 9)	MRI	WATSf: hyperintense and ≥ 1 mm thick	WATSf: hyperintense layer not visible; or STIR: focal collection of hyperintense signal between articular surfaces
Central osteophyte (Figs. 7 and 9)	MRI	—	Hypointense projections from the mineralisation front
Subchondral bone hyperintensity	MRI	< 1 mm hyperintense area/s	≥ 1 mm diameter hyperintense area/s
Articular mineralisation front defect (Figs. 7- 9)	CT	≤ 0.5 mm depth	> 0.5 mm depth
Marginal osteophyte (Fig. 9)	CT	Small	Large
Intra-articular and chondral mineralisation (Fig. 10)	CT	—	Mineral density material between the mineralisation fronts
Subchondral cyst-like lesion	CT	< 1 mm	≥ 1 mm
Subchondral sclerosis	CT	Focal sclerosis	Generalized sclerosis
Subchondral lysis	CT	Focal lysis	Generalized lysis

— = Not applicable; MRI = magnetic resonance imaging; CT = computed tomography; WATSf = water saturated fluid; STIR = short tau inversion recovery.

Coregistration of the CT and MRI images via a manual rigid registration algorithm (OsiriX v 4.1.2, Pixmeo, Geneva, Switzerland) on the basis of at least four anatomic landmarks was used during image evaluation so the locations of lesions identified via CT and MRI could be compared. The 5 mm diameter area that had the highest summed grade was identified as the image-guided sample site. The midpoints of these sites were marked with regions of interest on the CT image.

Bone slab CT images were coregistered by means of a manual rigid registration algorithm on the basis of at least four points to the tarsal CT images marked with the image-guided specimen collection site position (Fig. 6). With the tarsal CT images as a guide and the assistance of the localizer function in the imaging software (OsiriX v 4.1.2, Pixmeo, Geneva, Switzerland) locations of the image-guided specimen collection sites were marked as regions of interest on a corresponding 3D volumetric reconstruction bone slab CT image (Fig. 6). Osteochondral regions representing these sites were removed via bandsaw with guidance from the labelled bone slab CT images. The sections of the slab that contained the image-guided specimen collection site were removed as small blocks (5 to 15 mm in size).

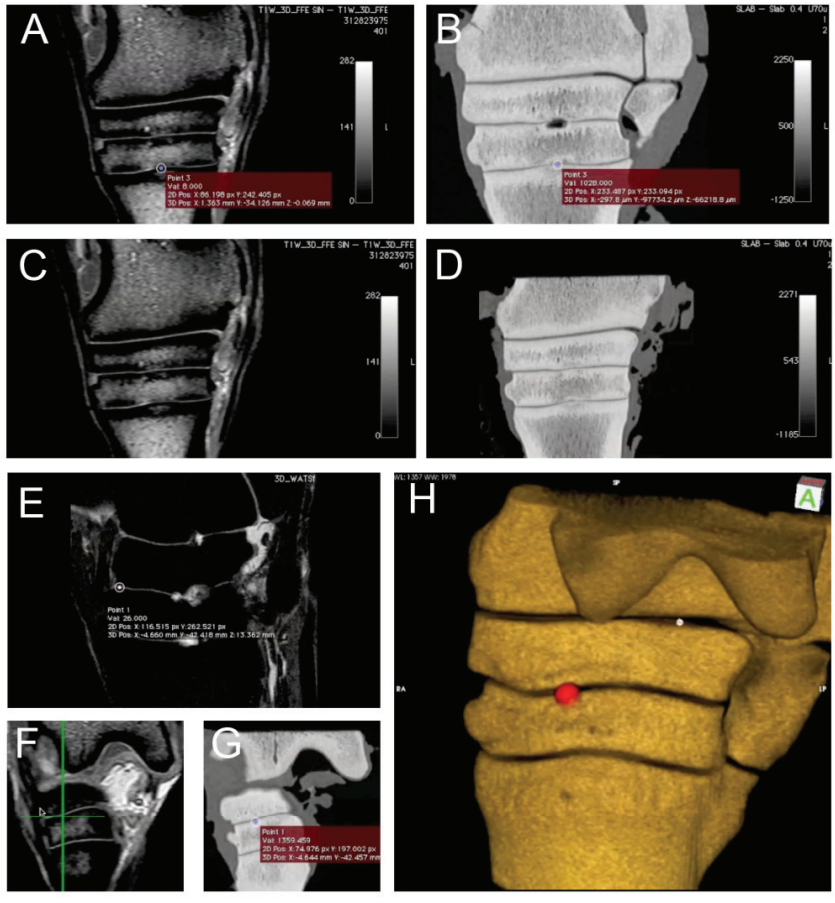

Figure 6. Sequence of images showing the coregistration process and localisation of an image-guided sample site in one of the tarsal specimens from the study. For a video presentation of this figure click on the following text (link to figure 6 video). (A and C) The same image slice from a T1-weighted magnetic resonance imaging (MRI) of the entire tarsus. (B and D) Computed tomography (CT) dorsal plane reconstructions of a tarsal bone slab from the tarsus. (A) and (B) image planes are not aligned, so corresponding anatomical structures are marked with regions of interest in the series of images. One of these regions of interest is shown (white circle with central blue dot called 'Point 3') marking the same anatomical point (the tarsometatarsal interosseus foramina) in both (A) and (B). Using these regions of interest the computer constructs a coregistered slab CT image series. After coregistration the (C) T1-weighted MRI and the (D) tarsal slab CT are now aligned. (E) Sagittal plane water saturation fluid (WATSf) MRI of the same tarsal joint shown in (A to D) with a centrodistal joint lesion marked (white circle with central white dot called 'point 1'). (F) Dorsal plane T1-weighted MRI where the localiser function has been used to identify the location of the lesion (centre of the green cross) marked in the (E) WATSf MRI. (G) Slab CT image that is aligned with the (F) WATSf MRI and the MRI image change is marked on the slab CT image (white circle with central blue dot called 'point 1'). (H) Three-dimensional volumetric reconstruction of the (F) CT series showing the location of the centrodistal lesion (red dot) in an image that can be rotated and viewed from all angles.

4.3.3 Image-guided sampling for SEM and CSLM (paper II)

In order to select osteochondral specimens containing a high frequency and degree of OA lesions and examples of specific lesion-types, the number of specimens taken from each joint and the microscopic technique used for each specimen was chosen subjectively, based on the information in the 1.5 Tesla MRI and CT images (AB, SE and CJL). The most severe lesion regions of interest in centrodistal joints (up to a maximum of four for each joint) were sampled using the MRI and CT image-guided sampling method and these specimens often included adjacent tarsometatarsal and/or talocalcaneal-centroquartal joints. If possible attempts were made to include multiple lesion regions of interest in one specimen. If no CT or MRI changes were detected in the centrodistal joint then a specimen of the centrodistal joint was removed using a predetermined sampling method (Björnsdottir *et al.*, 2004) without MRI/CT guidance. Lesion regions of interest in tarsometatarsal and talocalcaneal-centroquartal joints were then sampled and these specimens often included adjacent centrodistal joints or occasionally also tarsometatarsal and/or talocalcaneal-centroquartal joints. All joints included in a specimen were subsequently evaluated with microscopy regardless of whether or not MRI or CT abnormalities had been detected.

Osteochondral specimens were subsampled using a diamond saw (Labcut, DR Bennett LTD, London, UK) with guidance from the MRI and CT images. Where ever possible parallel adjacent specimens were taken for PMMA embedding and for processing for paraffin-embedding. The aim of this was to have adjacent light microscopy and BSE SEM/CSLM sections to allow comparison of these microscopic methods. Unfortunately an incompatibility between the 70% ethanol, which the specimens were immersed in prior to subsampling, and the decalcifying solution which they were immersed in after subsampling resulted in destruction of most of the paraffin-embedded specimens. For preparation of PMMA embedded specimens, 1.5 to 4 mm thick osteochondral slabs were made. Osteochondral blocks 5 to 15 mm thick were taken for BSE SEM studies after maceration of non-mineralised material.

4.4 Microscopic imaging methods (papers I-III)

4.4.1 Paraffin embedded light microscopy (papers I and III)

After decalcification in 3.4% (wt/vol) sodium formiate and 15.1% (wt/vol) formic acid, block specimens were trimmed with a scalpel into thin flat

sections. For the image-guided method, the radiologist was present to guide the block trimming with the aid of MRI and CT images, with the aim of collecting specimens as close as possible to the site of image lesions. Sections were dehydrated, embedded in paraffin blocks, cut into 3-6 μm thick sections, and stained with hematoxylin and eosin, and toluidine blue. Sections were then examined using light microscopy.

4.4.2 Polymethyl methacrylate (PMMA) embedded BSE SEM and CSLM (papers II and III)

Osteochondral slab specimens were embedded in PMMA and prepared as plane parallel slabs (Boyde, 2012a). The examination surface was ground and polished using a graded series of silicon carbide papers and diamond abrasives down to one micron.

Specimens embedded in PMMA used for BSE SEM were carbon coated, and examined using a Zeiss DSM962 SEM (Zeiss UK Ltd, Welwyn Garden City, Herts, UK) at 20 kV accelerating voltage with a 4 sector solid state BSE detector (KE Electronics, Toft, Cambs, UK) as previously described (Boyde & Firth, 2008; Boyde & Firth, 2005). Later in the study a Zeiss EVO MA10 SEM (Carl Zeiss NTS Ltd, Cambridge, UK) was acquired, which enabled scanning of uncoated PMMA embedded specimens when operated at 50 Pa chamber pressure and 20 kV for BSE imaging. Subsequently procedures for staining non-mineralised cell and matrix components using iodine were developed by AB (Boyde, 2013; Boyde, 2012b). Blocks were repolished to remove any carbon coating and stained with solutions of triiodide in potassium or ammonium iodide (triiodide ion) or stained dry with elemental iodine vapour, simply by placing the PMMA embedded specimens in a sealed container containing the iodine vapour.

Uncoated PMMA embedded specimens examined with CSLM were coverslipped with glycerol and examined using a Leica DMRBE with a SP2 confocal scan head and using 10/0.4 dry and 25/0.7 oil objectives (Leica Microsystems Ltd, Knowlhill, Milton Keynes, U.K.). The 488 nm line from an argon ion laser was used for excitation, and autofluorescence emission was collected into green (band from 498 – 578 nm) and red (588 – 734 nm) channels.

4.4.3 Macerated specimen BSE SEM (paper II)

Block specimens of joint surfaces were macerated using 2% Tergazyme (alkaline pronase enzyme detergent, Alconox Inc., New York, NY, USA) to remove hyaline articular cartilage and other soft tissue, washed and air dried. If Tergazyme treatment failed to remove cartilage, tendon or ligament, the

specimens were further treated by immersion in 5% hydrogen peroxide solution until clean. These specimens were either carbon coated and examined using the Zeiss DSM962 SEM at 20 kV, or examined uncoated in the Zeiss EVO MA10 SEM operated at 50 Pa chamber pressure, and again at 20 kV using BSE. Images were recorded in 3D by taking multiple images with 1° or 2° angle tilt difference and processed into movies to allow 3D to be appreciated through motion parallax; or by taking two images with a 6° tilt angle difference giving a stereoscopic pair and these were processed to give red-cyan anaglyphs that could be viewed with colour-filter spectacles.

4.4.4 Micro-CT (paper II)

Further investigation of macerated and PMMA embedded specimens was done with high resolution micro-CT (Scanco μCT40, Scanco Medical AG, Switzerland) when highly mineralised mineralisation front protrusions were seen or suspected. Macerated and PMMA embedded specimens were cut and trimmed to a cross-sectional size of less than 7 mm, permitting 6 μm micro-CT resolution.

4.5 Evaluation of microscopic imaging (papers I-III)

When light microscopy histology sections and BSE SEM images were graded the sections and images were evaluated individually by two of the authors (SE and CJL). All sections were coded so that the evaluators were blinded to identification information for the joints. If there was disagreement between evaluators then the final microscopy OA classification was decided by consensus.

4.5.1 Grading for comparison of methods (paper I)

In paper I the results of grading of microscopy sections from the osteochondral tissues were used to compare the OA detection rates of image-guided sampling compared to predetermined sampling. Light microscopy was used to evaluate 24 centrodistal joints in this study. Specimens were classified as OA negative and OA positive on the basis of a modification of a published grading system (McIlwraith *et al.*, 2010). For a specimen to be classified as OA positive, at least 3 of the following features had to be present, otherwise the section was classified as OA negative: chondrocyte necrosis, articular cartilage fibrillation, chondrocyte clusters with > 3 chondrocytes/lacuna, increase or decrease in articular cartilage thickness, osteochondral splitting, loss of toluidine blue staining, and tidemark (the interface between the mineralized and non-mineralized articular cartilage, which is considered to be equivalent to the

articular mineralisation front in the MRI, CT and BSE SEM images) fragmentation, reduplication, or absence.

4.5.2 Microscopy as the 'gold' standard (papers I and III)

In papers I and III grading of microscopy from the osteochondral tissues sampled using the image-guided method were used as the 'gold' standard to determine the OA status of the joints and investigate sensitivities and specificities of diagnostic imaging techniques.

The method of grading for the microscopy 'gold' standard in paper I was the same as was used for the comparison of the sampling methods in paper I (see 4.5.1).

In paper III light microscopy was used to evaluate 52 centrodistal joints and BSE SEM was used to evaluate 23 centrodistal joints (one sample was excluded due to loss of part of the specimen). The grading system from paper I was modified so that only morphological features were evaluated and thus the modified system could be used for both light microscopy and BSE SEM images. Thus evaluation of toluidine blue staining was removed from the light microscopy grading and to compensate for the loss of this feature the criteria for classification of OA positive was modified so that at least two of the osteochondral lesion-types had to be present; otherwise the specimen was classified as OA negative.

4.5.3 Evaluation of early OA osteochondral lesions using combined high resolution imaging (paper II)

Lesion classifications (lesion-types) were proposed from the morphological changes observed in the specimens. When multiple microscopic techniques were used images were correlated to evaluate the range of lesions present.

The PMMA embedded BSE SEM images were systematically re-examined and the lesion-types present in each specimen were determined. This information was used to record the frequency of osteochondral lesion-types in talocalcaneal-centroquartal, centrodistal and tarsometatarsal joints and to calculate associations and correlations between the lesion-types in the centrodistal joints.

4.6 Evaluation of radiography and low field MRI for detection of early OA (paper III)

Images from radiography and low-field MRI were examined for presence or absence, and distribution of lesions in the centrodistal joints by three of the authors (CJL, KH and SB). The initial image evaluations were done

individually and radiographs were examined before low-field MRI. Where there was disagreement between readers this was followed by simultaneous examination of the images by all readers and a majority consensus agreement. All images were coded, identification information was hidden and the order of the presentation of the joints was randomised.

Lesion categories for the radiographs and low-field MRI images were established based on the expected radiographic and low-field MRI appearance of lesion categories described in paper I and in high detail radiographic studies of centrodistal joints of young horses (Björnsdottir *et al.*, 2004; Barneveld & van Weeren, 1999; Laverty *et al.*, 1991). Lesion categories were constructed for radiography and low-field MRI to reflect the specific imaging characteristics of each modality and the images were subsequently evaluated for the presence of these lesions.

Lesion categories causing shape changes of the mineralised joint tissues were sought in both radiographs and the low-field MRI sequence T1-weighted-gradient echo (T1W-GRE). Joint margin changes were defined as abnormally enlarged margins (bone overproduction) or pointed or peaked shaped margins (caused by bone overproduction or undercutting bone resorption) as opposed to the normal angular or rounded joint margin shape. Evaluation for joint margin changes could not be done in areas of T1W-GRE images where hypointense ligament or joint capsule were confluent with the joint margin. Central osteophytes were defined as areas of focal convex bumps on the mineralisation front. Mineralisation front defects were defined as focal concave regions in the mineralisation front that usually resulted in a focal region of increased distance between the mineralisation fronts of the joint. Care was taken not to include regions suspected to be partial volume artefacts as central osteophytes or mineralisation front defects.

Several lesion categories that resulted from changes of joint tissue mineral opacity were sought in radiographs only. Regions of reduced opacity in the mineralised tissues adjacent to the joint surfaces were defined as mineralised joint tissue lysis. Regions of thickening of the mineralised tissues proximal or distal to the joint surfaces were defined as subchondral sclerosis. Narrowing of the lucent space between the mineralisation fronts (combination of joint space and hyaline articular cartilage) was defined as a narrow joint space. Focal mineral opacities detected between the mineralisation fronts were defined as a joint space mineral opacity.

In low-field MRI images several lesion categories defined by changes in MRI intensity patterns were sought. Abnormal MRI signal in the region between the mineralisation fronts was considered to represent an articular cartilage lesion resulting either from abnormal articular cartilage MRI signal or

an articular cartilage surface defect filled with synovial fluid, and this change was recorded according to sequence type. Lesions were recorded when focal T2-weighted-fast spin echo (T2W-FSE) and STIR- fast spin echo (FSE) hyperintensity, T1W-GRE hypointensity, T2-star-weighted-gradient echo (T2*W-GRE) hyperintensity or hypointensity were detected. Regions of T2W-FSE and STIR-FSE hyperintensity in the mineralised tissues adjacent to the articular surfaces were classified as subchondral hyperintensity and considered to represent oedema-like signal and/or cyst-like lesions. Regions of definite abnormal thickening of the signal void dense subchondral bone plate in T1W-GRE, T2*W-GRE and T2W-FSE sequences were classified as subchondral sclerosis.

The lesion distribution in each joint was classified as focal, multifocal or generalised. Readers also recorded the radiographic projection in which each lesion was detected. In low-field MRI images the location of lesions were judged subjectively by the readers with the assistance of the transverse pilot image at the level of the centrodistal joint. Possible lesion regions were lateral, dorsolateral, dorsal, dorsomedial, medial and plantar. For anatomical orientation the mid-sagittal plane was considered to divide the centrodistal joint region into two approximately symmetrically shaped halves.

4.7 Data analyses

4.7.1 Paper I

Osteoarthritis detection results for the two different specimen collection methods were compared with Chi-squared tests (Minitab 15 statistical software program, State College, Pa., USA).

To analyse the imaging grades the microscopic classification (OA positive or negative) of specimens from the image-guided collection sites was used as the ‘gold’ standard and the sums of the imaging grades were grouped into four categories. The association between these summed imaging grade categories and the microscopic OA classification of sites was assessed via logistic regression and production of receiver operating characteristic curves (SAS, version 9.2, SAS Institute, Cary, NC., USA)

The summed image grades were evaluated for their usefulness as a possible diagnostic tool for OA detection by calculation of the area under the curve for the receiver operating characteristic curves. Diagnostic sensitivity and specificity, including 95% confidence intervals, were calculated for image lesion-types and grades detected within each image-guided sample region, with results of microscopic classification of each image-guided sample considered

the ‘gold’ standard (Interactive Statistical Calculation Pages. Available at: statpages.org/ctab2x2.html).

Fisher’s exact tests were used to identify image lesion-types and grades that were associated with the microscopic OA classification (SAS, version 9.2, SAS Institute, Cary, NC., USA).

Values of $P < 0.05$ were considered significant for all statistical tests.

4.7.2 Paper II

The frequencies of lesion-types were recorded as percentages of joints examined according to joint (talocalcaneal-centroquartal, centrodistal or tarsometatarsal joint) and specimen type (PMMA embedded or macerated).

Count data of lesion-types detected in PMMA embedded centrodistal joint specimens was tested for associations between the presence of osteochondral lesion-types using Fisher’s exact tests (SAS, version 9.2, SAS Institute, Cary, NC., USA). To control type-1 errors, the Benjamini and Hochberg false discovery rate procedure was applied to $P = 0.05$ to determine significant P-values for individual tests of association (Benjamini & Hochberg, 1995). *Phi* coefficients were calculated from the same centrodistal joint lesion-type data to investigate the degree and direction of correlations between the osteochondral lesion-types.

4.7.3 Paper III

All analyses for paper III were performed using the PROC FREQ procedure in SAS (SAS, version 9.2, SAS Institute, Cary, NC, USA) and values of $P \leq 0.05$ were considered significant. Fisher’s exact tests were used to investigate associations between lesion categories detected in radiographs and the microscopic OA classification of the joint and lesion categories detected in low-field MRI. Microscopic OA classification was used as the ‘gold’ standard used to calculate sensitivity and specificity including 95% confidence intervals for radiography and low-field MRI. McNemar’s exact tests were used to compare the sensitivities and the specificities of radiography compared to low-field MRI, for pooled lesion categories, and for single lesion categories found to have a statistically significant association with microscopic OA. For lesion categories found to have a significant association with microscopic OA histograms were constructed showing the frequency of lesion detection in radiographs according to the angle of projection and in low-field MRI according to the anatomical region location of the detected lesion.

5 Results

This section summarises the results from the studies performed for this thesis. Detailed descriptions of the results are presented in each of the papers.

5.1 Paper I

5.1.1 Detection of OA according to the specimen collection method

The predetermined and image-guided specimen collection methods showed significantly different rates of OA detection (P = 0.02). Osteoarthritis lesions were detected with microscopy in 7 of 24 (29%) joints when the specimens were collected from the predetermined location and in 15 (62%) joints when the sites from which specimens were collected were identified with the aid of MRI and CT. All joints with OA changes detected using the predetermined specimen collection also had OA changes detected via the image-guided method.

5.1.2 Association of image grades and microscopic OA

Twenty-two joints were classified as microscopic OA positive and 26 joints classified as microscopic OA negative. An association was detected between the guided-sample summed image grade categories and the microscopic classification of OA (positive vs negative; P = 0.018). The area under the curve calculated from the receiver operating characteristic curve was 0.89, indicating that the summed image grades were a good predictor of microscopic OA.

5.1.3 Abnormalities identified in MRI and CT images

Moderate to high numbers of image-guided specimen collections sites had evidence in the images of articular mineralisation front defects (Figs. 8 and 9), marginal osteophytes (Fig. 9), central osteophytes (Fig. 7), articular cartilage thickness abnormalities (Fig. 7), articular cartilage hypointensities and intra-

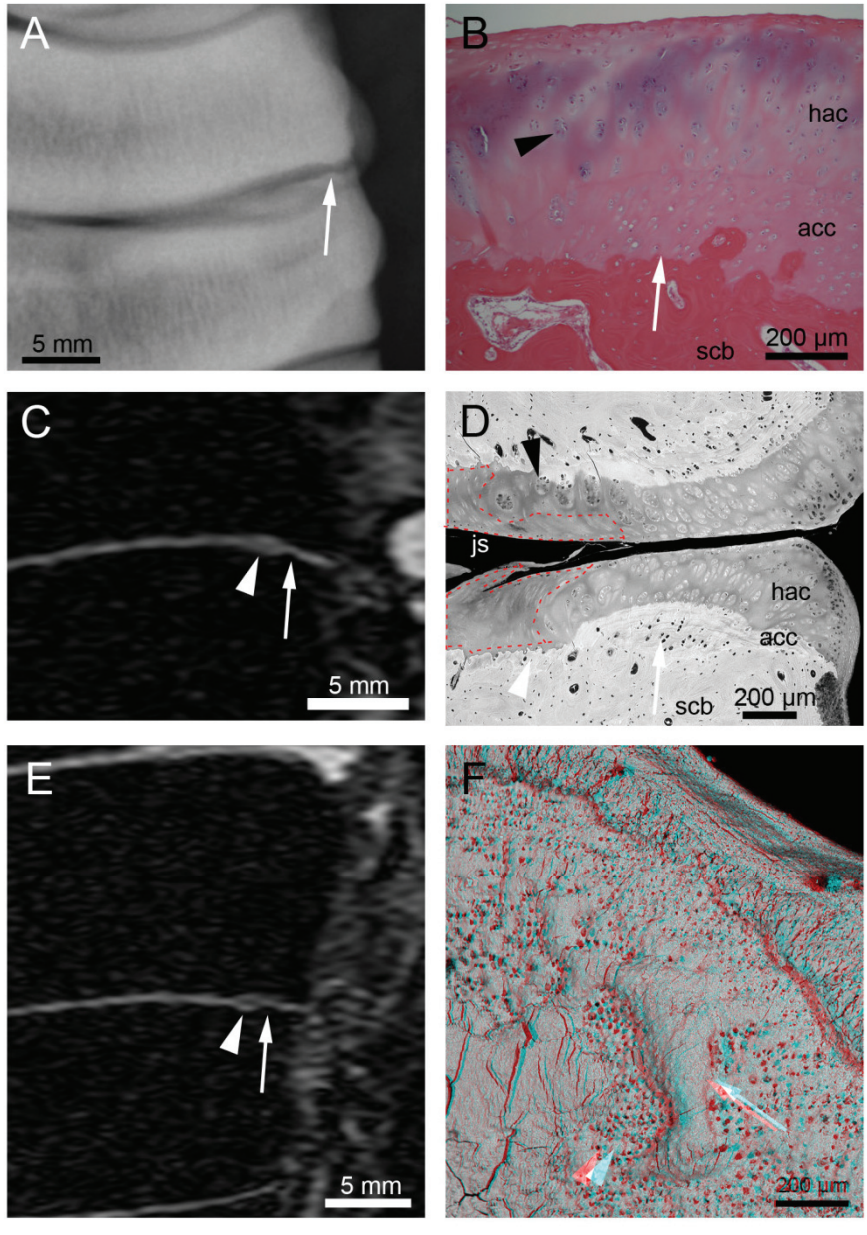
A
5 mm
B
hac
acc
scb
200 µm
C
5 mm
D
js
hac
acc
scb
200 µm
E
5 mm
F
200 µm

Figure 7. Correlation and comparison of diagnostic and microscopic imaging showing examples of the lesion-types central osteophytes/articular calcified cartilage advancement (white arrows), and articular cartilage thickening/articular calcified cartilage arrest (white arrowheads) in centrodistal joints. (A) Radiograph and corresponding (B) light microscopy histology of the same joint and region. (C) Water saturation fluid (WATSf) magnetic resonance imaging (MRI) and corresponding (D) iodine stained back scattered electron scanning electron microscopy (BSE SEM) images of the same joint and region. (E) WATSf MRI and corresponding (F) macerated specimen BSE SEM anaglyph image (requires red-cyan colour filter spectacles for viewing) of the same joint and region. The central osteophytes in (C) and (E) correspond to regions of articular calcified cartilage advancement in (D) and (F) respectively. The regions of articular cartilage thickening in (C) and (E) correspond to regions of articular calcified cartilage arrest in (D) and (F) respectively. Additionally (B) and (D) shows examples of chondrocyte clusters (black arrowheads) and (D) shows areas of chondrocyte necrosis (regions within the red dashed lines) and fibrillation of the hyaline articular cartilage. hac = hyaline articular cartilage; acc = articular calcified cartilage; scb = subchondral bone; js = joint space. (D) and (F) by A. Boyde.

chondral/articular mineralisation (Fig. 10). On the other hand, low numbers had signs of subchondral sclerosis, subchondral lysis, subchondral cyst, and subchondral hyperintensity.

5.1.4 Validated OA lesions

An association was identified between histologic detection of OA and the following lesions identified in MRI or CT images: grade-2 articular mineralisation front defects ($P = 0.022$, Fig. 8), and grade-2 marginal osteophytes ($P = 0.022$, Fig. 9), central osteophytes ($P < 0.001$, Fig. 7), combined grades-1 and -2 of articular cartilage thickness abnormalities ($P = 0.009$, Fig. 7).

5.1.5 Sensitivity and specificity of image lesions for OA detection

The specificity of image lesions and grades for OA detection was generally high, with the exception of articular mineralisation front defects grade 1 (very low specificity) and articular cartilage hypointensities (moderately low specificity). Large variation was evident in the sensitivities of the various image lesions and grades for OA detection, with image lesions and grades that were uncommon (detected in less than seven joints) having low sensitivity.

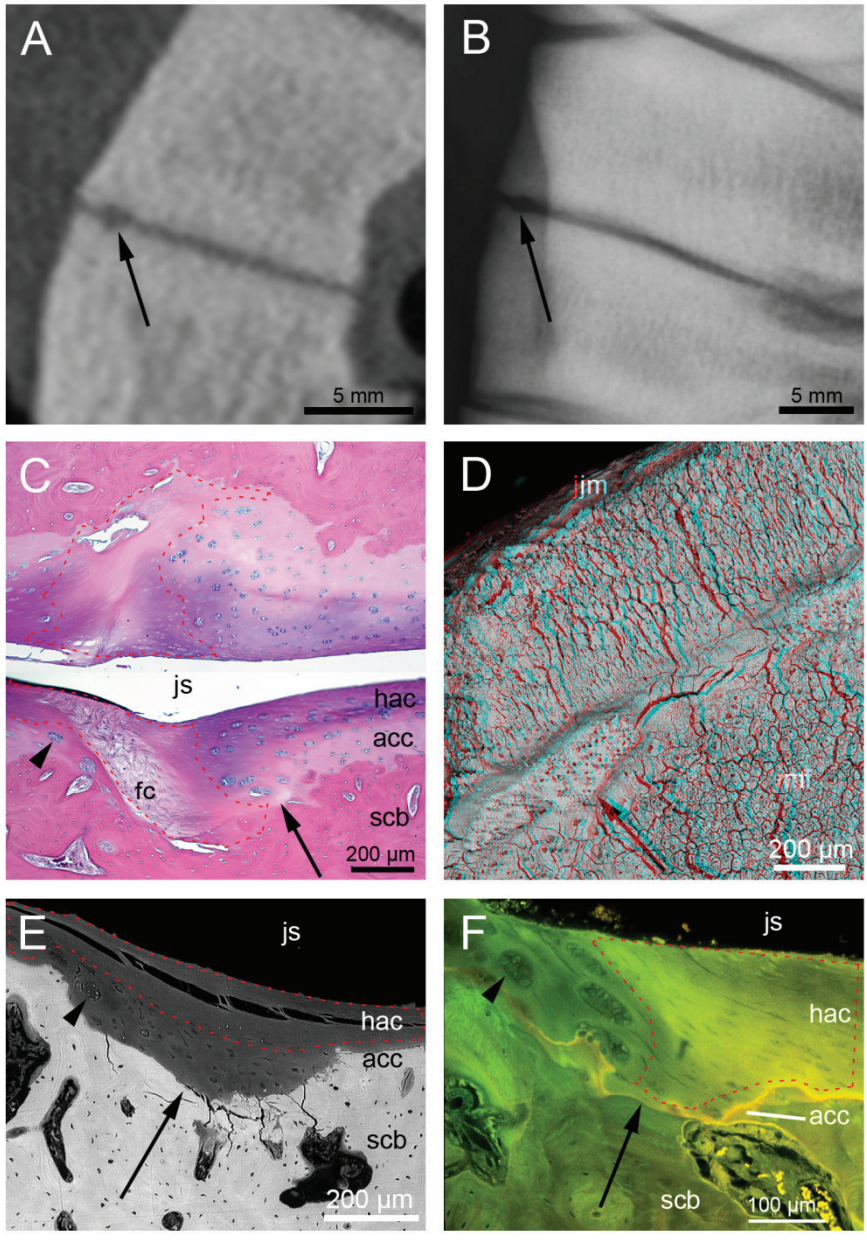
A
5 mm
B
5 mm
C
js
hac
acc
fc
scb
200 µm
D
jm
mi
200 µm
E
js
hac
acc
scb
200 µm
F
js
hac
acc
scb
100 µm

Figure 8. Correlation and comparison of diagnostic and microscopic imaging, and examples of the lesion-type of articular mineralisation front defects/articular calcified cartilage arrest (black arrows) in centrodistal joints. (A) Computed tomography, (B) radiography and (C) light microscopy histology from the same joint and region showing an articular mineralisation front defect lesion. (D to F) Examples of lesions in three other joints. Articular mineralisation front defects were called articular calcified cartilage arrest (black arrows) in (D) macerated specimen backscatter electron scanning electron microscopy (BSE SEM) (this is an anaglyph image and requires red-cyan colour filter spectacles for viewing), (E) iodine stained BSE SEM and (F) confocal scanning light microscopy. Additionally (C), (E) and (F) show examples of chondrocyte clusters (black arrowheads), areas of chondrocyte necrosis (regions within the red dashed lines) and (C) shows an area of fibrocartilage (fc). hac = hyaline articular cartilage; acc = articular calcified cartilage; scb = subchondral bone; js = joint space; jm = joint margins. (D), (E) and (F) by A. Boyde.

5.2 Paper II

Thirteen lesion-types were detected in PMMA embedded specimens and seven of these lesion-types were detected in macerated specimens (Table 6, Figs. 7 to 10).

5.2.1 Lesion-type frequency in PMMA embedded specimens

Lesions were detected in all centrodistal joints that had PMMA embedded specimens taken (n = 22) and all 13 lesion-types were detected. Lesion-type frequencies in the centrodistal joint were moderate to high in the hyaline articular cartilage, variable in the articular calcified cartilage, low in the subchondral bone, high on the joint margins and low for hypermineralised infill phase lesions.

Lesions were detected in all tarsometatarsal joints that had PMMA embedded specimens taken (n = 20) and 11 of 13 lesion-types were detected. Lesion-type frequencies in the hyaline articular cartilage of the tarsometatarsal joints were low except for marginal chondrocyte clusters, which had a high frequency similar to that seen in the centrodistal joint. Lesion-types of the tarsometatarsal joint margins had a moderate to high frequency with joint margin erosions having a similar frequency to that seen in the centrodistal joints.

Lesion-type frequencies in the talocalcaneal-centroquartal joints were low. Only five of 13 lesion-types were identified and lesions were detected in only three of seven joints.

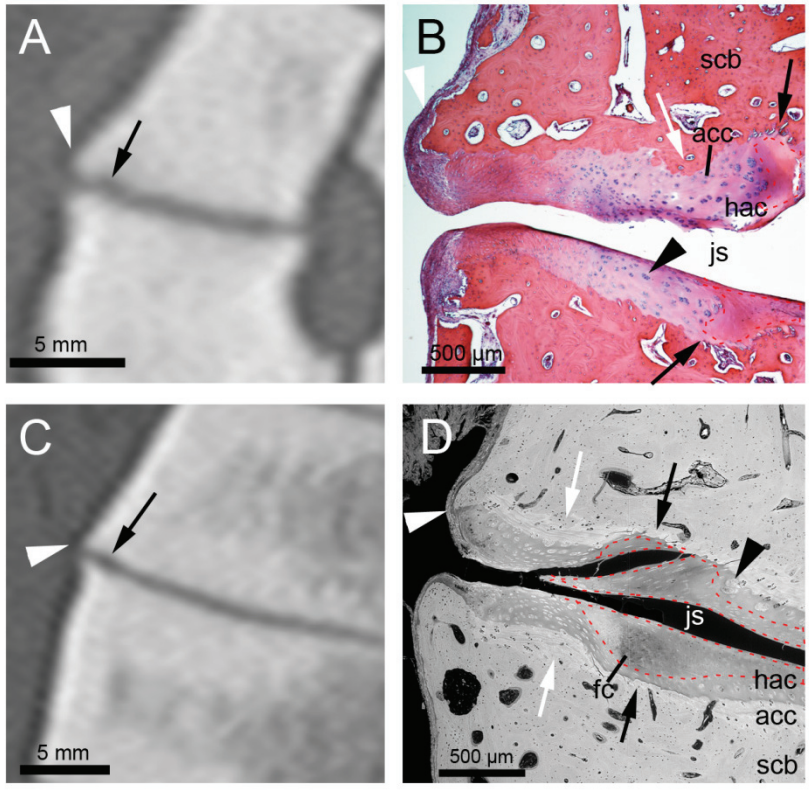

Figure 9. Correlation and comparison of diagnostic and microscopic imaging showing examples of lesion-types, marginal osteophytes (white arrowheads), articular mineralisation front defects/articular calcified cartilage arrest (black arrows) and central osteophytes/articular calcified cartilage advancement (white arrows) in centrodistal joints. (A) Computed tomography (CT) and correlated (B) light microscopy histology images of the same joint and region. (C) CT and correlated (D) iodine stained backscattered electron scanning electron microscopy images of the same joint and region. Additionally, chondrocyte clusters (black arrowheads) and areas of chondrocyte necrosis (regions within the red dashed lines) are shown in (B) and (D), and fibrocartilage (fc) and a full thickness split of the hyaline articular cartilage are shown in (D). hac = hyaline articular cartilage; acc = articular calcified cartilage; scb = subchondral bone; js = joint space. (D) by A. Boyde.

Table 6. *Descriptions of lesion-types in polymethyl methacrylate embedded and macerated specimens from joints of the distal tarsal region,*

Hyaline articular cartilage lesion-types (Figs. 7 to 9)	
Chondrocyte loss	**PMMA**: Regions that contained empty chondrocyte lacunae, small often flattened faint silhouettes of chondrocytes or hypo- or acellular HAC
Central chondrocyte clusters	**PMMA**: Groups of chondrocytes within a chondron ≥ 2 cells wide located > 500 µm from the joint margin
Marginal chondrocyte clusters	**PMMA**: Groups of chondrocytes within a chondron ≥ 2 cells wide located < 500 µm from the joint margin
Fibrillation	**PMMA**: Articular surface discontinuities, fissures, splits and erosions
Articular calcified cartilage lesion-types (Figs. 7 to 9)	
Chondrocyte loss	**PMMA**: Hypo- or acellular regions
Chondrocyte clusters	**PMMA**: Groups of chondrocytes within a chondron ≥ 2 cells wide
	Macerated: Imprints in the MF of chondrons ≥ 2 chondrocytes wide
Arrest	**PMMA**: Areas of thin, moderate to high mineralisation density, hypo- or acellular ACC which when focal caused a concave contour of the MF
	Macerated: Grooves and furrows formed by concave MF regions
Advancement	**PMMA**: Areas of thick ACC, which when focal caused a convex contour of the MF. Poorly defined and hazy mineralising front and superficial layer of low density
	Macerated: Ridges or mounds formed by convex MF regions
Joint margin lesion-types (Fig. 9)	
Extensions	**PMMA**: The joint margin at the level of the articular cartilage was enlarged by mineralised fibrous joint capsule and periosteum, mineralised fibrocartilage or bone
	Macerated: Extension or enlargement of the joint margin
Erosions	**PMMA**: Concave areas of bone resorption on non-articular aspects of the joint margin
	Macerated: Patches or craters of bone resorption on non-articular aspects of the joint margin
Hypermineralised infill phase lesion-types (Fig. 10)	
ACC HIP	**PMMA**: Focal linear or irregularly shaped HIP material within the ACC and occasionally extending into the SCB
HIP protrusions	**PMMA**: Focal protrusions of HIP within the articular cartilage that extended from the ACC into the HAC
	Macerated: Focal protrusions of HIP through the MF
Subchondral bone lesion-types	
Resorption	**PMMA**: Concave to circular regions of SCB resorption
	Macerated: Concave areas of resorption extending into the SCB

ACC = articular calcified cartilage, HAC = hyaline articular cartilage, HIP = hypermineralised infill phase, MF = mineralisation front, PMMA = polymethyl methacrylate embedded, SCB = subchondral bone.

5.2.2 Lesion-type frequency in macerated specimens

Lesions were detected in all centrodistal joints that had macerated specimens taken (n = 9) and all seven lesion-types were detected. Lesion-types of the articular calcified cartilage in the centrodistal joints had a moderate to high frequency. Margin erosions were detected in all the centrodistal joints examined and margin extensions were detected in four joints (44%).

Lesions were detected in all tarsometatarsal joints that had macerated specimens examined (n = 6) and the only lesion-type not detected was subchondral bone resorption. The tarsometatarsal joints had a mildly lower frequency of articular calcified cartilage lesion-types compared to the centrodistal joints. The frequency of joint margin lesion-types was almost identical to that of the centrodistal joints.

Four of the five talocalcaneal-centroquartal joints that had macerated specimens taken had at least one lesion detected and all seven lesion-types were detected in these joints. Similar to the frequency pattern in PMMA embedded specimens, marginal lesions of the talocalcaneal-centroquartal joint in macerated specimens had a low frequency.

5.2.3 Associations and correlations between lesion-types in PMMA embedded centrodistal joint specimens

Centrodistal joint lesion-types with moderate to high frequency that had significant associations and strong positive correlations were; hyaline articular cartilage chondrocyte loss, hyaline articular cartilage central chondrocyte clusters, hyaline articular cartilage fibrillation, articular calcified cartilage arrest, articular calcified cartilage advancement and articular calcified cartilage chondrocyte loss.

Lesion-types with high frequency that had no significant associations with other joint lesion-types were hyaline articular cartilage marginal chondrocyte clusters and lesion-types of the joint margins.

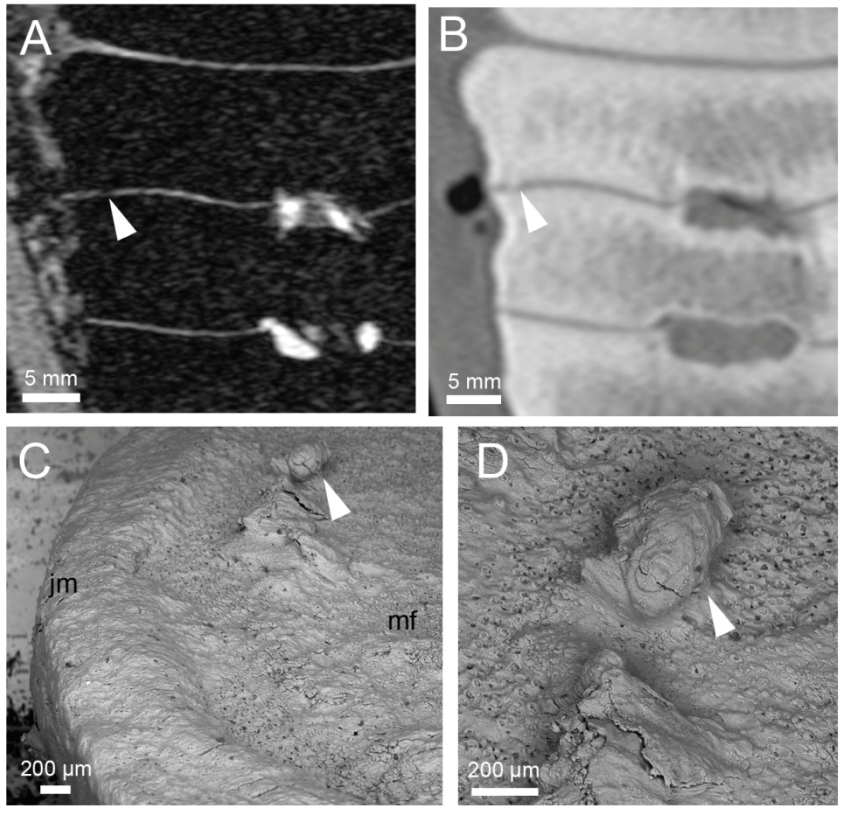

Figure 10. Correlation and comparison of diagnostic and microscopic imaging showing hypermineralised infill phase protrusions (white arrowheads) from the same region of the same centrodistal joint. (A) Water saturation fluid magnetic resonance imaging. (B) Computed tomography. (C and D) Macerated specimen back scattered electron scanning electron microscopy. Panel (D) is a close-up image of part of the hypermineralised infill phase protrusion shown in (C) and the location of the white arrowheads in (C) and (D) correspond. jm = joint margin; mf = mineralisation front. (C) and (D) by A. Boyde.

5.3 Paper III

The microscopy evaluation classified 42/75 joints OA positive and 33/75 OA negative. Lesions were detected in radiographs of 38/75 joints and in low-field MRIs of 40/75 joints. Radiographic lesions in 32/38 joints were classified as OA positive by microscopy and distributions of these radiographic lesions were focal in 9/32 joints, multifocal in 23/32 and no joints with generalised changes were detected. Low-field MRI lesions in 28/40 joints were classified as OA positive by microscopy and distributions for these MRI lesions were

focal for 9/28 joints, multifocal in 19/28 and no joints with generalised changes were detected.

5.3.1 Associations between radiographs and microscopic OA

Associations were identified between the detection of lesions in radiographs (pooled results of all lesion categories) and the presence of microscopic OA ($P < 0.0001$). The sensitivity and specificity for pooled radiographic lesion categories for detecting OA was high. Joint margin lesions and mineralisation front defects (Fig. 8) were the most frequently detected lesion categories and both had associations with the presence of OA ($P < 0.0001$), and moderate sensitivity and high (joint margin lesions) or almost perfect (mineralisation front defects) specificity for the detection of OA. Mineralisation front defects were detected in 29/75 joints and all but one of these joints were classified as OA positive by microscopy. Central osteophytes (Fig. 7) were detected with low frequency but still had an association with the presence of OA ($P = 0.03$). Central osteophytes were only detected in centrodistal joints that were classified positive for microscopic OA and in every joint where a central osteophyte was detected both mineralisation front defects and joint margin changes were always present. Mineralised joint tissue lysis, subchondral sclerosis, narrow joint space and joint space mineral opacity were detected with very low frequency and showed no association with OA.

5.3.2 Associations between low-field MRI and microscopic OA

Associations were detected between the detection of lesions in low-field MRI (pooled results of all lesion categories) and the presence of microscopic OA ($P = 0.01$). The sensitivity and specificity of pooled low-field MRI lesion categories for detecting OA were moderate. Joint margin lesions were the most frequently detected lesion category and had associations with the presence of OA ($P = 0.02$) and moderate sensitivity and high specificity for the detection of OA. Mineralisation front defects were detected with moderate frequency and had associations with the presence of OA ($P = 0.01$), and low sensitivity and very high specificity for the detection of OA. Articular cartilage lesions were detected with high frequency and had associations with the presence of OA ($P = 0.0003$), and low sensitivity and very high specificity for the detection of OA. All of the articular cartilage lesions detected in low-field MRI were suspected articular cartilage surface defects indicated by focal collections of T2W-FSE or STIR hyperintensity between the articular cartilage layers. It was noted that in these areas of T2W-FSE or STIR hyperintensity there was often a corresponding area of T1W hyperintensity. No joints were detected with focal T1W-GRE hypointensities within the intermediate signal articular cartilage

region. Subchondral hyperintensity and subchondral sclerosis were detected with very low frequency and showed no association to OA. Central osteophytes were not detected with low-field MRI.

5.3.3 Comparison of radiography and low-field MRI for detection of centrodistal joint OA

No differences were detected between radiography and low-field MRI when all lesion categories were pooled, although there was a trend towards radiography having a higher specificity. When frequently detected radiography lesion categories that were associated with OA (joint margin lesions and mineralisation front defects) were compared to pooled results for all low-field MRI lesion categories, radiography had a higher specificity. Frequently detected low-field MRI lesion categories that were associated with OA (joint margin lesions, mineralisation front defects and articular cartilage lesions) had a higher sensitivity compared to pooled results for all radiography lesion categories.

Mineralisation front defects detected in radiographs were more sensitive at detecting OA compared to mineralisation front defects in low-field MRI, but there was no difference in specificity. An association was detected between the presence of mineralisation front defects in radiographs and low-field MRI of the same joint ($P = 0.0218$) and when mineralisation front defects were detected with both modalities in a joint, OA was always detected with microscopy.

There was no difference between the sensitivity and specificity of radiography joint margin lesions and low-field MRI joint margin lesions for the detection of OA. An association was detected between the presence of joint margin lesions in radiographs and low-field MRI of the same joint ($P < 0.0001$) and when joint margin lesions were detected with both modalities in a joint, the joint was positive for OA in 18/21 joints.

5.3.4 Locations of lesions associated with microscopic OA

Lesions detected with radiography in joints with OA were identified most frequently in the Pl10Di45L-DPrMO projection, with moderate frequency in the LM and D35L-PlMO projections and with low frequency in DPl projections.

Lesions detected with low-field MRI in joints with OA were identified with high frequency in the dorsolateral region of the centrodistal joints, and with low frequency in the lateral, dorsal, dorsomedial and medial regions. No low-field MRI lesions were detected in the plantarolateral, plantar or plantaromedial regions.

6 General discussion

6.1 Image guidance for detection of early OA in cadaver distal tarsal joints

The morphological changes of early OA are typically focal and small compared to the much larger joint organ (Pritzker *et al.*, 2006; Squires *et al.*, 2003; Veje *et al.*, 2003; Dieppe & Kirwan, 1994). This is a major challenge for early OA detection and for the investigation of early OA morphological lesions. Furthermore the anatomy of the joints of the equine distal tarsal region makes access to the articular surfaces for macroscopic evaluation impossible without extensive dissection of the joint capsule and ligaments. With these challenges in mind the method using clinical diagnostic imaging equipment for sampling cadaver joints using image guidance was developed in paper I. In this method the images of the osteochondral tissues of the entire centrodistal joint were evaluated to localise focal lesions, then using coregistration of CT images of sawn joint slabs it was possible to sample the regions of these lesions. The image-guided sampling method had a higher sensitivity for the detection of centrodistal joint OA detected by light microscopy compared to specimens taken using a predetermined sampling method. These results support the use of an image guidance method when sampling joints of the centrodistal joint from equine cadavers to investigate the frequency of early OA.

6.2 Early distal tarsal OA lesions

By using a combination of microscopic techniques (paper II) it was possible to investigate lesions in the mineralised and non-mineralised joint tissues and examine of joint tissues in cross-section, *en face* and with 3D volumetric reconstructions. Additionally the MRI and CT guided osteochondral sampling technique allowed localisation of focal regions of change in the joints and

selection of optimal microscopic methods to examine these regions. Furthermore the validation of several lesion-types detected in radiographs, MRI and CT images for OA detection (papers I and III) opens possibilities to use these imaging methods that evaluate the entire joint to further investigate spatial patterns of these lesion-types in centrodistal joints.

The BSE SEM studies of PMMA embedded articular tissues (paper II) produced high contrast and spatial resolution images of the mineralised tissue morphology and density thus these techniques were ideal for examining the articular calcified cartilage and mineralisation front. This is in contrast to light microscopy histology (paper I) where the decalcification required for tissue preparation resulted in removal of some of the mineralised tissue information, which in some cases made identification and detailed evaluation of the mineralisation front region uncertain (Figs. 8C and 9B). Of particular value to paper II was the development by Alan Boyde of novel iodine staining methods for BSE SEM examinations of PMMA embedded blocks, which resulted in excellent quality high-resolution images of both mineralised and non-mineralised tissues. Additionally, the attribute of BSE SEM to acquire detailed images of the mineralisation front in cross-section in PMMA embedded specimens and *en face* in macerated specimens allowed examination of mineralisation front changes at very high magnification and resolution, and showed patterns of changes of relatively large areas of the articular surface. Further information was acquired in paper II about changes deep to the mineralisation front lesions detected in macerated specimens by using microCT, particularly in the case of hypermineralised protrusions. MicroCT was also useful to guide re-surfacing, re-polishing and further imaging of PMMA embedded specimens when lesions were suspected under the block surface.

In human OA research early OA is considered to occur before radiographic changes of the joint are detectable (Palmer *et al.*, 2013; Bay-Jensen *et al.*, 2010; Cibere *et al.*, 2009), but in paper III lesions were detected in radiographs that were associated with focal microscopic osteochondral lesions in the centrodistal joints. A possible explanation for why early OA of the centrodistal joint was possible to detect with radiographs is that these small focal lesions were often located close to the periphery of the joint in regions that could be radiographed with minimal summation from the adjacent tissues (Figs. 7 and 8). Additionally, narrowed joint space and subchondral bone sclerosis and lysis, which are lesions commonly detected in radiographs of horses with advanced OA of the distal tarsal region (Labens *et al.*, 2007a), were very rarely detected (paper III).

Some of the articular cartilage lesions detected with microscopy (paper I-III) were similar to lesions classified as severe in general OA and equine OA grading systems (McIlwraith *et al.*, 2010; Pritzker *et al.*, 2006) but the focal distribution of these lesions that was observed in the MRI and CT images (paper I) and the microscopy images (paper II) is consistent with early OA (Pritzker *et al.*, 2006; Squires *et al.*, 2003; Veje *et al.*, 2003; Dieppe & Kirwan, 1994).

In humans early OA is considered to occur in the preclinical stage of the disease before symptoms are established (Luyten *et al.*, 2012). The horses in the study were not trained to lead or ride, thus detailed lameness and orthopaedic examinations of the horses were not possible, although the horses in group-09 were evaluated with an objective lameness detection system (Lameness locator®, Equinosis, Columbia, Missouri, USA). For the examinations the horses trotted freely in pairs in an approximately 3 m wide 50 m long laneway. Gait recordings were considered suitable for measurement in 13 of 14 horses. One horse would only pace or tolt and thus gait measurements of this horse were not possible. Using published lameness criteria (Keegan *et al.*, 2011) no systematic lameness's were detected in the 13 horses recorded. In these horses microscopic OA was detected in both centrodistal joints in three horses, in one centrodistal joint in five horses and was not detected in the centrodistal joints of the remaining five horses.

6.2.1 Articular cartilage lesions

The terminology used to name lesion-types in the papers included in the thesis differs depending on the imaging technique used. The lesions articular mineralisation front defect and focal mineralisation front defects in paper I and paper III respectively are considered to correspond to articular calcified cartilage arrest lesions identified in paper II (Figs. 7 to 9). The lesion central osteophyte in papers I and III is considered to correspond to articular calcified cartilage advancement lesions identified in paper II (Figs. 7 and 9). It is likely that many of the focal articular cartilage thickness and joint space lesions detected with high-field MRI are a result of articular calcified cartilage advancement and arrest lesions (paper I). Other studies utilizing light microscopy of paraffin embedded specimens have described subchondral bone defects and subchondral bone plate irregularities in the joints of the equine distal tarsal region (Björnsdottir *et al.*, 2004; Laverty *et al.*, 1991) and it is likely these are also equivalent to the articular calcified cartilage advancement and arrest lesions described in this thesis. It was only with the microscopic imaging methods used in paper II that it was always possible to localise these lesions specifically to the articular calcified cartilage, since it was not

uncommon in the paraffin embedded specimens that the tidemark could not be clearly defined in regions of articular cartilage lesions (Figs. 8C and 9B).

In paper II the lesion-types of the hyaline and calcified articular cartilage were most common and strong correlations were found between the presence of hyaline articular cartilage chondrocyte loss, hyaline articular cartilage central chondrocyte clusters, articular calcified cartilage arrest and articular calcified cartilage advancement. Chondrocyte loss and clusters are typical lesions described in early OA (McIlwraith *et al.*, 2010; Pritzker *et al.*, 2006; Björnsdottir *et al.*, 2004; Barneveld & van Weeren, 1999) but the articular calcified cartilage lesion-types arrest and advancement have not been described in detail previously. The reason for selection of the terms advancement and arrest for these lesion-types was that the morphological features of these lesion-types suggested different rates of progression of the mineralisation front into the hyaline articular cartilage. Advancement lesions appeared to be due to an increased mineralisation rate of the deep layer of the hyaline articular cartilage matrix thus creating a convex bulge of the mineralisation front and thick articular calcified cartilage (Figs. 7 and 9). Whereas, in regions of arrest lesions there appeared to be a slowing or complete stop of the rate of mineralisation of the deep layer of the hyaline articular cartilage. Since mineralisation of the adjacent regions of the hyaline articular cartilage continued and ossification of the deep aspect of the articular calcified cartilage appeared to continue this resulted in concave regions of the mineralisation front and thin articular calcified cartilage (Figs. 7 to 9). The study horses were at the age where endochondral ossification of the articular epiphyseal cartilage had only recently finished but it is likely that some lesions developed during the previous months when endochondral ossification was occurring. Since the mineralisation front region is very active and rapidly changing during articular epiphyseal endochondral ossification this is likely to be a period when injuries to these tissues may result in changes in the development and subsequent morphology of the mineralisation front. Thus, the lesions detected in these studies in this thesis are likely to be not only injuries of tissue structure but also injuries that have affected tissue growth. This raises the very important question: what happens to these lesions? Do these lesions progress to involve more of the osteochondral tissues and the other associated joint tissues, or is it possible for these early OA lesions to heal?

In radiographs and CT images the mineralisation front should always be the articular aspect of the articular calcified cartilage except in regions where there is a defect in the articular calcified cartilage. The appearance of lesions in the MRI images (paper I) suggests that the articular aspect of the border of the hypointense region representing dense bone is in the region of the

mineralisation front. However, this does not agree with a study that compared articular cartilage thickness in MRI images with histology images and concluded that the border was probably the osteochondral junction rather than the articular aspect of the articular calcified cartilage (Murray *et al.*, 2005).

Spatial relations were apparent between the four strongly correlated hyaline articular cartilage and articular calcified cartilage lesion-types (paper II). Hyaline articular cartilage chondrocyte clusters often occurred on either side of focal regions of hyaline articular cartilage chondrocyte loss. Articular calcified cartilage arrest often occurred deep to focal regions of hyaline articular cartilage chondrocyte loss. Articular calcified cartilage advancement often occurred on either side of focal regions of articular calcified cartilage arrest and deep to regions of hyaline articular cartilage chondrocyte clusters. Focal regions containing this pattern of these four lesion-types were often seen in apposing articular surfaces located toward the periphery of the joint. In macerated specimens it was common to see articular calcified cartilage arrest trenches and articular calcified cartilage advancement ridges on the lateral, dorsal and medial peripheral articular surfaces and following the shape of the joint margins. This peripheral location on the joint surface and following the joint margins was also evident in the articular mineralisation front defects seen in CT images (paper I), articular cartilage thickness lesions in high-field MRI (paper I) and mineralisation front defects in radiography and low-field MRI (paper III).

The spatial relations detected suggest a possible sequence of events in the early stages of distal tarsal joint OA. Focal hyaline and calcified articular cartilage damage could be caused by focal increased overloading (most likely static due to the low-motion characteristics of the distal tarsal joints) or the presence of osteochondral tissue with increased susceptibility to loading in the peripheral articular surface regions. Chondrocyte death and related to this articular calcified cartilage arrest may occur in the regions of maximum overloading damage. The resulting thinning or even loss of the articular calcified cartilage likely causes a reduction of the selective barrier function of the articular calcified cartilage (Pan *et al.*, 2012; Suri & Walsh, 2012; Pan *et al.*, 2009). This provides an opportunity for the perpetuation of the OA cascade due to the possible increased access of inflammatory substances between the subchondral bone and intra-articular compartments.

On the edge of highly loaded areas the damage to the articular cartilage is less and the injury to chondrocytes in these areas may result in the activation of anabolic processes in the articular cartilage and the development of clusters of hypertrophic chondrocytes. Hypertrophic chondrocytes in the hyaline cartilage are associated with an increased rate of mineralisation of the cartilage (Chen-An *et al.*, 2013; Lotz *et al.*, 2010). The increased rate of mineralisation occurs due to release of substances such as bone morphogenetic protein 2 by the clusters (van der Kraan & van den Berg, 2007). Extracellular membrane vesicles distribute substances produced by chondrocytes that induce calcification to the surrounding cartilage matrix (Anderson *et al.*, 2010).

6.2.2 Joint margin lesions

Joint margin lesions were evaluated in the diagnostic imaging studies and in the microscopy studies. Marginal osteophytes detected by CT were used as a criterion for the image-guided sampling method (paper I) and it was found that large marginal osteophytes were associated with presence of OA, but small marginal osteophytes were not. Joint margin changes were also evaluated using radiography and low-field MRI (paper III) and detection of these lesions was frequent and found to be associated with the detection of microscopic OA. When the joints were examined with BSE SEM and CSLM (paper II) a range of joint margin changes were discovered. This included joint margin erosions, seen as patches or craters on the non-articular aspects of the joints, and joint margin extensions by mineralised fibrous joint capsule and periosteum, mineralised fibrocartilage or bone. However, all these types of joint margin changes resulted in similar peaked marginal osteophyte shape. Shape is the basis of evaluation for joint margins in radiography, CT and MRI and because of this it is unlikely these methods can differentiate between marginal erosions and the variety of causes of marginal extensions.

Joint margin changes were very common in the centrodistal and tarsometatarsal joints but there was no association between the types of joint margin lesion or between joint margin lesions and osteochondral OA lesions (paper II). In contrast to paper I the joint margin changes in paper II were not graded according to size but rather were graded according to type, thus it appears that the size of a joint margin change is more important for the prediction of osteochondral OA rather than the type of joint margin change.

The BSE SEM and CSLM techniques in paper II resulted in very high resolution of the mineralised joint margin compared to that of papers I and III. With BSE SEM it was possible to detect joint margin extensions and erosions that may have been too small to be detectable in paper III and either too small to be detected or in the grade 1 category in described paper I. Furthermore, the

maceration technique used in paper II meant it was possible to survey large regions of the non-articular joint margin with high resolution. Thus the detection rate of joint margin lesions in paper II, particularly small and mild lesions is likely to be higher than the studies that used light microscopy histology, MRI, CT or radiography (papers I and III). A method to differentiate small from larger joint margin lesions was not used in paper II due to problems of classifying size in joint margins that often had both margin erosion and margin extension.

The variation of the association between joint margin changes and OA found in papers I-III are consistent with reports in the literature. When examining joints with radiography, CT or MRI marginal osteophytes are considered indicative of OA (Hunter *et al.*, 2011a) although osteophytes are reported in joints without OA (Brandt *et al.*, 2009) and osteophyte formation and articular cartilage destruction have been found to be independent in OA (Kaneko *et al.*, 2013). Laverty *et al*. found that isolated joint margin bony productive lesions on equine distal tarsal joints were not always associated with other histological changes in the joint and suggested that margin changes alone have minimal clinical significance (Laverty *et al.*, 1991).

6.2.3 Hypermineralised infill phase lesions

The lesion-type name hypermineralised infill phase was coined in paper II to describe highly mineralised material that fills spaces within the osteochondral tissues. Similar lesions have been described in BSE SEM studies of the equine metacarpophalangeal joint (Whitton *et al.*, 2013; Boyde *et al.*, 2011; Boyde & Firth, 2008) and third tarsal bone (Boyde, 2003). The hypermineralised infill phase material is proposed to arise from traumatic cracks and spaces within the osteochondral tissues that fill with extracellular fluid, blood or plasma forming an aqueous organic matrix (Boyde *et al.*, 2011). The water component of this organic matrix progressively mineralises and if the contents of the crack or cavity are isolated from the surrounding tissues there will be a lack of mineralisation inhibitors allowing very high concentrations of mineralisation to develop. Thus, these lesions are characterised by accumulations of material that have levels of mineralisation that are higher than articular calcified cartilage or bone. Hypermineralised infill phase lesions are very likely to be removed by the decalcification and microtomy procedures required for the preparation of light microscopy sections (Boyde *et al.*, 2011) and this is the most likely reason of the very rare mention of these lesion-types in the literature. Interestingly the larger hypermineralised infill phase protrusions were clearly visible in CT images of the joints and this was used to identify some of these lesions (paper II). In paper I

hypermineralised infill phase protrusions were categorised as intra-articular and chondral mineralisation in CT images and in retrospective evaluation of the high-field MRI images some of these lesions could be seen as focal articular cartilage hypointensities.

Hypermineralised infill phase protrusions occurred with a relatively low frequency in the joints but this lesion-type was always associated with OA changes in the surrounding osteochondral tissues (papers I and II). Hypermineralised infill phase protrusions will result in a focal region of very hard inflexible tissue surrounded by flexible hyaline articular cartilage, giving a high risk of eventual exposure of the hypermineralised protrusion through the articular surface and even fracture and displacement of the hypermineralised protrusion into the joint space. Such exposed or displaced hypermineralised protrusions have tremendous potential to cause extensive mechanical damage to the articular surfaces.

The relation of articular calcified cartilage hypermineralised infill phase material, which is usually seen in the form of linear hypermineralised crack-like lesions, and distal tarsal joint OA is less clear. These lesions were seen in distal tarsal joints with and without articular cartilage OA lesions and so it uncertain if this lesion occurs at a stage of OA before morphological changes are seen in the articular cartilage or whether this lesion is an overload or fatigue injury that does not necessarily progress to OA. These findings have similarities to those of a recent BSE SEM study of the distal articular surface of the third metacarpal bone in Thoroughbred racehorses where 36% of horses with third metacarpal condyle fractures but 63% of control horses (euthanised for reasons other than third metacarpal condyle fractures) had hypermineralised crack-like articular calcified cartilage lesions (Whitton *et al.*, 2013).

All of the methods used to evaluate the subchondral bone in this thesis have been used in other equine studies to successfully detect subchondral bone changes (Whitton *et al.*, 2013; Olive *et al.*, 2010a; Boyde & Firth, 2008; Murray *et al.*, 2007; Young *et al.*, 2007; Boyde & Firth, 2005) so if subchondral bone lesion were present they should have been readily detectable. The subchondral bone was evaluated with CT (paper I), MRI (papers I and III), radiography (paper I), and BSE SEM (paper II) and in all cases the frequencies of subchondral bone lesions in joints were low and associations with articular cartilage OA lesions were not detected (papers I-III), although the few subchondral bone resorptive lesions that were detected (paper II) were always seen together with articular cartilage lesions. These findings are in agreement with several other diagnostic imaging and microscopy studies of equine centrodistal joints. A study with high-detail radiography shows that microscopic articular cartilage lesions were associated with joint margin

demineralisation but not subchondral bone sclerosis (Laverty *et al.*, 1991), whilst another study shows some association between bone sclerosis and chondronecrosis in the lateral part of the joint, but no association medially (Björnsdottir *et al.*, 2004). The low frequency and low or lack of association of microscopic OA and subchondral bone changes detectable with CT, radiography and MRI means that using these methods the evaluation of centrodistal joints from young horses for changes within the subchondral bone is unlikely to assist in the detection of individuals with early microscopic OA. Furthermore it is doubtful that the initiating events of early OA occur in the subchondral bone in the joints in the distal tarsal region of horses.

6.3 Microscopy - the 'gold' standard

The 'gold' standard used to evaluate the detection of early OA by the diagnostic imaging methods used in this thesis was microscopic morphological changes in the osteochondral tissues. The microscopic classification systems used in this thesis were comparable to grades 1 to 3 of the Osteoarthritis Research Society International system (Pritzker *et al.*, 2006), grades 1 to 4 of a proposed microscopic grading system for OA in equine fetlock and carpal joints (McIlwraith *et al.*, 2010) and a recently proposed definition of histological early-stage OA in humans (Madry *et al.*, 2012). To allow use of light microscopy histology in some joints and iodine stained BSE SEM in others (paper III) a classification system was used that evaluated morphological features that could be assessed using either technique. Thus even though light microscopy histology and BSE SEM provide some different tissue information it was considered that both methods were suitable and comparable for grading OA.

6.4 An imaging biomarker for early distal tarsal OA in Icelandic horses

Screening programs for heritable forms of disease, investigations of the evolution of naturally developing diseases and studies of early intervention treatment strategies require biomarkers that are validated, widely available, cost-effective and easily allow for follow up examinations (ESR, 2013). In this thesis several imaging biomarkers have been identified and validated for early OA of the equine centrodistal joint.

The investigation of lesions detected in the MRI and CT images of the sampled regions of centrodistal joints and OA changes detected in microscopic sections from these sampled regions (paper I) showed that central osteophytes

and articular cartilage thickness abnormalities detected with MRI, and moderate or larger articular mineralisation front defects and moderate or larger marginal osteophytes detected with CT were associated with OA. These lesion-types had very high or perfect specificity and variable sensitivity for OA detection thus validating these lesion-types for the detection of early OA. The imaging methods in paper I were designed for examination of cadaver specimens rather than screening live horses. The WATSf MRI sequence used in paper I is not suitable for scanning live animals due to the extremely long scan time (approximately 54 minutes). However the CT protocol used is suitable for scanning live horses although a general anaesthetic is required for the examination. Thus the CT method is not suitable for screening large numbers of live horses.

Radiography and low-field MRI (paper III) are methods that are currently available for examining standing sedated horses. Due to the isolated location of the study horses it was only possible to perform the radiographic examinations on live horses whilst the low-field MRIs were made on cadaver tarsal specimens from the same horses. Thus the low-field MRI studies lack the effects of weight bearing and horse motion. Additionally the low-field MRI sequences used in paper III were in all cases except STIR sequences higher resolution than the standard sequence protocols in the low-field MRI system and thus had relatively long scan times and small pixel sizes. The likelihood of motion degradation increases as image spatial resolution improves since any motion greater than half the pixel size degrades the image (McKnight *et al.*, 2004). Various motion-correction techniques have been developed (Lange *et al.*, 2013; McKnight *et al.*, 2004) and although motion-insensitive sequences were available in the low-field MRI system used they were included since motion artefacts were not anticipated in the specimens. To reduce the effects of motion artefacts when doing low-field MRI on the tarsal regions general anaesthesia can be used for the scanning procedure.

The comparison of radiography of standing horses and low-field MRI of cadaver specimens showed that radiography was equal to or better than low-field MRI for detecting early stage centrodistal joint OA. This result disagreed with the study hypothesis that MRI would have a higher sensitivity for early OA detection. The major reason for the lower than expected sensitivity and specificity of low-field MRI most likely relates to low image resolution relative to the small osteochondral lesions. Morphological changes in the early stages of OA are focal and mild (Pritzker *et al.*, 2006; Veje *et al.*, 2003; Brama *et al.*, 2000; Palmer *et al.*, 1995; Dieppe & Kirwan, 1994) thus the detectability of early lesions is heavily dependent on image resolution (Alhadlaq *et al.*, 2004). The acquisition in-plane pixel resolutions in the low-field MRI sequences were

between 0.44-1.03 mm and slice thicknesses were between 3.5-5 mm and this compares to a pixel pitch of 0.16 mm for the radiographs. Thus the 2D spatial resolution of the radiographic image is considerably higher than the low-field MRI images. The 2D nature of radiographs results in summation and overlap of opacities and this can obscure anatomical detail and hide lesions despite high image resolution. However, convex curved bone surfaces that are tangential to the x-ray beam are projected free from other skeletal structures, thus summation is minimal and very high resolution images of these surfaces are possible (May *et al.*, 1986). A radiograph taken with an x-ray beam that is both parallel to an articular surface and tangential to a convex curved joint margin can result in high resolution images of focal regions of the peripheral regions of a joint, and the angles of projection used in paper III resulted in these types of images. Therefore, each set of radiographs from a joint provided high resolution images of multiple small peripheral joint regions without overlap of other skeletal structures and it was in these peripheral joint regions that almost all of the radiographic changes that were associated with microscopic OA were detected.

A study of the image resolution required for MRI to detect OA changes in human and bovine patella articular cartilages concludes that images with in-plane pixel resolutions greater than 0.3 mm do not reliably show mild alterations of articular cartilage (Rubenstein *et al.*, 1997). A study of articular cartilage volume measurements in human stifle joints suggests 0.275 mm in-plane resolution and 1 mm slice-thickness reduced partial volume averaging effects to acceptable levels for accurate repeated cartilage volume measurements (Hardy *et al.*, 2000). Furthermore the articular cartilage in equine centrodistal joints is thin compared to human and bovine knee articular cartilage (Malda *et al.*, 2013; Salo *et al.*, 2012; Tranquille *et al.*, 2009) and thus would be expected to require even higher pixel resolutions in images to show mild cartilage lesions. Lesions that are similar or smaller than image voxels suffer partial volume averaging effects due to dilution of the lesion signal in the surrounding tissue signal within that voxel. The pixel and voxel sizes in the low-field MRI images were larger than those suggested in the human and bovine studies and often had dimensions larger than lesion sizes detected in paper II. This was a major limitation for the MRI cartilage assessment and the likely reason that the sensitivity values for detecting lesions of the articular cartilage were low, or in the case of central osteophytes not detected.

To increase spatial resolution (decrease pixel/voxel size) in digital images there is always a trade off for a lower signal-to-noise ratio or a longer scan time. An adequate signal-to-noise ratio must be maintained otherwise lesion detectability will decrease (Rubenstein *et al.*, 1997). Scan times for clinical

sequences must be relatively short and it is the amount of tissue signal resulting from an MRI sequence that has the strongest influence on the maximum image spatial resolutions possible. Since tissue signal increases in proportion to magnetic field strength, high field strengths allow higher resolution imaging and it has been shown that higher field strengths improve the sensitivity of MRI for detection of OA changes (Kijowski *et al.*, 2009; Stahl *et al.*, 2009; Wong *et al.*, 2009; Masi *et al.*, 2005). Studies that compare high- and low-field MRI for the detection of artificially created and natural articular cartilage lesions in equine cadaver specimens show high-field MRI to be superior (Werpy *et al.*, 2011; Murray *et al.*, 2009b). High-field MRI is validated in multiple studies for the detection of morphological changes in human OA (Hunter *et al.*, 2011b; Quatman *et al.*, 2011) and is used with success to evaluate focal osteochondral changes and early stage OA in the human knee (Chundru *et al.*, 2013; Ding *et al.*, 2006; Ding *et al.*, 2005a; Ding *et al.*, 2005b). Anaesthesia is currently required for high-field MRI examination of the equine tarsus and the high costs and potential complications associated with this procedure virtually excludes high-field MRI as a screening technique for early OA.

The paper III results validate mineralisation front defects and joint margins lesions in both radiography and low-field MRI, central osteophytes in radiographs and focal T2W/STIR hyperintensity between the articular surfaces in low-field MRI as changes of early centrodistal joint OA. The specificity and sensitivity results show that all these lesion categories have high or very high specificity but there is considerable variation in the sensitivity of these lesion categories for the detection of OA. Mineralisation front defects detected by radiography had the highest sensitivity and this suggests that evaluation for this lesion in radiographs may be useful for screening young Icelandic horses for early centrodistal joint OA.

6.5 The Icelandic horse as a model for OA research

Animal models with naturally occurring OA provide valuable information for human OA research (Madry *et al.*, 2012; Innes & Clegg, 2010). Horses offer several advantages over other animal species in regards to joint structure. Compared to other animal models used in OA research horses provide the closest approximation to human articular cartilage thickness (Malda *et al.*, 2013; Frisbie *et al.*, 2006) and chondrocyte volume density (Aigner *et al.*, 2010). Due to the heritability and high frequency of distal tarsal OA in the Icelandic horse population (Björnsdottir *et al.*, 2000a; Björnsdottir *et al.*, 2000b; Eksell *et al.*, 1998) and the relatively low genetic diversity of the breed

(Glowatzki-Mullis *et al.*, 2006) the Icelandic horse provides a valuable general model for the study of naturally occurring OA. In agreement with previous studies (Björnsdottir *et al.*, 2004) this thesis shows that early OA is common in the joints of the distal tarsal region in young Icelandic horses. Thus studies of the distal tarsal joints of young Icelandic horses provide an opportunity to study a spectrum of osteochondral lesions during the period when the early stages of OA are occurring. Information from such studies has potential applications for the development of diagnostic and therapeutic methods in all species.

7 Conclusions

- An image-guided method for collecting specimens for microscopy resulted in a higher detection rate of early OA in cadaver equine centrodistal joints compared to predetermined sampling.
- An image-guided method for collecting specimens is recommended when microscopic examination will be used as the 'gold' standard for the detection of early OA in cadaver centrodistal joints of horses.
- The early morphological changes of distal tarsal OA in Icelandic horses occur in the hyaline and calcified articular cartilage, rather than in the subchondral bone.
- Central osteophytes and articular cartilage thickness abnormalities detected with high-field MRI were validated by light microscopy histology as OA lesions.
- Moderate or larger articular mineralisation front defects and moderate or larger marginal osteophytes detected with CT were validated by light microscopy histology as OA lesions.
- Mineralisation front defects and joint margins lesions detected with radiography and low-field MRI were validated by a combination of light microscopy histology and BSE SEM as OA lesions.
- Central osteophytes detected with radiographs were validated by a combination of light microscopy histology and BSE SEM as OA lesions.
- Focal T2W/STIR hyperintensity between the articular surfaces detected with low-field MRI were validated by a combination of light microscopy histology and BSE SEM as OA lesions.
- Young Icelandic horses offer a promising model for the study of calcified articular cartilage behaviour in early OA of low-motion joints
- Morphological changes of early stage centrodistal joint OA were detectable with both radiography of standing horses and low-field MRI of cadaver joints.

- Radiography is equal to or better than low-field MRI for detecting early stage centrodistal joint OA in Icelandic horses.
- Detection of mineralisation front defects in radiographs may be a useful screening method for detection of early OA in centrodistal joints of young Icelandic horses.

8 Future research

During the collection of the data from the horses in this study it was attempted to maximise the opportunities for parallel and future studies that were outside the framework for this thesis. The results of this thesis also open possibilities for further development of screening programmes in Icelandic horses and wider applications to other horse breeds and models for early OA research.

The diagnostic images acquired in this thesis work contain an enormous amount of morphological information about the horses in the study and there are several further studies that can be made using these images:

- The locations of the lesions detected in the MRI and CT images were thoroughly marked during the imaging guidance process and methods for spatial mapping of lesions in joints with confirmed OA can provide valuable information about the lesion distributions within the joint. This information has importance in the further development of imaging diagnostic methods for early distal tarsal OA and the search for the factors that initiate and predispose for the development of distal tarsal OA.
- The CT images contain readily accessible 3D information that can be applied to investigating the conformation of the bones of the tarsal joints and possible associations with the conformation and the presence of early distal tarsal OA.
- The CT images also contain quantitative mineral density information in the form of Hounsfield units that can be used to investigate patterns of bone density in the tarsal region and their associations to early distal tarsal OA and leg conformation.
- Spatial information of osteochondral lesions, bone conformation and mineral density information can be evaluated in relation to known loading patterns of the tarsal joint to investigate associations between mechanical joint loading and the development of OA.

- Multi-echo MRI sequences for T2-mapping were acquired from all the tarsal joints in the study and these images are not yet evaluated.

Remaining tissue specimens and sections from the study horses will provide possibilities for further investigation of:

- Specific osteochondral lesion-types using techniques such as immunohistochemistry.
- Evaluation of frozen specimens for genetic and biochemical research.
- Further processing of the PMMA embedded specimens for investigation of subchondral bone structure.

Parallel to this study the conformations of the study horses were evaluated using 3D videomorphometry and this information gives possibilities for investigation of associations between external conformation and the presence of early distal tarsal OA.

Most importantly the findings from paper III provide a non-invasive, cost effective, widely available and highly specific method for the detection of early distal tarsal OA in Icelandic horses. Possible future research using this method includes:

- Longitudinal studies of groups of Icelandic horses starting at a young age to investigate whether the radiographic changes validated for early distal tarsal OA in paper III progress or heal as the horses get older and associations with future lameness problems arising from the distal tarsal region.
- Retrospective studies of archives of tarsal radiographs of young Icelandic horses to evaluate the prevalence of the validated radiographic changes and attempts to re-radiograph these now older horses and investigate associations with lameness detected since the taking of the radiographs.

If correlations are found between the validated radiographic changes and the subsequent development of advanced distal tarsal OA and lameness arising from the region then the radiographic method described in paper III could be:

- Applied as a screening method to remove horses with early distal tarsal OA from the Icelandic horses breeding population.
- Used to investigate genetic screening methods for distal tarsal OA in Icelandic horses.
- Used to select horses for study groups to evaluate early intervention treatments for early OA in horses and as a general early OA model.

It remains uncertain whether or not distal tarsal OA has a common pathogenesis in all horse breeds or whether Icelandic horses have a separate subtype of the disease. Evaluation of other breeds of horse using the methods described in this thesis should help to clarify this.

The image-guided sampling method has applications in joint research where osteochondral specimens are collected. This includes specimen collection guidance for large and/or inaccessible joints to guiding specimen collection between multiple joints in an individual animal.

References

Adrian, A.M., Koene, M., Roberts, S., Doughty, P., Bolas, N., Kinns, J., Brehm, W. & Gerlach, K. (2012). The influence of temperature and age on the T1 relaxation time of the equine distal limb. *Veterinary Radiology and Ultrasound* 53(3), 296-303.

Aigner, T. (2012). Osteoarthritis histopathology grading criteria - a never ending story? *Osteoarthritis and Cartilage* 20(6), 469-70.

Aigner, T., Cook, J.L., Gerwin, N., Glasson, S.S., Laverty, S., Little, C.B., McIlwraith, W. & Kraus, V.B. (2010). Histopathology atlas of animal model systems – overview of guiding principles. *Osteoarthritis and Cartilage* 18, Supplement 3(0), S2-S6.

Alhadlaq, H.A., Xia, Y., Moody, J.B. & Matyas, J.R. (2004). Detecting structural changes in early experimental osteoarthritis of tibial cartilage by microscopic magnetic resonance imaging and polarised light microscopy. *Annals of the Rheumatic Diseases* 63(6), 709-17.

Ameye, L.G. & Young, M.F. (2006). Animal models of osteoarthritis: lessons learned while seeking the "Holy Grail". *Current Opinion in Rheumatology* 18(5), 537-47.

Amin, S., LaValley, M.P., Guermazi, A., Grigoryan, M., Hunter, D.J., Clancy, M., Niu, J., Gale, D.R. & Felson, D.T. (2005). The relationship between cartilage loss on magnetic resonance imaging and radiographic progression in men and women with knee osteoarthritis. *Arthritis and Rheumatism* 52(10), 3152-9.

Anderson, H.C., Mulhall, D. & Garimella, R. (2010). Role of extracellular membrane vesicles in the pathogenesis of various diseases, including cancer, renal diseases, atherosclerosis, and arthritis. *Laboratory Investigation* 90(11), 1549-57.

Arnason, T. & Björnsdóttir, S. (2003). Heritability of age-at-onset of bone spavin in Icelandic horses estimated by survival analysis. *Livestock Production Science* 79, 285-293.

Aubin, J.E. (1979). Autofluorescence of viable cultured mammalian cells. *The journal of histochemistry and cytochemistry* 27(1), 36-43.

Aula, A.S., Jurvelin, J.S. & Töyräs, J. (2009). Simultaneous computed tomography of articular cartilage and subchondral bone. *Osteoarthritis and Cartilage* 17(12), 1583-1588.

Axelsson, M., Bjornsdottir, S., Eksell, P., Haggstrom, J., Sigurdsson, H. & Carlsten, J. (2001). Risk factors associated with hindlimb lameness and degenerative joint disease in the distal tarsus of Icelandic horses. *Equine Veterinary Journal* 33(1), 84-90.

Axelsson, M., Eksell, P., Roneus, B., Brostrom, H., Haggstrom, J. & Carlsten, J. (1998). Relationship between hind limb lameness and radiographic signs of bone spavin in Icelandic horses in Sweden. *Acta Veterinaria Scandinavica* 39(3), 349-57.

Bansal, P.N., Joshi, N.S., Entezari, V., Malone, B.C., Stewart, R.C., Snyder, B.D. & Grinstaff, M.W. (2011). Cationic contrast agents improve quantification of glycosaminoglycan (GAG) content by contrast enhanced CT imaging of cartilage. *Journal of Orthopaedic Research* 29(5), 704-9.

Barneveld, A. & van Weeren, P.R. (1999). Early changes in the distal intertarsal joint of Dutch Warmblood foals and the influence of exercise on bone density in the third tarsal bone. *Equine Veterinary Journal* Suppl. 31, 67-73.

Baum, T., Joseph, G.B., Arulanandan, A., Nardo, L., Virayavanich, W., Carballido-Gamio, J., Nevitt, M.C., Lynch, J., McCulloch, C.E. & Link, T.M. (2012). Association of magnetic resonance imaging-based knee cartilage T2 measurements and focal knee lesions with knee pain: data from the Osteoarthritis Initiative. *Arthritis Care and Research* 64(2), 248-55.

Bay-Jensen, A.C., Hoegh-Madsen, S., Dam, E., Henriksen, K., Sondergaard, B.C., Pastoureau, P., Qvist, P. & Karsdal, M.A. (2010). Which elements are involved in reversible and irreversible cartilage degradation in osteoarthritis? *Rheumatology International* 30(4), 435-42.

Bell, B.T., Baker, G.J., Foreman, J.H. & Abbott, L.C. (1993). In vivo investigation of communication between the distal intertarsal and tarsometatarsal joints in horses and ponies. *Veterinary Surgery* 22(4), 289-92.

Benjamini, Y. & Hochberg, Y. (1995). Controlling the False Discovery Rate - a Practical and Powerful Approach to Multiple Testing. *Journal of the Royal Statistical Society Series B-Methodological* 57(1), 289-300.

Bergsten, G. (1983). Sjukdomsfrekvenser i rörelseorganen hos ett material försäkrade hästar 1973-1981. *Svensk Veterinartidning* 35(14, Supplement 3), 14-20.

Biswal, S., Hastie, T., Andriacchi, T.P., Bergman, G.A., Dillingham, M.F. & Lang, P. (2002). Risk factors for progressive cartilage loss in the knee: a longitudinal magnetic resonance imaging study in forty-three patients. *Arthritis and Rheumatism* 46(11), 2884-92.

Bittersohl, B., Mamisch, T.C., Welsch, G.H., Stratmann, J., Forst, R., Swoboda, B., Bautz, W., von Rechenberg, B. & Cavallaro, A. (2009). Experimental

model to evaluate in vivo and in vitro cartilage MR imaging by means of histological analyses. *European Journal of Radiology* 70(3), 561-569.
Björnsdottir, S., Arnason, T., Axelsson, M., Eksell, P., Sigurðsson, H. & Carlsten, J. (2000a). The heritability of degenerative joint disease in the distal tarsal joints in Icelandic horses. *Livestock Production Science* 63, 77-83.
Björnsdottir, S., Árnason, T. & Lord, P. (2003). Culling rate of Icelandic horses due to bone spavin. *Acta Veterinaria Scandinavica* 44, 161-169.
Björnsdottir, S., Axelsson, M., Eksell, P., Sigurðsson, H. & Carlsten, J. (2000b). Radiographic and clinical survey of degenerative joint disease in the distal tarsal joints in Icelandic horses. *Equine Veterinary Journal* 32(3), 268-272.
Björnsdottir, S., Ekman, S., Eksell, P. & Lord, P. (2004). High detail radiography and histology of the centrodistal tarsal joint of young Icelandic horses. *Equine Veterinary Journal* 36(1), 5-11.
Bousson, V., Lowitz, T., Laouisset, L., Engelke, K. & Laredo, J.D. (2012). CT imaging for the investigation of subchondral bone in knee osteoarthritis. *Osteoporosis International* 23 Suppl. 8, 861-5.
Boyde, A. (2003). The real response of bone to exercise. *Journal of Anatomy* 203(2), 173-89.
Boyde, A. (2012a). Scanning electron microscopy of bone. In: Helfrich, M.H.*, et al.* (Eds.) *Bone Research Protocols*. pp. 365-400. New York: Springer science + Business Media. (Methods in Molecular Biology; 816). ISBN 978-1-61779-414-8.
Boyde, A. (2012b). Staining plastic blocks with triiodide to image cells and soft tissues in backscattered electron SEM of skeletal and dental tissues. *European cells & materials* 24, 154-160; discussion 160-161.
Boyde, A. (2013). Joint histology by iodine staining. *Journal of Anatomy* 223, 84.
Boyde, A. & Firth, E.C. (2004). Articular calcified cartilage canals in the third metacarpal bone of 2-year-old thoroughbred racehorses. *Journal of Anatomy* 205(6), 491-500.
Boyde, A. & Firth, E.C. (2005). Musculoskeletal responses of 2-year-old Thoroughbred horses to early training. 8. Quantitative back-scattered electron scanning electron microscopy and confocal fluorescence microscopy of the epiphysis of the third metacarpal bone. *New Zealand Veterinary Journal* 53(2), 123-32.
Boyde, A. & Firth, E.C. (2008). High resolution microscopic survey of third metacarpal articular calcified cartilage and subchondral bone in the juvenile horse: possible implications in chondro-osseous disease. *Microscopy Research and Technique* 71(6), 477-88.
Boyde, A., Lovicar, L. & Zamecnik, J. (2005). Combining confocal and BSE SEM imaging for bone block surfaces. *European cells & materials* 9, 33-8.
Boyde, A., Riggs, C.M., Bushby, A.J., McDermott, B., Pinchbeck, G.L. & Clegg, P.D. (2011). Cartilage damage involving extrusion of mineralisable matrix from the articular calcified cartilage and subchondral bone. *European cells & materials* 21, 470-8; discussion 478.

Brama, P.A., Tekoppele, J.M., Bank, R.A., Karssenberg, D., Barneveld, A. & van Weeren, P.R. (2000). Topographical mapping of biochemical properties of articular cartilage in the equine fetlock joint. *Equine Veterinary Journal* 32(1), 19-26.

Branch, M.V., Murray, R.C., Dyson, S.J. & Goodship, A.E. Magnetic resonance imaging of distal tarsal osteochondral structure: normal variation or pathological change? In: *Proceedings of workbook from American Association of Equine Practitioners, Focus on Joints Meeting*, July 22-24 2004. pp. 28-41.

Brandt, K.D., Dieppe, P. & Radin, E. (2009). Etiopathogenesis of Osteoarthritis. *Medical Clinics of North America* 93(1), 1-24.

Brandt, K.D., Radin, E.L., Dieppe, P.A. & van de Putte, L. (2006). Yet more evidence that osteoarthritis is not a cartilage disease. *Annals of the Rheumatic Diseases* 65(10), 1261-4.

Brown, M.P. & Valko, K. (1980). A technique for intra-articular injection of the equine tarsometatarsal joint. *Veterinary Medicine, Small Animal Clinician* 75(2), 265-70.

Buck, R.J., Wyman, B.T., Le Graverand, M.P., Hudelmaier, M., Wirth, W. & Eckstein, F. (2010). Osteoarthritis may not be a one-way-road of cartilage loss--comparison of spatial patterns of cartilage change between osteoarthritic and healthy knees. *Osteoarthritis and Cartilage* 18(3), 329-35.

Buckwalter, J.A. & Hunziker, E.B. (1999). Articular cartilage morphology and biology. In: Archer, C.W.*, et al.* (Eds.) *Biology of the synovial joint*. pp. 75 - 100. Amsterdam: Harwood academic publishers. ISBN 90-5702-327-X.

Burr, D.B. (2004a). Anatomy and physiology of the mineralized tissues: Role in the pathogenesis of osteoarthrosis. *Osteoarthritis and Cartilage* 12, Supplement(0), 20-30.

Burr, D.B. (2004b). The importance of subchondral bone in the progression of osteoarthritis. *Journal of Rheumatology. Supplement* 70, 77-80.

Burr, D.B. (2005). Increased biological activity of subchondral mineralized tissues underlies the progressive deterioration of articular cartilage in osteoarthritis. *Journal of Rheumatology* 32(6), 1156-8; discussion 1158-9.

Burstein, D. & Hunter, D.J. (2009). "Why aren't we there yet?" Re-examining standard paradigms in imaging of OA: Summary of the 2nd annual workshop on imaging based measures of osteoarthritis. *Osteoarthritis and Cartilage* 17(5), 571-578.

Bushberg, J., Seibert, J., Leidholdt, E. & Boone, J. (2012). *The essential physics of medical imaging*. 3rd. ed. Philadelphia: Lippincott Williams & Wilkins. ISBN 9780781780575; 0781780578; 9781451118100 (International ed.).

Calvo, E., Palacios, I., Delgado, E., Sánchez-Pernaute, O., Largo, R., Egido, J. & Herrero-Beaumont, G. (2004). Histopathological correlation of cartilage swelling detected by magnetic resonance imaging in early experimental osteoarthritis. *Osteoarthritis and Cartilage* 12(11), 878-886.

Chen-An, P., Andreassen, K.V., Henriksen, K., Karsdal, M.A. & Bay-Jensen, A.C. (2013). Investigation of chondrocyte hypertrophy and cartilage calcification in a full-depth articular cartilage explants model. *Rheumatology International* 33(2), 401-11.

Chiba, K., Ito, M., Osaki, M., Uetani, M. & Shindo, H. (2011). In vivo structural analysis of subchondral trabecular bone in osteoarthritis of the hip using multi-detector row CT. *Osteoarthritis and Cartilage* 19(2), 180-5.

Chiba, K., Uetani, M., Kido, Y., Ito, M., Okazaki, N., Taguchi, K. & Shindo, H. (2012). Osteoporotic changes of subchondral trabecular bone in osteoarthritis of the knee: a 3-T MRI study. *Osteoporosis International* 23(2), 589-97.

Chundru, R., Baum, T., Nardo, L., Nevitt, M.C., Lynch, J., McCulloch, C.E. & Link, T.M. (2013). Focal knee lesions in knee pairs of asymptomatic and symptomatic subjects with OA risk factors-Data from the Osteoarthritis Initiative. *European Journal of Radiology*.

Cibere, J., Zhang, H., Garnero, P., Poole, A.R., Lobanok, T., Saxne, T., Kraus, V.B., Way, A., Thorne, A., Wong, H., Singer, J., Kopec, J., Guermazi, A., Peterfy, C., Nicolaou, S., Munk, P.L. & Esdaile, J.M. (2009). Association of biomarkers with pre-radiographically defined and radiographically defined knee osteoarthritis in a population-based study. *Arthritis and Rheumatism* 60(5), 1372-80.

Cluzel, C., Blond, L., Fontaine, P., Olive, J. & Laverty, S. (2013). Foetal and postnatal equine articular cartilage development: magnetic resonance imaging and polarised light microscopy. *European cells & materials* 26, 33-47; discussion 47-8.

D'Anjou, M.-A., Moreau, M., Troncy, É., Martel-Pelletier, J., Abram, F., Raynauld, J.-P. & Pelletier, J.-P. (2008). Osteophytosis, Subchondral Bone Sclerosis, Joint Effusion and Soft Tissue Thickening in Canine Experimental Stifle Osteoarthritis: Comparison Between 1.5T Magnetic Resonance Imaging and Computed Radiography. *Veterinary Surgery* 37(2), 166-177.

Dalrymple, N.C., Prasad, S.R., Freckleton, M.W. & Chintapalli, K.N. (2005). Introduction to the language of three-dimensional imaging with multidetector CT. *Radiographics* 25(5), 1409-28.

Dawson, J., Gustard, S. & Beckmann, N. (1999). High-resolution three-dimensional magnetic resonance imaging for the investigation of knee joint damage during the time course of antigen-induced arthritis in rabbits. *Arthritis and Rheumatism* 42(1), 119-128.

De Clerck, N. & Postnov, A. (2007). High Resolution X-ray Microtomography: Applications in Biomedical Research. In: Ntziachristos, V*., et al.* (Eds.) *Textbook of in vivo Imaging in Vertebrates*. pp. 57-78. Chichester, UK: John Wiley & Sons Ltd. ISBN 978-0-470-01528-5.

Desbrosse, F.G., Vandeweerd, J.M.E.F., Perrin, R.A.R., Clegg, P.D., Launois, M.T., Brogniez, L. & Gehin, S.P. (2008). A technique for computed

tomography (CT) of the foot in the standing horse. *Equine Veterinary Education* 20(2), 93-98.
Dieppe, P. & Kirwan, J. (1994). The localization of osteoarthritis. *British Journal of Rheumatology* 33(3), 201-3.
Ding, C., Cicuttini, F. & Jones, G. (2007). Tibial subchondral bone size and knee cartilage defects: relevance to knee osteoarthritis. *Osteoarthritis and Cartilage* 15(5), 479-86.
Ding, C., Cicuttini, F., Scott, F., Cooley, H., Boon, C. & Jones, G. (2006). Natural history of knee cartilage defects and factors affecting change. *Archives of Internal Medicine* 166(6), 651-8.
Ding, C., Cicuttini, F., Scott, F., Cooley, H. & Jones, G. (2005a). Association between age and knee structural change: a cross sectional MRI based study. *Annals of the Rheumatic Diseases* 64(4), 549-55.
Ding, C., Garnero, P., Cicuttini, F., Scott, F., Cooley, H. & Jones, G. (2005b). Knee cartilage defects: association with early radiographic osteoarthritis, decreased cartilage volume, increased joint surface area and type II collagen breakdown. *Osteoarthritis and Cartilage* 13(3), 198-205.
Ding, C., Jones, G., Wluka, A.E. & Cicuttini, F. (2010). What can we learn about osteoarthritis by studying a healthy person against a person with early onset of disease? *Current Opinion in Rheumatology* 22(5), 520-527.
Doube, M., Firth, E.C. & Boyde, A. (2007). Variations in articular calcified cartilage by site and exercise in the 18-month-old equine distal metacarpal condyle. *Osteoarthritis and Cartilage* 15(11), 1283-92.
Egenvall, A., Penell, J.C., Bonnett, B.N., Olson, P. & Pringle, J. (2006). Mortality of Swedish horses with complete life insurance between 1997 and 2000: variations with sex, age, breed and diagnosis. *The Veterinary Record* 158(12), 397.
Eksell, P., Axelsson, M., Brostrom, H., Roneus, B., Haggstrom, J. & Carlsten, J. (1998). Prevalence and risk factors of bone spavin in Icelandic horses in Sweden: a radiographic field study. *Acta Veterinaria Scandinavica* 39(3), 339-48.
Eksell, P., Uhlhorn, H. & Carlsten, J. (1999). Evaluation of different projections for radiographic detection of tarsal degenerative joint disease in Icelandic Horses. *Veterinary Radiology and Ultrasound* 40(3), 228-232.
ESR (2013). European society of radiology (ESR) statement on the stepwise development of imaging biomarkers. *Insights into imaging* 4(2), 147-52.
Felson, D.T. (2013). Osteoarthritis as a disease of mechanics. *Osteoarthritis and Cartilage* 21(1), 10-5.
Felson, D.T. & Neogi, T. (2004). Osteoarthritis: Is it a disease of cartilage or of bone? *Arthritis and Rheumatism* 50(2), 341-344.
Finn, P. *New rules aimed to reduce the prevalence of bone spavin in Icelandic horses*. [online] Available from: http://www.feiffengur.com/documents/brspavin06.pdf. [Accessed 26th April 2013].

Frisbie, D.D., Cross, M.W. & McIlwraith, C.W. (2006). A comparative study of articular cartilage thickness in the stifle of animal species used in human pre-clinical studies compared to articular cartilage thickness in the human knee. *Veterinary and comparative orthopaedics and traumatology* 19(3), 142-6.

Gahunia, H.K., Babyn, P., Lemaire, C., Kessler, M.J. & Pritzker, K.P.H. (1995). Osteoarthritis staging: comparison between magnetic resonance imaging, gross pathology and histopathology in the rhesus macaque. *Osteoarthritis and Cartilage* 3(3), 169-180.

Gaschen, L. & Burba, D.J. (2012). Musculoskeletal injury in thoroughbred racehorses: correlation of findings using multiple imaging modalities. *Veterinary Clinics of North America. Equine Practice* 28(3), 539-61.

Glowatzki-Mullis, M.L., Muntwyler, J., Pfister, W., Marti, E., Rieder, S., Poncet, P.A. & Gaillard, C. (2006). Genetic diversity among horse populations with a special focus on the Franches-Montagnes breed. *Animal Genetics* 37(1), 33-9.

Gold, G.E., Chen, C.A., Koo, S., Hargreaves, B.A. & Bangerter, N.K. (2009). Recent advances in MRI of articular cartilage. *American Journal of Roentgenology* 193(3), 628-38.

Goldring, M.B. & Goldring, S.R. (2007). Osteoarthritis. *Journal of Cellular Physiology* 213(3), 626-34.

Guermazi, A., Niu, J., Hayashi, D., Roemer, F.W., Englund, M., Neogi, T., Aliabadi, P., McLennan, C.E. & Felson, D.T. (2012). Prevalence of abnormalities in knees detected by MRI in adults without knee osteoarthritis: population based observational study (Framingham Osteoarthritis Study). *BMJ* 345, e5339.

Guermazi, A., Roemer, F.W., Burstein, D. & Hayashi, D. (2011). Why radiography should no longer be considered a surrogate outcome measure for longitudinal assessment of cartilage in knee osteoarthritis. *Arthritis research & therapy* 13(6), 247.

Guermazi, A., Roemer, F.W., Felson, D.T. & Brandt, K.D. (2013a). Motion for debate: osteoarthritis clinical trials have not identified efficacious therapies because traditional imaging outcome measures are inadequate. *Arthritis and Rheumatism* 65(11), 2748-58.

Guermazi, A., Roemer, F.W., Haugen, I.K., Crema, M.D. & Hayashi, D. (2013b). MRI-based semiquantitative scoring of joint pathology in osteoarthritis. *Nature reviews. Rheumatology* 9(4), 236-51.

Hardy, P.A., Newmark, R., Liu, Y.M., Meier, D., Norris, S., Piraino, D.W. & Shah, A. (2000). The influence of the resolution and contrast on measuring the articular cartilage volume in magnetic resonance images. *Magnetic Resonance Imaging* 18(8), 965-72.

Hayashi, D., Guermazi, A. & Roemer, F.W. (2012a). MRI of osteoarthritis: the challenges of definition and quantification. *Seminars in musculoskeletal radiology* 16(5), 419-30.

Hayashi, D., Roemer, F.W. & Guermazi, A. (2012b). Osteoarthritis year 2011 in review: imaging in OA--a radiologists' perspective. *Osteoarthritis and Cartilage* 20(3), 207-14.

Heinegard, D. (2009). Proteoglycans and more--from molecules to biology. *International Journal of Experimental Pathology* 90(6), 575-86.

Heinegard, D. & Saxne, T. (2011). The role of the cartilage matrix in osteoarthritis. *Nature reviews. Rheumatology* 7(1), 50-6.

Hinz, A. & Fischer, A.T., Jr. (2011). Comparison of the accuracy of radiography and ultrasonography for detection of articular lesions in horses. *Veterinary Surgery* 40(7), 881-5.

Howell, P.G. & Boyde, A. (1994). Monte Carlo simulations of electron scattering in bone. *Bone* 15(3), 285-91.

Howell, P.G. & Boyde, A. (2003). Volumes from which calcium and phosphorus X-rays arise in electron probe emission microanalysis of bone: Monte Carlo simulation. *Calcified Tissue International* 72(6), 745-9.

Hunter, D.J., Arden, N., Conaghan, P.G., Eckstein, F., Gold, G., Grainger, A., Guermazi, A., Harvey, W., Jones, G., Hellio Le Graverand, M.P., Laredo, J.D., Lo, G., Losina, E., Mosher, T.J., Roemer, F. & Zhang, W. (2011a). Definition of osteoarthritis on MRI: results of a Delphi exercise. *Osteoarthritis and Cartilage* 19(8), 963-969.

Hunter, D.J. & Eckstein, F. (2011). From joint anatomy to clinical outcomes in osteoarthritis and cartilage repair: summary of the fifth annual osteoarthritis imaging workshop. *Osteoarthritis and Cartilage* 19(11), 1263-9.

Hunter, D.J. & Guermazi, A. (2012). Imaging techniques in osteoarthritis. *PM & R* 4(5 Suppl), S68-74.

Hunter, D.J., Lo, G.H., Gale, D., Grainger, A.J., Guermazi, A. & Conaghan, P.G. (2008). The reliability of a new scoring system for knee osteoarthritis MRI and the validity of bone marrow lesion assessment: BLOKS (Boston Leeds Osteoarthritis Knee Score). *Annals of the Rheumatic Diseases* 67(2), 206-11.

Hunter, D.J., Zhang, W., Conaghan, P.G., Hirko, K., Menashe, L., Li, L., Reichmann, W.M. & Losina, E. (2011b). Systematic review of the concurrent and predictive validity of MRI biomarkers in OA. *Osteoarthritis and Cartilage* 19(5), 557-588.

Innes, J.F. & Clegg, P. (2010). Comparative rheumatology: what can be learnt from naturally occurring musculoskeletal disorders in domestic animals? *Rheumatology* 49(6), 1030-1039.

Inoué, S. (1995). Foundations of confocal scanned imaging in light microscopy. In: Pawley, J.B. (Ed.) *Handbook of Biological Confocal Microscopy*. pp. 1-17. New York: Plenum Press.

Jeffery, A.K., Blunn, G.W., Archer, C.W. & Bentley, G. (1991). Three-dimensional collagen architecture in bovine articular cartilage. *The Journal of bone and joint surgery. British volume* 73(5), 795-801.

Jones, G., Ding, C., Scott, F., Glisson, M. & Cicuttini, F. (2004). Early radiographic osteoarthritis is associated with substantial changes in cartilage volume and tibial bone surface area in both males and females. *Osteoarthritis and Cartilage* 12(2), 169-74.

Kaneko, H., Ishijima, M., Futami, I., Tomikawa-Ichikawa, N., Kosaki, K., Sadatsuki, R., Yamada, Y., Kurosawa, H., Kaneko, K. & Arikawa-Hirasawa, E. (2013). Synovial perlecan is required for osteophyte formation in knee osteoarthritis. *Matrix Biology* 32(3-4), 178-87.

Keegan, K.G., Kramer, J., Yonezawa, Y., Maki, H., Pai, P.F., Dent, E.V., Kellerman, T.E., Wilson, D.A. & Reed, S.K. (2011). Assessment of repeatability of a wireless, inertial sensor-based lameness evaluation system for horses. *American Journal of Veterinary Research* 72(9), 1156-63.

Kellgren, J.H. & Lawrence, J.S. (1957). Radiological assessment of osteo-arthrosis. *Annals of the Rheumatic Diseases* 16(4), 494-502.

Kerkhof, H.J., Meulenbelt, I., Akune, T., Arden, N.K., Aromaa, A., Bierma-Zeinstra, S.M., Carr, A., Cooper, C., Dai, J., Doherty, M., Doherty, S.A., Felson, D., Gonzalez, A., Gordon, A., Harilainen, A., Hart, D.J., Hauksson, V.B., Heliovaara, M., Hofman, A., Ikegawa, S., Ingvarsson, T., Jiang, Q., Jonsson, H., Jonsdottir, I., Kawaguchi, H., Kloppenburg, M., Kujala, U.M., Lane, N.E., Leino-Arjas, P., Lohmander, L.S., Luyten, F.P., Malizos, K.N., Nakajima, M., Nevitt, M.C., Pols, H.A., Rivadeneira, F., Shi, D., Slagboom, E., Spector, T.D., Stefansson, K., Sudo, A., Tamm, A., Tamm, A.E., Tsezou, A., Uchida, A., Uitterlinden, A.G., Wilkinson, J.M., Yoshimura, N., Valdes, A.M. & van Meurs, J.B. (2011). Recommendations for standardization and phenotype definitions in genetic studies of osteoarthritis: the TREAT-OA consortium. *Osteoarthritis and Cartilage* 19(3), 254-64.

Kijowski, R., Blankenbaker, D.G., Davis, K.W., Shinki, K., Kaplan, L.D. & De Smet, A.A. (2009). Comparison of 1.5- and 3.0-T MR imaging for evaluating the articular cartilage of the knee joint. *Radiology* 250(3), 839-48.

Kornaat, P.R., Ceulemans, R.Y.T., Kroon, H.M., Riyazi, N., Kloppenburg, M., Carter, W.O., Woodworth, T.G. & Bloem, J.L. (2005). MRI assessment of knee osteoarthritis: Knee Osteoarthritis Scoring System (KOSS)—inter-observer and intra-observer reproducibility of a compartment-based scoring system. *Skeletal Radiology* 34(2), 95-102.

Kraus-Hansen, A.E., Jann, H.W., Kerr, D.V. & Fackelman, G.E. (1992). Arthrographic analysis of communication between the tarsometatarsal and distal intertarsal joints of the horse. *Veterinary Surgery* 21(2), 139-44.

Labens, R., Innocent, G.T. & Voute, L.C. (2007a). Reliability of a quantitative rating scale for assessment of horses with distal tarsal osteoarthritis. *Veterinary Radiology and Ultrasound* 48(3), 204-11.

Labens, R., Mellor, D.J. & Voute, L.C. (2007b). Retrospective study of the effect of intra-articular treatment of osteoarthritis of the distal tarsal joints in 51 horses. *Veterinary Record* 161(18), 611-6.

Lacourt, M., Gao, C., Li, A., Girard, C., Beauchamp, G., Henderson, J.E. & Laverty, S. (2012). Relationship between cartilage and subchondral bone lesions in repetitive impact trauma-induced equine osteoarthritis. *Osteoarthritis and Cartilage* 20(6), 572-83.

Lane, N.E., Brandt, K., Hawker, G., Peeva, E., Schreyer, E., Tsuji, W. & Hochberg, M.C. (2011). OARSI-FDA initiative: defining the disease state of osteoarthritis. *Osteoarthritis and Cartilage* 19(5), 478-482.

Lange, T., Maclaren, J., Herbst, M., Lovell-Smith, C., Izadpanah, K. & Zaitsev, M. (2013). Knee cartilage MRI with in situ mechanical loading using prospective motion correction. *Magnetic Resonance in Medicine*.

Lanovaz, J.L., Khumsap, S., Clayton, H.M., Stick, J.A. & Brown, J. (2002). Three-dimensional kinematics of the tarsal joint at the trot. *Equine Veterinary Journal* Supplement 34, 308-13.

Laverty, S., Stover, S.M., Belanger, D., O'Brien, T.R., Pool, R.R., Pascoe, J.R., Taylor, K. & Harrington, T. (1991). Radiographic, high detail radiographic, microangiographic and histological findings of the distal portion of the tarsus in weanling, young and adult horses. *Equine Veterinary Journal* 23(6), 413-21.

Loeser, R.F., Goldring, S.R., Scanzello, C.R. & Goldring, M.B. (2012). Osteoarthritis: a disease of the joint as an organ. *Arthritis and Rheumatism* 64(6), 1697-707.

Loeuille, D. & Chary-Valckenaere, I. (2012). MRI in OA: from cartilage to bone marrow lesion. *Osteoporosis International* 23 Suppl 8, 867-9.

Loeuille, D., Olivier, P., Mainard, D., Gillet, P., Netter, P. & Blum, A. (1998). Magnetic resonance imaging of normal and osteoarthritic cartilage. *Arthritis and Rheumatism* 41(6), 963-975.

Lotz, M.K., Otsuki, S., Grogan, S.P., Sah, R., Terkeltaub, R. & D'Lima, D. (2010). Cartilage cell clusters. *Arthritis and Rheumatism* 62(8), 2206-18.

Luyten, F., Denti, M., Filardo, G., Kon, E. & Engebretsen, L. (2012). Definition and classification of early osteoarthritis of the knee. *Knee Surgery, Sports Traumatology, Arthroscopy* 20(3), 401-406.

Madry, H., Luyten, F.P. & Facchini, A. (2012). Biological aspects of early osteoarthritis. *Knee Surgery, Sports Traumatology, Arthroscopy* 20(3), 407-22.

Madry, H., van Dijk, C. & Mueller-Gerbl, M. (2010). The basic science of the subchondral bone. *Knee Surgery, Sports Traumatology, Arthroscopy* 18(4), 419-433.

Mair, T.S., Kinns, J., Jones, R.D. & Bolas, N.M. (2005). Magnetic resonance imaging of the distal limb of the standing horse. *Equine Veterinary Education* 17(2), 74-78.

Malda, J., de Grauw, J.C., Benders, K.E., Kik, M.J., van de Lest, C.H., Creemers, L.B., Dhert, W.J. & van Weeren, P.R. (2013). Of mice, men and

elephants: the relation between articular cartilage thickness and body mass. *PloS one* 8(2), e57683.
Mankin, H.J., Dorfman, H., Lippiello, L. & Zarins, A. (1971). Biochemical and metabolic abnormalities in articular cartilage from osteo-arthritic human hips. II. Correlation of morphology with biochemical and metabolic data. *The Journal of Bone and Joint Surgery. American Volume* 53(3), 523-37.
Martel-Pelletier, J., Wildi, L.M. & Pelletier, J.P. (2011). Future therapeutics for osteoarthritis. *Bone* 51(2), 297-311.
Masi, J.N., Sell, C.A., Phan, C., Han, E., Newitt, D., Steinbach, L., Majumdar, S. & Link, T.M. (2005). Cartilage MR imaging at 3.0 versus that at 1.5 T: preliminary results in a porcine model. *Radiology* 236(1), 140-50.
May, S.A., Wyn-Jones, G. & Peremans, K.Y. (1986). Importance of oblique views in radiography of the equine limb. *Equine Veterinary Journal* 18(1), 7-13.
McGibbon, C.A., Bencardino, J., Yeh, E.D. & Palmer, W.E. (2003). Accuracy of cartilage and subchondral bone spatial thickness distribution from MRI. *Journal of Magnetic Resonance Imaging* 17(6), 703-15.
McGibbon, C.A., Dupuy, D.E., Palmer, W.E. & Krebs, D.E. (1998). Cartilage and subchondral bone thickness distribution with MR imaging. *Academic Radiology* 5(1), 20-25.
McGibbon, C.A. & Trahan, C.A. (2003). Measurement accuracy of focal cartilage defects from MRI and correlation of MRI graded lesions with histology: a preliminary study. *Osteoarthritis and Cartilage* 11(7), 483-493.
McGonagle, D., Tan, A.L., Carey, J. & Benjamin, M. (2010). The anatomical basis for a novel classification of osteoarthritis and allied disorders. *Journal of Anatomy* 216(3), 279-91.
McIlwraith, C.W., Fortier, L.A., Frisbie, D.D. & Nixon, A.J. (2011). Equine Models of Articular Cartilage Repair. *Cartilage* 2(4), 317-326.
McIlwraith, C.W., Frisbie, D.D., Kawcak, C.E., Fuller, C.J., Hurtig, M. & Cruz, A. (2010). The OARSI histopathology initiative – recommendations for histological assessments of osteoarthritis in the horse. *Osteoarthritis and Cartilage* 18, Supplement 3(0), S93-S105.
McKnight, A.L., Manduca, A., Felmlee, J.P., Rossman, P.J., McGee, K.P. & Ehman, R.L. (2004). Motion-correction techniques for standing equine MRI. *Veterinary Radiology and Ultrasound* 45(6), 513-9.
Menashe, L., Hirko, K., Losina, E., Kloppenburg, M., Zhang, W., Li, L. & Hunter, D.J. (2012). The diagnostic performance of MRI in osteoarthritis: a systematic review and meta-analysis. *Osteoarthritis and Cartilage* 20(1), 13-21.
Modl, J.M., Sether, L.A., Haughton, V.M. & Kneeland, J.B. (1991). Articular cartilage: correlation of histologic zones with signal intensity at MR imaging. *Radiology* 181(3), 853-855.
Monici, M. (2005). Cell and tissue autofluorescence research and diagnostic applications. *Biotechnology annual review* 11, 227-56.

Mow, V.C., Ratcliffe, A. & Robin Poole, A. (1992). Cartilage and diarthrodial joints as paradigms for hierarchical materials and structures. *Biomaterials* 13(2), 67-97.

Moyer, W. (1978). Bone spavin: a clinical review. *The Journal of Equine Medicine and Surgery* 2(9), 362, 370-371.

Murray, R.C., Blunden, T.S., Branch, M.V., Tranquille, C.A., Dyson, S.J., Parkin, T.D. & Goodship, A.E. (2009a). Evaluation of age-related changes in the structure of the equine tarsometatarsal osteochondral unit. *American Journal of Veterinary Research* 70(1), 30-6.

Murray, R.C., Blunden, T.S., Schramme, M.C. & Dyson, S.J. (2006). How does magnetic resonance imaging represent histologic findings in the equine digit? *Veterinary Radiology and Ultrasound* 47(1), 17-31.

Murray, R.C., Branch, M.V., Tranquille, C. & Woods, S. (2005). Validation of magnetic resonance imaging for measurement of equine articular cartilage and subchondral bone thickness. *American Journal of Veterinary Research* 66(11), 1999-2005.

Murray, R.C., Dyson, S., Branch, M. & Schramme, M. (2007). Validation of Magnetic Resonance Imaging Use in Equine Limbs. *Clinical Techniques in Equine Practice* 6(1), 26-36.

Murray, R.C., Mair, T.S., Sherlock, C.E. & Blunden, A.S. (2009b). Comparison of high-field and low-field magnetic resonance images of cadaver limbs of horses. *The Veterinary record* 165(10), 281-8.

Myers, S.L., Flusser, D., Brandt, K.D. & Heck, D.A. (1992). Prevalence of cartilage shards in synovium and their association with synovitis in patients with early and endstage osteoarthritis. *The Journal of rheumatology* 19(8), 1247-51.

O'Brien, T., Baker, T.A., Brounts, S.H., Sample, S.J., Markel, M.D., Scollay, M.C., Marquis, P. & Muir, P. (2011). Detection of Articular Pathology of the Distal Aspect of the Third Metacarpal Bone in Thoroughbred Racehorses: Comparison of Radiography, Computed Tomography and Magnetic Resonance Imaging. *Veterinary Surgery* 40(8), 942-951.

Oegema, T.R., Jr., Carpenter, R.J., Hofmeister, F. & Thompson, R.C., Jr. (1997). The interaction of the zone of calcified cartilage and subchondral bone in osteoarthritis. *Microscopy Research and Technique* 37(4), 324-32.

Oehler, S., Neureiter, D., Meyer-Scholten, C. & Aigner, T. (2002). Subtyping of osteoarthritic synoviopathy. *Clinical and Experimental Rheumatology* 20(5), 633-40.

Olive, J. (2010). Distal interphalangeal articular cartilage assessment using low-field magnetic resonance imaging. *Veterinary Radiology and Ultrasound* 51(3), 259-266.

Olive, J., D'Anjou, M.-A., Girard, C., Laverty, S. & Theoret, C.L. (2009). Imaging and histological features of central subchondral osteophytes in racehorses with metacarpophalangeal joint osteoarthritis. *Equine Veterinary Journal* 41(9), 859-864.

Olive, J., D'Anjou, M., Alexander, K., Laverty, S. & Theoret, C. (2010a). Comparison of magnetic resonance imaging, computed tomography, and radiography for assessment of noncartilaginous changes in equine metacarpophalangeal osteoarthritis. *Veterinary Radiology and Ultrasound* 51(3), 267-279.

Olive, J., D'Anjou, M., Girard, C., Laverty, S. & Theoret, C. (2010b). Fat-suppressed spoiled gradient-recalled imaging of equine metacarpophalangeal articular cartilage. *Veterinary Radiology and Ultrasound* 51(2), 107-115.

Palmer, A.J., Brown, C.P., McNally, E.G., Price, A.J., Tracey, I., Jezzard, P., Carr, A.J. & Glyn-Jones, S. (2013). Non-invasive imaging of cartilage in early osteoarthritis. *The bone & joint journal* 95-B(6), 738-46.

Palmer, J.L., Bertone, A.L., Malemud, C.J., Carter, B.G., Papay, R.S. & Mansour, J. (1995). Site-specific proteoglycan characteristics of third carpal articular cartilage in exercised and nonexercised horses. *American Journal of Veterinary Research* 56(12), 1570-6.

Pan, J., Wang, B., Li, W., Zhou, X., Scherr, T., Yang, Y., Price, C. & Wang, L. (2012). Elevated cross-talk between subchondral bone and cartilage in osteoarthritic joints. *Bone* 51(2), 212-7.

Pan, J., Zhou, X., Li, W., Novotny, J.E., Doty, S.B. & Wang, L. (2009). In situ measurement of transport between subchondral bone and articular cartilage. *Journal of Orthopaedic Research* 27(10), 1347-52.

Peterfy, C.G., Guermazi, A., Zaim, S., Tirman, P.F.J., Miaux, Y., White, D., Kothari, M., Lu, Y., Fye, K., Zhao, S. & Genant, H.K. (2004). Whole-Organ Magnetic Resonance Imaging Score (WORMS) of the knee in osteoarthritis. *Osteoarthritis and Cartilage* 12(3), 177-190.

Pool, R.R. (1996). Pathological manifestations of joint disease in the athletic horse. In: McIlwraith, C.W*., et al.* (Eds.) *Joint Disease in the Horse*. 1st. ed. pp. 87-104. Philadelphia: W. B. Saunders Co.

Pritzker, K.P.H. & Aigner, T. (2010). Terminology of osteoarthritis cartilage and bone histopathology – a proposal for a consensus. *Osteoarthritis and Cartilage* 18, Supplement 3(0), S7-S9.

Pritzker, K.P.H., Gay, S., Jimenez, S.A., Ostergaard, K., Pelletier, J.P., Revell, P.A., Salter, D. & van den Berg, W.B. (2006). Osteoarthritis cartilage histopathology: grading and staging. *Osteoarthritis and Cartilage* 14(1), 13-29.

Quasnichka, H.L., Anderson-MacKenzie, J.M., Tarlton, J.F., Sims, T.J., Billingham, M.E. & Bailey, A.J. (2005). Cruciate ligament laxity and femoral intercondylar notch narrowing in early-stage knee osteoarthritis. *Arthritis and Rheumatism* 52(10), 3100-9.

Quatman, C.E., Hettrich, C.M., Schmitt, L.C. & Spindler, K.P. (2011). The clinical utility and diagnostic performance of magnetic resonance imaging for identification of early and advanced knee osteoarthritis: a systematic review. *The American journal of sports medicine* 39(7), 1557-68.

Raes, E.V., Bergman, E.H., van der Veen, H., Vanderperren, K., Van der Vekens, E. & Saunders, J.H. (2011). Comparison of cross-sectional anatomy and computed tomography of the tarsus in horses. *American Journal of Veterinary Research* 72(9), 1209-21.

Raynauld, J.P., Martel-Pelletier, J., Berthiaume, M.J., Labonte, F., Beaudoin, G., de Guise, J.A., Bloch, D.A., Choquette, D., Haraoui, B., Altman, R.D., Hochberg, M.C., Meyer, J.M., Cline, G.A. & Pelletier, J.P. (2004). Quantitative magnetic resonance imaging evaluation of knee osteoarthritis progression over two years and correlation with clinical symptoms and radiologic changes. *Arthritis and Rheumatism* 50(2), 476-87.

Roemer, F.W., Crema, M.D., Trattnig, S. & Guermazi, A. (2011). Advances in imaging of osteoarthritis and cartilage. *Radiology* 260(2), 332-54.

Rubenstein, J.D., Li, J.G., Majumdar, S. & Henkelman, R.M. (1997). Image resolution and signal-to-noise ratio requirements for MR imaging of degenerative cartilage. *American Journal of Roentgenology* 169(4), 1089-96.

Sack, W.O. & Orsini, P.G. (1981). Distal intertarsal and tarsometatarsal joints in the horse: communication and injection sites. *Journal of the American Veterinary Medical Association* 179(4), 355-9.

Salo, E.N., Nissi, M.J., Kulmala, K.A.M., Tiitu, V., Töyräs, J. & Nieminen, M.T. (2012). Diffusion of Gd-DTPA2− into articular cartilage. *Osteoarthritis and Cartilage* 20(2), 117-126.

Sanchez, C., Deberg, M.A., Piccardi, N., Msika, P., Reginster, J.Y. & Henrotin, Y.E. (2005). Subchondral bone osteoblasts induce phenotypic changes in human osteoarthritic chondrocytes. *Osteoarthritis and Cartilage* 13(11), 988-97.

Scanzello, C.R. & Goldring, S.R. (2012). The role of synovitis in osteoarthritis pathogenesis. *Bone* 51(2), 249-57.

Schamhardt, H.C., Hartman, W. & Lammertink, J.L. (1989). Forces loading the tarsal joint in the hind limb of the horse, determined from in vivo strain measurements of the third metatarsal bone. *American Journal of Veterinary Research* 50(5), 728-33.

Schiphof, D., Oei, E.H., Hofman, A., Waarsing, J.H., Weinans, H. & Bierma-Zeinstra, S.M. (2014). Sensitivity and associations with pain and body weight of an MRI definition of knee osteoarthritis compared with radiographic Kellgren and Lawrence criteria: a population-based study in middle-aged females. *Osteoarthritis and Cartilage* 22(3), 440-6.

Schmitz, N., Laverty, S., Kraus, V.B. & Aigner, T. (2010). Basic methods in histopathology of joint tissues. *Osteoarthritis and Cartilage* 18, Supplement 3(0), S113-S116.

Shelley, J. & Dyson, S. (1984). Interpreting radiographs 5: radiology of the equine hock. *Equine Veterinary Journal* 16(6), 488-95.

Shively, M.J. (1982). Correct anatomic nomenclature for the joints of the equine tarsus. *Equine Practice* 4(4), 9-13.

Sisson, S. (1975). Equine syndesmology. In: Getty, R. (Ed.) *The anatomy of the domestic animals*. 5th. ed. pp. 349–375. Philadelphia: Saunders.

Smith, M.A., Dyson, S.J. & Murray, R.C. (2012). Reliability of high- and low-field magnetic resonance imaging systems for detection of cartilage and bone lesions in the equine cadaver fetlock. *Equine Veterinary Journal* 44(6), 684-691.

Sokoloff, L. (1993). Microcracks in the calcified layer of articular cartilage. *Archives of Pathology and Laboratory Medicine* 117(2), 191-5.

Squires, G.R., Okouneff, S., Ionescu, M. & Poole, A.R. (2003). The pathobiology of focal lesion development in aging human articular cartilage and molecular matrix changes characteristic of osteoarthritis. *Arthritis and Rheumatism* 48(5), 1261-70.

Stahl, R., Krug, R., Kelley, D.A., Zuo, J., Ma, C.B., Majumdar, S. & Link, T.M. (2009). Assessment of cartilage-dedicated sequences at ultra-high-field MRI: comparison of imaging performance and diagnostic confidence between 3.0 and 7.0 T with respect to osteoarthritis-induced changes at the knee joint. *Skeletal Radiology* 38(8), 771-83.

Stokes, D. (2009). *Principles and Practice of Variable Pressure: Environmental Scanning Electron Microscopy (VP-ESEM)*. Chichester, GBR: Wiley.

Strand, E., Braathen, L.C., Hellsten, M.C., Huse-Olsen, L. & Bjornsdottir, S. (2007). Radiographic closure time of appendicular growth plates in the Icelandic horse. *Acta Veterinaria Scandinavica* 49, 19.

Strimbu, K. & Tavel, J.A. (2010). What are biomarkers? *Current opinion in HIV and AIDS* 5(6), 463-6.

Suri, S. & Walsh, D.A. (2012). Osteochondral alterations in osteoarthritis. *Bone* 51(2), 204-11.

Tranquille, C.A., Blunden, A.S., Dyson, S.J., Parkin, T.D.H., Goodship, A.E. & Murray, R.C. (2009). Effect of exercise on thicknesses of mature hyaline cartilage, calcified cartilage, and subchondral bone of equine tarsi. *American Journal of Veterinary Research* 70(12), 1477-1483.

Tranquille, C.A., Dyson, S.J., Blunden, A.S., Collins, S.N., Parkin, T.D.H., Goodship, A.E. & Murray, R.C. (2011). Histopathologic features of distal tarsal joint cartilage and subchondral bone in ridden and pasture-exercised horses. *American Journal of Veterinary Research* 72(1), 33-41.

Trattnig, S., Huber, M., Breitenseher, M.J., Trnka, H.-J., Rand, T., Kaider, A., Helbich, T., Imhof, H. & Resnick, D. (1998). Imaging Articular Cartilage Defects with 3D Fat-Suppressed Echo Planar Imaging: Comparison with Conventional 3D Fat-Suppressed Gradient Echo Sequence and Correlation with Histology. *Journal of Computer Assisted Tomography* 22(1), 8-14.

Turmezei, T.D., Fotiadou, A., Lomas, D.J., Hopper, M.A. & Poole, K.E. (2014). A new CT grading system for hip osteoarthritis. *Osteoarthritis and Cartilage*.

Vajda, E.G., Humphrey, S., Skedros, J.G. & Bloebaum, R.D. (1999). Influence of topography and specimen preparation on backscattered electron images of bone. *Scanning* 21(6), 379-87.

Waldschmidt, J.G., Braunstein, E.M. & Buckwalter, K.A. (1999). Magnetic resonance imaging of osteoarthritis. *Rheumatic Diseases Clinics of North America* 25(2), 451-65.

van der Kraan, P.M. & van den Berg, W.B. (2007). Osteophytes: relevance and biology. *Osteoarthritis and Cartilage* 15(3), 237-244.

van der Kraan, P.M. & van den Berg, W.B. (2012). Chondrocyte hypertrophy and osteoarthritis: role in initiation and progression of cartilage degeneration? *Osteoarthritis and Cartilage* 20(3), 223-32.

van der Veen, G., Kingmans, J., van Veldhuizen, A.E., van de Watering, C.C., Barneveld, A., Dik, K.J., van der Meij, G.J.W. & van de Belt, A.J. (1994). *The Frequency and Heredity of Navicular Disease, Sesamoidosis, Fetlock Joint arthrosis, Bone Spavin, Osteochondrosis of the Hock: A Radiographic Progeny Study.*: Royal Dutch Warmblood Studbook.

van Hoogmoed, L.M., Snyder, J.R., Thomas, H.L. & Harmon, F.A. (2003). Retrospective evaluation of equine prepurchase examinations performed 1991–2000. *Equine Veterinary Journal* 35(4), 375-381.

Vande Berg, B.C., Lecouvet, F.E. & Malghem, J. (2002). Frequency and topography of lesions of the femoro-tibial cartilage at spiral CT arthrography of the knee: a study in patients with normal knee radiographs and without history of trauma. *Skeletal Radiology* 31(11), 643-9.

Wang, Y., Ding, C., Wluka, A.E., Davis, S., Ebeling, P.R., Jones, G. & Cicuttini, F.M. (2006). Factors affecting progression of knee cartilage defects in normal subjects over 2 years. *Rheumatology* 45(1), 79-84.

Wang, Y., Wluka, A.E., Jones, G., Ding, C. & Cicuttini, F.M. (2012). Use magnetic resonance imaging to assess articular cartilage. *Therapeutic advances in musculoskeletal disease* 4(2), 77-97.

Watrous, B.J., Hultgren, B.D. & Wagner, P.C. (1991). Osteochondrosis and juvenile spavin in equids. *American Journal of Veterinary Research* 52(4), 607-12.

Veje, K., Hyllested-Winge, J.L. & Ostergaard, K. (2003). Topographic and zonal distribution of tenascin in human articular cartilage from femoral heads: normal versus mild and severe osteoarthritis. *Osteoarthritis and Cartilage* 11(3), 217-227.

Werpy, N.M., Ho, C.P., Pease, A.P. & Kawcak, C.E. (2011). The effect of sequence selection and field strength on detection of osteochondral defects in the metacarpophalangeal joint. *Veterinary Radiology and Ultrasound* 52(2), 154-60.

Verschooten, F. & Schramme, M. (1994). Radiological examination of the tarsus. *Equine Veterinary Education* 6(6), 323-332.

Whitton, R.C., Mirams, M., Mackie, E.J., Anderson, G.A. & Seeman, E. (2013). Exercise-induced inhibition of remodelling is focally offset with fatigue fracture in racehorses. *Osteoporosis International* 24(7), 2043-8.

WHO *Biomarkers in Risk Assessment: Validity and Validation*. [online] Available from: http://www.inchem.org/documents/ehc/ehc/ehc222.htm. [Accessed 28th April 2014].

Wieland, H.A., Michaelis, M., Kirschbaum, B.J. & Rudolphi, K.A. (2005). Osteoarthritis - an untreatable disease? *Nature reviews. Drug discovery* 4(4), 331-44.

Winter, V.D., Bruns, E., Glodek, P. & Hertsch, B. (1996). Genetic disposition of Bone Diseases in Sport Horses. *Zuchtungskunde* 68(2), 92-108.

Wirth, W., Duryea, J., Hellio Le Graverand, M.P., John, M.R., Nevitt, M., Buck, R.J. & Eckstein, F. (2013). Direct comparison of fixed flexion, radiography and MRI in knee osteoarthritis: responsiveness data from the Osteoarthritis Initiative. *Osteoarthritis and Cartilage* 21(1), 117-25.

Wluka, A.E., Stuckey, S., Snaddon, J. & Cicuttini, F.M. (2002). The determinants of change in tibial cartilage volume in osteoarthritic knees. *Arthritis and Rheumatism* 46(8), 2065-2072.

Wong, S., Steinbach, L., Zhao, J., Stehling, C., Ma, C. & Link, T. (2009). Comparative study of imaging at 3.0 T versus 1.5 T of the knee. *Skeletal Radiology* 38(8), 761-769.

Yoshioka, H., Stevens, K., Hargreaves, B.A., Steines, D., Genovese, M., Dillingham, M.F., Winalski, C.S. & Lang, P. (2004). Magnetic resonance imaging of articular cartilage of the knee: comparison between fat-suppressed three-dimensional SPGR imaging, fat-suppressed FSE imaging, and fat-suppressed three-dimensional DEFT imaging, and correlation with arthroscopy. *Journal of Magnetic Resonance Imaging* 20(5), 857-64.

Young, B.D., Samii, V.F., Mattoon, J.S., Weisbrode, S.E. & Bertone, A.L. (2007). Subchondral bone density and cartilage degeneration patterns in osteoarthritic metacarpal condyles of horses. *American Journal of Veterinary Research* 68(8), 841-9.

Acknowledgements

The work included in this thesis was performed at the Department of Clinical Sciences, Division of Large Animals and Diagnostics, Swedish University of Agricultural Sciences (SLU), with support of the former and present heads of department Torkel Ekman and Björn Ekesten, and former and present heads of division Bernt Jones and Ove Wattle.

Funding for the project was provided by the Swedish-Norwegian Foundation for Equine Research (Stiftelsen Hästforskning). Additional funding for the high-resolution microscopy studies with Professor Alan Boyde was provided by the Carl-Fredrik von Horns Grant from the Royal Swedish Academy of Agriculture and Forestry (Kungliga Skogs- och Lantbruksakademien) and the SLU Fund for Internationalisation of Postgraduate Studies. Support for attendance of conferences was provided by Gunnar Philipssons Stipendium.

This thesis has been supported by a team of dedicated, supportive, enthusiastic and expert supervisors.

My sincere thanks to my diagnostic imaging supervisor Kerstin Hansson. Thank you for your hard work getting the thesis project off the ground and keeping it flying from start to finish. Thank you for your great enthusiasm for the project, the constant encouragement, your thorough, accurate and honest feedback and sharing your ability to see things from new perspectives. I have great admiration for your radiology skills and appreciate how willing you are to share those skills with your peers.

My sincere thanks to my pathology supervisor Stina Ekman. Thank you for patiently teaching the radiologist some pathology and working through the large amount of microscopic grading that we have done for this thesis. Your solid support, optimistic encouragement and rapid thorough feedback has kept the project moving forward and your enthusiasm for research is infectious.

My sincere thanks to my Icelandic horse supervisor Sigríður Björnsdóttir. The study of this group of Icelandic horses to investigate the early stages of distal tarsal OA was something that Sigríður had planned for many years and this thesis is only part of a much larger study. Thank you Sigríður for inviting us to be part of this most exciting and unique equine OA project and for the generous hospitality offered by you and your family during our visits to Iceland. Your determination and thoroughness in establishing and carrying through this study is truly impressive.

My sincere thanks to my osteoarthritis supervisor Leif Dahlberg. Thank you for introducing me to the world of human OA research and the discussions we have had about the project.

My sincere thanks to my head supervisor Björn Ekesten. Thank you for your regular and uplifting encouragement and keeping my PhD on track.

During this thesis project I have been privileged to have worked with Alan Boyde and his unique and remarkable microscopic methods. Thank you Alan for sharing your immense knowledge, lab, newly discovered techniques, house and life in general. I am grateful for the enormous amount of work you have done in the study and the time you have spent teaching, helping and editing me. Your attitude to discovery is uplifting and it really is very enjoyable to work with you.

Special thanks to:

All of the staff at the Department of Clinical Sciences, SLU, for having such a positive and active attitude to veterinary research and teaching. I feel privileged to have done a PhD in this department.

The University Animal Hospital Diagnostic Imaging Department, SLU, where radiography, low-field MRI and some of the CT examinations were performed. Margareta Uhlhorn, Anna Straube, Carolina Nilemo, Frida Westgren, Helena Treffenberg Pettersson, Martin Rapp, Tove Hjorth, Jessica Ingman, Lisa Frilling, Chiaretta Mattei, Helena Nyman, Marion Grapperon-Mathis, Peter Lord, Christina Larsson, Vivan Eriksson, Marita Blom, Anna-Karin Thoresson, Jessica Johansson, Monica Sundqvist, Emilie Persson and Mieth Berger for making the department friendly, enthusiastic, highly competent and a pleasure to work in.

The Department of Biomedical Sciences and Veterinary Public Health, Division of Pathology, Pharmacology and Toxicology, SLU, where joint sampling and light microscopy histology were performed. Beate Hillman for your excellent assistance in collecting specimens from the joints and preparing the vast number of histology sections that were produced by the study. Agneta Boström for assistance with the preparation of histology sections. Hans

Kanbjer, Lars Hammarsten and Johan Karevik for assistance with sawing of tarsal joints.

Anders Lundberg, Gunilla Arvidsson, Monica Segelsjö and Lars Ove Magnusson from the Academic Hospital in Uppsala for assisting in development and performing MRI and CT examinations on the tarsal joints.

Eveliina Lammentausta from the Oulu University Hospital, Finland for assisting with MRI sequence development, and for valuable discussions about joint diagnostic imaging.

Maureen Arora in Alan Boyde's lab in London for preparation of the specimens for BSE SEM and CSLM examinations.

Sten-Olof Fredriksson and Kjell-Åke Ahlin for constructing and maintaining the study's computer systems that were, and are, so vital to working with images.

Sigurjon Einarsson for huge amounts of help with the horses in Iceland and the specimens of the tarsal joints in Uppsala. The Einarsson family for their generosity of lending breeding horses for the project and their hospitality when we visited Iceland.

Karl Zötterman for help with the horses and Iceland and a great undergraduate thesis work that helped clear the fog during the early parts of the study.

Carina Kubacki for an excellent undergraduate thesis work on the affect of temperature and post-mortem time on the MRI images of the pilot tarsal joint studies.

The SLU library for providing a superb, easily accessible and complete literature resource, and especially Michael Eklund for your assistance finding the tricky references.

Biostokastikum, SLU, particularly Claudia von Brömssen for very helpful statistical advice.

Susanne Pettersson, Annika Nyström, Anette Forsberg, Mikael Rosenius, Veiko Niemi from the Department of Clinical Sciences administration, SLU, for happy and helpful assistance with everything from course points to bills.

This thesis would not have been completed without the support, assistance, encouragement and tolerance of my family. Thank you Timothy, Kristoffer and Edward for you love, happiness and keeping life in perspective. Thank you Cecilia for taking this journey with me. Your love makes anything possible.